NTNU – Trondheim
Norwegian University of
Science and Technology

Epigenetic changes in human bronchial epithelial cells after *in vitro* transformation with chemical carcinogens

Analysis of cell migration and DNA methylation in *FOXA* genes

Ida Øvre Andersen

Biotechnology (5 year)
Submission date: May 2013
Supervisor: Aage Haugen, IBT
Co-supervisor: Steen Mollerup, Statens arbeidsmiljøinstitutt (Stami), Oslo

Norwegian University of Science and Technology
Department of Biotechnology

Acknowledgements

The work with this thesis was performed at the National Institute of Occupational Health, Oslo, as a part of the Master in Science in Biotechnology at the Norwegian University of Science and Technology (NTNU), Trondheim. The work started in august 2012 and ended in May 2013. First of all, I would like to thank the group of toxicology and my supervisors, Professor Aage Haugen and PhD Steen Mollerup, for giving me the opportunity to complete my master thesis here.

A special thank to Steen Mollerup for being an excellent supervisor and for his enthusiasm in the project. I'm grateful for all of his good advice, theoretical guidance and valuable input during my time here. I would like to thank Audun Bersaas for invaluable support, guidance and patience both in the laboratory and with analysis of results. Many thank to Rita Bæra for tutoring in the laboratory and assistance with data analysis.

Thanks to Ragnhild Askeland Sandbu for your time proofreading. To Mayes Kasem, thank you for your help and for the joy you spread at work. To all of the master students at the top floor, thank you for many good times this year. Especially to Jenny Dugstad, for cooperation with this study.

I would like to thank my family for their love and support. At last, but not least, to Erik, thank you for always making me smile.

Oslo, 15.05.2013
Ida Øvre Andersen

Content

Abstract

Lung cancer is the leading cause of cancer related deaths worldwide. Cancer is caused by an accumulation of genetic and epigenetic changes that leads to alterations in gene activity and phenotype. There is emerging evidence of the epigenetic events in initiation and progression of cancer. Tobacco smoking is the major cause of lung cancer, involving numerous carcinogens. An *in vitro* transformation model had previously been established at STAMI, where human bronchial epithelial cells (HBECs) were exposed to tobacco smoke carcinogens (benzo[*a*]pyrene, cigarette smoke condensate and *N*-methylnitrosourea) for up to 15 weeks. Two transformed cell lines (HBEC-2KT and HBEC-12KT) were used as models to investigate molecular changes associated with transformation. The first aim of this thesis was to investigate how transformation affected cell migration. The second aim was to investigate whether DNA methylation of *FOXA1* and *FOXA2* genes could explain their downregulation in transformed cells relative to non-transformed cells.

Two methods, the manual *in vitro* scratch assay and a semi-automated technique using IncuCyte ZOOM, were used to study cell migration. Both methods involve creating a wound in the cell monolayer and further measure the cells migration into the wound during a set time period. Light microscope images were acquired after 0 and 12 hours for the manual method, and on an hourly basis for 24 hours for the semi-automated method. DNA methylation studies were carried out by bisulfite treatment of DNA followed by pyrosequencing.

Transformed HBEC-12KT showed decreased migration compared to their control cells (DMSO). HBEC-2KT transformed cells also showed decreased migration compared to their control cells (DMSO) when analysed by IncuCyte ZOOM. However, an increased migration was observed when transformed HBEC-2KT were analysed by *in vitro* scratch assay. Previous gene expression analysis of transformed cell lines showed reduced expression of E-cadherin (*CDH1*) and increased expression of N-cadherin (*CDH2*), which indicates a hallmark of EMT known as the cadherin switch. This was supported by downregulation of the *FOXA1* and *FOXA2* genes, which may be an essential step of EMT in cancer progression.

DNA methylation levels in the FOXA1_pyro1 assay varied between 35-90 % in both transformed HBEC-2KT and their control cells (DMSO). DNA methylation levels in this

assay were above 90 % in both transformed HBEC-12KT and their control cells (DMSO). DNA methylation levels in the FOXA1_pyro2 assay were above 80 % in transformed HBEC-2KT and their control cells (DMSO), and above 70 % in transformed HBEC-12KT and their control cells (DMSO). Therefore, it is difficult to draw conclusions on whether methylation of FOXA1 is related to its expression since non-transformed cells already had high methylation levels in the studied CpG sites. In addition, it might be speculated that the inspected sites are not involved in gene silencing since control cells express the gene despite high levels of methylation.

Both *FOXA2* assays showed overall lower DNA methylation levels than the *FOXA1* assays. In the FOXA2_cpg1 assay the DNA methylation levels were below 10 % in all of the transformed cell lines (HBEC-2KT and HBEC-12KT), and also their control cells (DMSO). Methylation levels in FOXA2_TSS ranged between 0-50 % for transformed HBEC-2KT and their control cells (DMSO). The majority of the transformed HBEC-12KT cells showed DNA methylation levels between 20-50 % in the FOXA2_TSS assay. Their control cells (DMSO) also showed DNA methylation levels in the same range. Thus, downregulation of *FOXA2* gene expression in transformed cell lines was in contrast to an overall low degree of DNA methylation and no outstanding changes in DNA methylation levels between non-transformed and transformed cell lines were observed.

In conclusion, changes in migration between transformed and non-transformed cell lines were observed. It is, however, clear that cell migration and EMT are not directly linked in this *in vitro* transformation model. Based on bisulfite/pyrosequencing analyses, no outstanding changes in DNA methylation of the CpG sites studied between non-transformed and transformed cells were observed. Hence, based on the results presented in this thesis, no conclusions can be drawn to whether downregulation of *FOXA1* and *FOXA2* gene expression is related to DNA methylation of the regions studied.

Sammendrag

Lungekreft er en ledende årsak til kreftdødsfall på verdensbasis. Kreft er forårsaket av akkumulering av genetiske og epigenetiske endringer. Dette vil føre til forandringer i genaktivitet og fenotype. Det kommer stadig nye bevis på at epigenetiske mekanismer er viktige for initiering og utvikling av kreft. Tobakk inneholder mange kreftfremkallende karsinogener og tobakksrøyking er den fremste årsaken til lungekreft. En *in vitro* transformasjonsmodell har tidligere blitt utviklet på STAMI, der humane bronkieepitelceller (HBECs) ble utsatt for karsinogener fra tobakk (benzo[*a*]pyren, sigarettrøyk kondensat og *N*-methylnitrosourea) i opptil 15 uker. To transformerte cellelinjer (HBEC-2KT og HBEC-12KT) ble brukt som modeller for å undersøke molekylære endringer knyttet til transformasjon. Det første målet med denne oppgaven var å undersøke hvordan celletransformasjon påvirket cellemigrasjon. Det andre målet var å undersøke om DNA-metylering kan forklare nedregulering av *FOXA1* og *FOXA2* genene i transformerte celler i forhold til ikke-transformerte celler.

To metoder, det manuelle *in vitro* sårhelings-assay og en delvis automatisert metode ved bruk av IncuCyte ZOOM, ble brukt til å studere cellemigrasjon. Begge metodene innebærer å lage et sår i cellens monolag, og videre måle cellemigrering inn i såret i løpet av en definert tidsperiode. Det ble tatt bilder med lysmikroskop etter 0 og 12 timer for den manuelle metoden, og på timesbasis i 24 timer for IncuCyte ZOOM-metoden. Studier av DNA-metylering ble utført ved bisulfitt-behandling av DNA etterfulgt av pyrosekvensering.

Transformerte HBEC-12KT viste redusert migrasjon i forhold til sine kontrollceller (DMSO). HBEC-2KT transformerte celler viste også redusert migrasjon i forhold til sine kontrollceller (DMSO) når analysert ved hjelp av IncuCyte ZOOM. På motsatt side ble det observert økt migrasjon av transformerte HBEC-2KT når de ble analysert med *in vitro* sårhelingsassay. Tidligere genuttrykksanalyser av transformerte cellelinjer viste redusert uttrykk av E-kadherin (*CDH1*) og økt uttrykk av N-kadherin (*CDH2*), noe som er kjent som den såkalte ”cadherin switch” og er et kjennetegn ved EMT. Nedregulering av *FOXA1* og *FOXA2* genene understøtter dette, og kan trolig være et viktig trinn for EMT i utviklingen av kreft.

Nivået av DNA-metylering i FOXA1_pyro1 assay varierte mellom 35-90 % i både transformerte HBEC-2KT og deres kontrollceller (DMSO). For transformerte HBEC-12KT og deres kontrollceller (DMSO) var nivået av DNA-metylering over 90 %. I FOXA1_pyro2 assay var nivået av DNA-metylering over 80 % i transformerte HBEC-2KT og deres kontrollceller (DMSO), og over 70 % i transformerte HBEC-12KT og deres kontrollceller (DMSO). Det er derfor vanskelig å trekke konklusjoner om hvorvidt metylering av *FOXA1* er relatert til genuttrykk siden ikke-transformerte celler allerede hadde høyt nivå av DNA-metylering i de undersøkte CpG områdene. I tillegg kan det spekuleres i om de undersøkte områdene ikke er involvert i stilning av genet siden kontrollcellene (DMSO) uttrykker genet til tross for høye nivåer av DNA metylering.

Begge assayene i *FOXA2* genet viste generelt lavere nivåer av DNA-metylering enn *FOXA1* genet. I FOXA2_cpg1 var nivået av DNA-metylering lavere enn 10 % i de transformerte cellelinjene (HBEC-2KT og HBEC-12KT), inkludert deres kontrollceller (DMSO). DNA-metyleringsnivåer i FOXA2_TSS varierte mellom 0-50 % i transformerte HBEC-2KT og deres kontrollceller (DMSO). Flertallet av de transformerte HBEC-12KT cellene hadde DNA-metyleringsnivåer mellom 20-50 % i FOXA2_TSS assay. Kontrollceller (DMSO) viste også samme nivå av DNA-metylering. Dermed var nedregulering av *FOXA2* genet i transformerte celle linjer i kontrast til generelt lave nivåer av DNA metylering. Det ble ikke observert noen betydelige endringer i DNA-metyleringsnivåer mellom ikke-transformerte og transformerte cellelinjer.

Det ble observert endringer i migrasjon mellom ikke-transformerte og transformerte cellelinjer. Det er imidlertid konkludert med at celle migrasjon og EMT ikke er direkte sammenkoblet i denne *in vitro* transformasjonsmodellen. Basert på bisulfitt/pyrosekvenseringsanalysene ble det ikke observert noen betydelige endringer i DNA-metylering i de undersøkte CpG områder mellom ikke-transformerte og transformerte celler. Derfor kan det, basert på resultatene i denne oppgaven, ikke konkluderes med om nedregulering av *FOXA1* og *FOXA2* er på grunn av DNA-metylering i de undersøkte regionene.

Abbreviations

ANOVA	Analysis of variance
ATP	Adenosine-5'-triphosphate
Benzo[*a*]pyrene	B[*a*]P
bp	Base pair
CpG	Cytosine-phosphate-guanine
CAM	Cell adhesion molecule
CDH	Cadherin
Cdk	Cyclin-dependent kinase
ChIP	Chromatin immunoprecipitation
CSC	Cigarette smoke condensate
DMSO	Dimethyl sulfoxide
DNA	Deoxyribonucleic acid
DNMT	DNA methyltransferase
E-cadherin	Epithelial cadherin
EMT	Epithelial-to-mesenchymal transition
FOXA	Forkhead-box A
GJIC	Gap junctional intercellular communication
GTP	Guanosine-5'-triphosphate
HBEC	Human bronchial epithelial cell
IARC	International Agency for Research on Cancer
MeDIP	Methyl-DNA immunoprecipitation
mRNA	Messenger RNA
miRNA	Micro RNA
MNU	*N*-methylnitrosourea
N-cadherin	Neural cadherin
NNK	4-(methylnitrosoamino)-1-(3-pyridyl)-1-butanone
NSCLC	Non-small cell lung cancer
PAH	Polycyclic aromatic hydrocarbons
PBS	Phosphate buffered saline
PCR	Polymerase chain reaction
RNA	Ribonucleic acid
RWD	Relative wound density

SD	Standard deviation
STAMI	National Institute of Occupational Health
TGF-β	Transforming growth factor beta
UTR	Untranslated region

1 Introduction

1.1 Cancer

Cancer is a major health problem for humans. According to Jemal et al. (2011), cancer is the leading cause of death in developed countries and the second leading cause in developing countries. However, there is an increasing problem of cancer in developing countries, due to aging and growth of the population. In addition, there is an increased adoption of cancer-associated lifestyles in the developing countries, as for example smoking, physical inactivity and unhealthy diets. Worldwide, in 2008 there were about 12.7 million cancer cases and 7.6 million cancer deaths (figure 1.1). Both estimated new cases and estimated deaths from cancer have increased the last years (Jemal et al., 2011; Parkin et al., 2005).

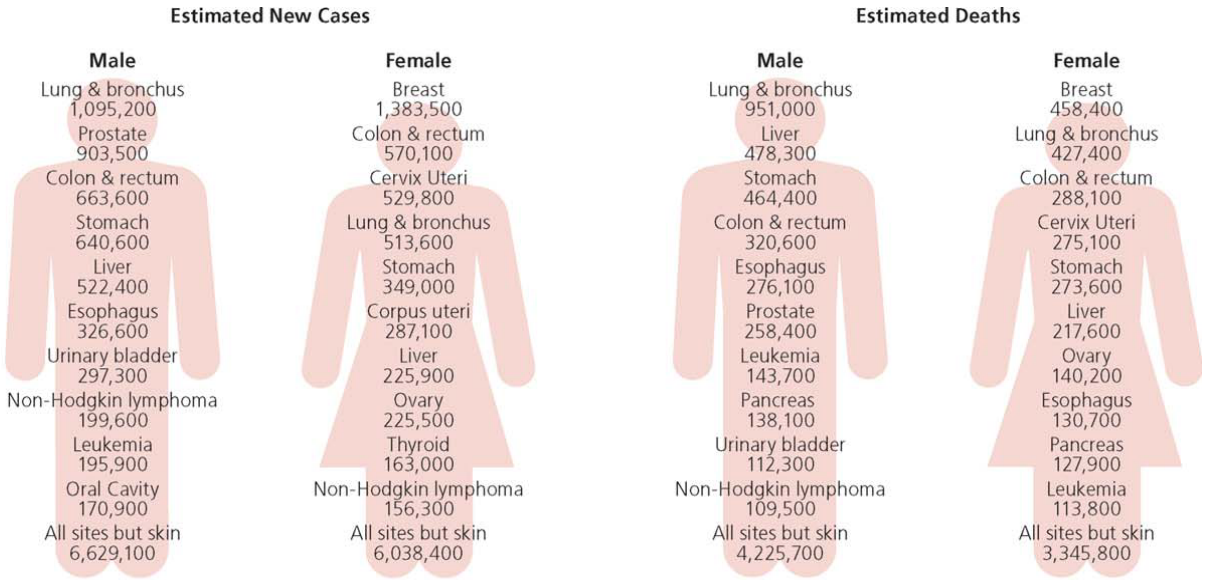

Figure 1.1: Estimated new cancer cases and deaths worldwide in 2008 (Jemal et al., 2011).

As can be seen from figure 1.1, lung and bronchus cancer were the most commonly diagnosed cancer for men in 2008, and also the leading cause of cancer-related deaths worldwide. Breast cancer was the most commonly diagnosed cancer among women in 2008 as well as the leading cause of cancer deaths globally. Lung and bronchus cancer among men accounted for about 17 % of estimated new cases and 23 % of cancer deaths worldwide in 2008. Breast cancer in women accounted for about 23 % of new cases and 14 % of cancer deaths (Jemal et al., 2011).

There is evidence of great variations in the risk of cancer according to geographical area. Most of the variations are due to risk factors in lifestyle and environment (Parkin et al., 2005). In 2008, the cancer incidence rates in the developing world were half the cancer incidence rates in the developed world, whereas the cancer mortality (number of deaths per 100 000 persons per year) was the same. This might be due to later diagnosis and limited access to treatment in the developing world, which will have an adverse effect on cancer survival. Tobacco smoking is a major cause of cancer globally and there are also differences in the stage and degree of the tobacco epidemic. As for example in China, where they consume one in three of all the cigarettes produced in the world. This is due to both the huge population in the country and high prevalence of smoking among men in China (Jemal et al., 2011; Youlden et al., 2008).

On the positive side, there has been a tremendous increase in the knowledge of the various molecular mechanisms and pathophysiology of human cancer during the past 20 years and so. These mechanisms might serve as new targets for drug development, that hopefully will be less toxic for the patients and have enhanced antitumor activity (Debeir et al., 2008).

1.1.1 Lung cancer

In 2008, lung cancer accounted for 13 % of total cases and 18 % of total deaths (Jemal et al., 2011; Parkin et al., 2005). During the last years, there have been improvements in treatment of lung cancer but the prognosis still remains poor. The 5-year survival rate is only 15 % (Deutsch et al., 2012).

There are two subtypes of lung cancer: small cell lung cancer (SCLC), which accounts for about 25 % of all lung cancers in Europe, and non-small cell lung cancer (NSCLC). NSCLC is divided into three histological types: squamous cell carcinoma, adenocarcinoma and large cell carcinoma. The most common are squamous cell carcinoma and adenocarcinoma. Squamous cell carcinoma is characterised by intercellular bridging and keratinization, but these morphologic features are difficult to detect in poorly differentiated tumours. Adenocarcinomas are highly heterogeneous and consist of a mixture of two or three histologic subtypes, as for example papillary adenocarcinoma and bronchioloalveolar carcinoma. Large cell carcinomas are poorly differentiated tumours, and shows no differentiation pattern for

classification into squamous cell carcinoma, adenocarcinoma or small cell carcinoma. Carcinomas arise from epithelia, which are cells that line walls of cavities and channels (Brambilla and Lantuejoul, 2008; Youlden et al., 2008; Weinberg, 2007). Lung tumours have a complex pattern of random cytogenetic and molecular genetic changes, and there are various substances that can increase the risk of development. A better understanding of mechanisms leading to lung cancer will provide a new insight into how to prevent the disease (Deutsch et al., 2012).

Some risk factors for lung cancer includes exposure to carcinogens, both occupational and environmental, as asbestos, arsenic, radon and polycyclic aromatic hydrocarbons (PAHs), indoor pollution from cooking fumes and cigarette smoke (Jemal et al., 2011; Haugen and Mollerup, 2008). Tobacco smoking is the major cause of lung cancer, accounting for 80 % of the lung cancer burden in men and 50 % in women (Jemal et al., 2011). Inhalation of tobacco smoke can cause genetic and epigenetic changes in the respiratory epithelium during the process of carcinogenesis, as tobacco smoke holds numerous carcinogens (Tang et al., 2011). According to IARC Monograph Volume 83 (2004) PAHs, as benzo[*a*]pyrene (B[*a*]P), and tobacco specific nitrosoamines, as 4-(methylnitrosoamino)-1-(3-pyridyl)-1-butanone (NNK), are considered to be major lung carcinogens (Jemal et al., 2011). Activation of proto-oncogenes and inactivation of tumour suppressor genes are some of the genetic changes that occur due to carcinogens in cigarette smoke (Tang et al., 2011). Hypermethylation of 5'methylcytosine in CpG (cytosine-phosphate-guanine) islands in tumour suppressor genes is an important epigenetic event in the development of cancer. Promoter hypermethylation is important for the inactivation of many tumour suppressor genes in for example NSCLC. This can lead to loss of gene transcription and is a critical event in the initiation and progression of cancer (Lin et al., 2007).

Lung cancer death rates for men in western countries are decreasing. However, in for example China and Africa, the smoking epidemic was established later and the prevalence of smoking is therefore still increasing in the majority of the areas. Females started smoking several decades after men, and lung cancers have a latency period of 20-40 years, hence the lung cancer trends of women are lagging behind and the cancer incidences are still increasing in many countries (Jemal et al., 2011; Klaassen and Watkins III, 2010).

1.1.2 Molecular biology of cancer

Cancer is a class of diseases that is characterised by cellular mutation, increased proliferation and aberrant cell growth (Klaassen and Watkins III, 2010). Cells accumulate genetic and epigenetic changes that can lead to changes in gene activity and alter the phenotype. Over time, a cell population that ignores normal controls of proliferation will become cancer (Ponder, 2001).

Cancer is caused by mutations in the genes that control proliferation or apoptosis. The vast majority arise as a consequence of chemical damage to DNA, and are referred to as genetic modifications. After DNA replication and subsequent cell division this damage is converted into a heritable change in DNA. Mutations giving cancer cells the ability to evade normal homeostatic mechanisms are the ones that are found in successful cancer cells (Bertram, 2001). In the later years there has been emerging evidence of epigenetic events in initiation and progression of cancer. Epigenetics is defined as heritable changes in the activity of gene expression without altering the DNA sequence itself. Key mechanisms in epigenetics are DNA methylation, histone modifications, nucleosome positioning and regulation by non-coding RNA (Jones and Baylin, 2002; Kanwal and Gupta, 2010). For example, methylation has several consequences for development of cancer. Cancer cells can enter cell cycle, avoid apoptosis and promote angiogenesis by methylations of genes involved in these processes. Also, it may lead to defects in DNA repair and loss of cell adhesion (Sharma et al., 2010). These processes will be dealt with in later paragraphs.

Two important types of genes that play a role in development of cancer are proto-oncogenes and tumour-suppressor genes, that are involved in controlling cell growth and proliferation. Proto-oncogenes encode proteins that have functions in regulation of cell growth, apoptosis and differentiation. They can be activated to oncogenes by structural alterations, which can lead to cancer as they can cause cells ought to die to survive. This is characterised as a gain-of-function mutation. Loss of function of tumour suppressor genes will contribute on the road to cancer, due to their role in inhibiting cell division and promote apoptosis when damage to cells cannot be repaired (Croce, 2008; Klaassen and Watkins III, 2010; Ponder, 2001).

1.1.3 Carcinogenesis

Carcinogens are exogenous agents, physical or chemical, which cause neoplasia (autonomous growth of tissue). They can be genotoxic, meaning that they interact directly with DNA and damage its structure or non-genotoxic (epigenetic), which modify gene expression without damaging DNA (Bertram, 2001; Klaassen and Watkins III, 2010). A series of genetic and epigenetic alterations that lead to uncontrolled cell growth is the foundation of carcinogenesis (Tost and Gut, 2007).

Carcinogenesis is the creation of cancer. This process involves a series of three definable and reproducible stages, known as initiation, promotion and progression (figure 1.2).

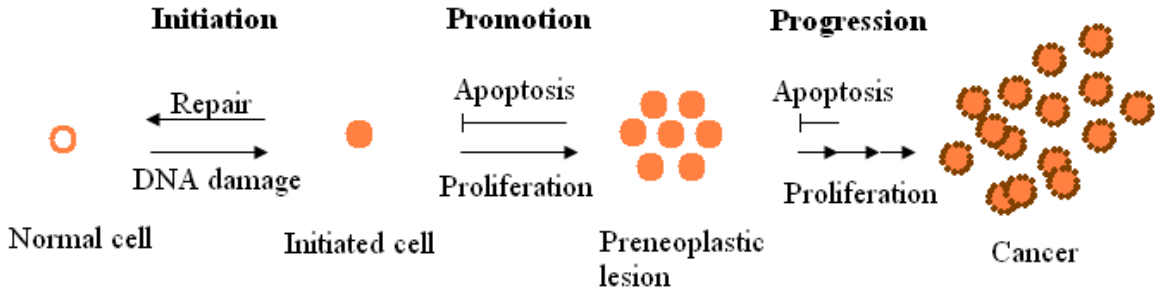

Figure 1.2: The process of carcinogenesis. Modified from Klaassen and Watkins III (2010).

Initiation is the first stage and it is a rapid and irreversible process that results in a stable and heritable carcinogen-induced mutation. Chemical carcinogens will bind covalently to DNA and form adducts. Carcinogens are known as initiating agents. The initiated cell undergoes selective clonal expansion and produces a preneoplastic lesion, a stage known as promotion. Tumour promoters function through various mechanisms, as gene expression changes, increasing proliferation and inhibiting apoptosis. This stage is reversed when tumour promoters are removed. A benign preneoplastic lesion is converted into neoplastic cancer during the non-reversible process of progression. Additional genotoxic events occur as the result of increased DNA synthesis and proliferation in the preneoplastic lesion. Autonomous growth, accumulation of chromosomal aberrations and karyotypic instability are hallmarks of progression (Klaassen and Watkins III, 2010).

1.1.4 Hallmarks of cancer

The hallmarks of cancer are six biological capabilities cells acquire during the multistep development of human cancer and this contributes to complexities of neoplastic diseases. They include sustaining proliferative signal, evading growth suppressors, enabling replicative immortality, resisting cell death, induce angiogenesis and activate invasion and metastasis (figure 1.3). These hallmarks provide a solid foundation for understanding the biology of cancer (Hanahan and Weinberg, 2011).

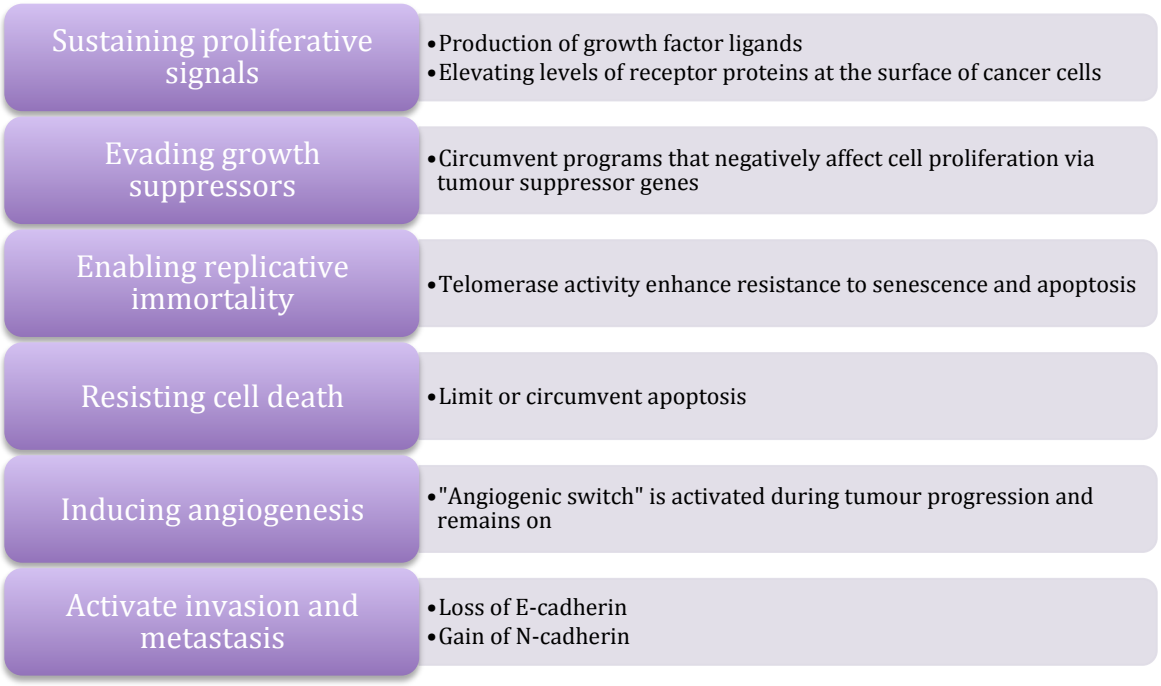

Figure 1.3: The six hallmarks of cancer (Hanahan and Weinberg, 2011).

Cancer is a disease that involves dynamic changes in the genome. The basis is, as mentioned earlier, in mutations that result in activated oncogenes and the loss of function of tumour suppressor genes. Oncogenic mutations in the *ras* gene disrupt the Ras GTPase activity, which usually functions as a negative-feedback circuit to control cell proliferation. The tumour suppressor protein 53 (p53) is central in regulatory circuits for control of proliferation and promoting senescence and apoptosis. The p53 protein arrests cells with damaged DNA in the G_1 phase of the cell cycle. Cancer cells circumvent apoptosis by the loss of p53, which is seen in more than 50 % of human cancers (Hanahan and Weinberg, 2000; Hanahan and Weinberg, 2011; Klaassen and Watkins III, 2010).

In order to generate macroscopic tumours cancer cells must obtain unlimited replicative potential. Telomeres are essential for protection of the ends of chromosomes. Telomerase is a specialised DNA polymerase, and its presence is correlated with resistance to both senescence and apoptosis (Hanahan and Weinberg, 2011).

Invasion and metastasis are important for the malignancy of cancers. Metastases are the cause of 90 % of human cancer deaths. One of the alterations during the process is the loss of E-cadherin (epithelial cadherin), a cell-to-cell adhesion molecule (Hanahan and Weinberg, 2000; Hanahan and Weinberg, 2011). This will be described in detail in section 1.3.

By acquisition of hallmark capabilities cancer cells can survive, proliferate and initiate metastasis. Various mechanisms contribute and they differ according to type of tumour and time during the process of carcinogenesis. Enabling characteristics associated with acquisition of hallmark capabilities are genomic instability and tumour-promoting inflammation. Genomic instability will lead to generation of random mutations, as chromosomal rearrangements, and the inflammatory state of premalignant and malignant lesions can serve to promote tumour progression. This shows the dual roles of the immune system in fighting diseases and promoting tumour formation. Inflammation by immune cells is designed to heal wounds and fight infections, but it can instead lead to its inadvertent support of hallmark capabilities. The process of inflammation will lead to an increased inflow of growth factors, survival factors, extracellular matrix-modifying enzymes and inductive signals for epithelial-to-mesenchymal transition (EMT) (Hanahan and Weinberg, 2011).

Evading destruction from immune cells and reprogramming energy metabolism are emerging hallmarks of cancer. The immune system can also act as a barrier to tumour formation and progression, and by evading the system cancer cells will not be eliminated. Cancer cells have a metabolic switch where they limit their energy production mostly to glycolysis, known as the “Warburg-effect”. This metabolic phenotype is characteristic for rapidly dividing cells. Hence, it must provide advantages during cell proliferation. A significant increase in uptake and utilization of glucose is documented in human tumours (Hanahan and Weinberg, 2011; Lunt and Heiden, 2011).

1.2 Chemicals in cigarette smoke

Upon inhalation, chemicals in cigarette smoke are deposited in airways and lungs. Genotoxic carcinogens in cigarette smoke may have mutagenic effects on lung cells. Cigarette smoke is a complex mixture of chemicals, and how it causes lung cancer is depicted in figure 1.4 (Hecht, 2012a; Pleasance et al., 2009).

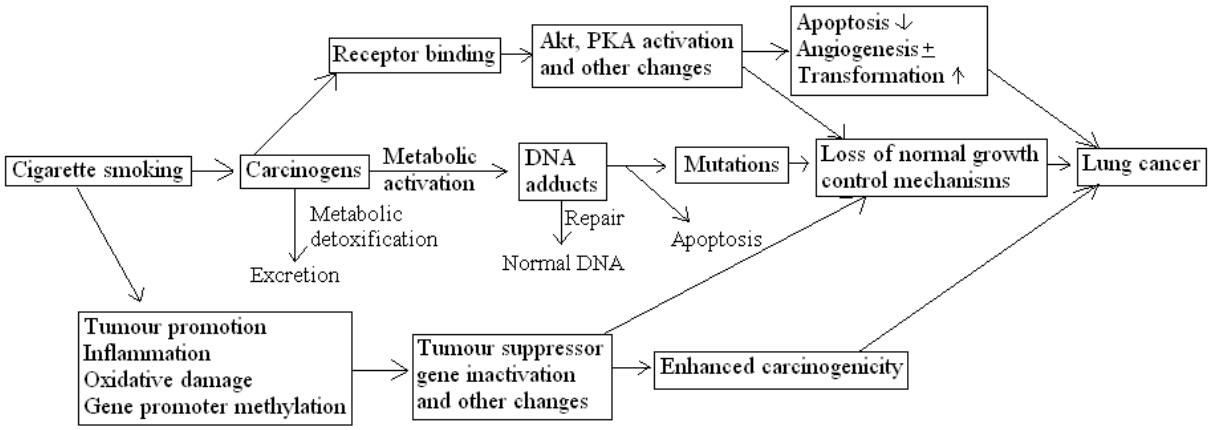

Figure 1.4: How cigarette smoking can cause the development of lung cancer. Modified from Hecht (2012a).

Cigarette smoke contains more than 5000 constituents, and only a few of them have been studied thoroughly considering toxic effects. International Agency for Research on Cancer (IARC) have evaluated more than 70 compounds for carcinogenicity and placed them in group 1 (carcinogenic to humans), 2A (probably carcinogenic to humans) or 2B (possibly carcinogenic to humans). Some of them are listed in table 1.1 (Hecht, 2012b).

Table 1.1: Major groups of carcinogens in cigarette smoke classified by IARC, and some specific examples of chemicals within each group. IARC classify the carcinogens into groups: group 1 (carcinogenic to humans), 2A (probably carcinogenic to humans) and 2B (possibly carcinogenic to humans). ND=not detected (Hecht, 2012b).

Chemical group	Specific examples	IARC group	Amount in mainstream cigarette smoke, per cigarette
Polycyclic aromatic hydrocarbons (PAH)	Benzo[*a*]pyrene (B[*a*]P)	1	1-15.2 ng
Other hydrocarbons	Naphthalene	2B	65-868 ng
***N*-Nitrosoamines**	N'-nitrosonornicotine (NNN)	1	5-270 ng
	4-(methylnitrosoamino)-1-(3-pyridyl)-1-butanone (NNK)	1	13-223 ng
Aromatic amines	2-Naphtylamine	1	1.47-17.2 ng
Aldehydes	Formaldehyde	1	1.6-75.5 μg
	Acetaldehyde	2B	32-828 μg
Phenolic compounds	Caffeic acid	2B	Present
Nitrohydrocarbons	Nitrobenzene	2B	Present
Miscellaneous organic compounds	Acrylamide	2A	2.3 μg
Metals and inorganic compounds	Arsenic	1	ND-5.5 ng
	Cadmium	1	1.6-101 ng

As for 2012, there was no regulation of harmful tobacco smoke constituents in the United States, but some countries have set maximum levels for certain harmful constituents, as tar, nicotine and carbon monoxide (CO). A proposal for lowering of toxicants in cigarette smoke, this regulation goes for example for acetaldehyde, formaldehyde, B[*a*]P and CO has been made (Hecht, 2012b).

1.2.1 Polycyclic aromatic hydrocarbons (PAHs)

PAHs are a group of genotoxic carcinogens present at high concentrations in tobacco smoke and various working environments. They are formed by incomplete combustion of organic

matter, and require metabolic activation to DNA-reactive intermediates as epoxides. Epoxides are mutagenic and carcinogenic. These substances react easily with DNA and form so-called adducts, with miscoding consequences during replication. DNA adducts are found at increased levels in the lungs of smokers, compared to non-smokers. B[*a*]P is classical PAH, and is metabolized to B[*a*]-7,8-diol-9,10-epoxide that is its ultimate carcinogen. It is known that B[*a*]P induces EMT-related gene expression in lung cancer cells (Hecht, 2012a; Yoshino et al., 2007). This will be discussed in section 1.3.

1.2.2 *N*-methylnitrosourea (MNU)

MNU, also known as nitrosomethylurea (NMU), is defined as a carcinogen. It is similar to NNK, which is a major lung carcinogen as mentioned earlier. It can induce benign and malignant tumours after administration by various routes. MNU has been shown to cause cancer in for example stomach, skin, kidney and nervous systems of animals (IARC, 1978). MNU is an alkylating agent, and attaches an alkyl group to DNA. It is also referred to as base-damaging (Xu et al., 2011). By exposure to MNU, there are formed pro-mutagenic methylated purines in DNA. This has been proposed as a critical initiating event of carcinogenesis. MNU is not dependent on metabolic activation (Faustman-Watts and Goodman, 1984).

1.2.3 Cigarette smoke condensate (CSC)

CSC is the particulate fraction of cigarette smoke, and has tumour promoting, co-carcinogenic and genotoxic properties. Tumour promoters are found in the weakly acidic/neutral fraction of the condensate. CSC is commercially produced and is often used in *in vitro* carcinogenesis studies (DeMarini, 2004; Hecht, 2012a; Hellermann et al., 2002).

Studies show that CSC induces a squamous morphology and growth inhibition in human bronchial epithelial cells, and that the effect is mostly pronounced when using the neutral fraction of CSC. Squamous cells are more flattened, hence adhered to the underlying matrix and they become less able to migrate. This effect was seen after longer exposures to CSC. Bronchial epithelium has three properties by which they undergo repair; attachment to matrix, migration and proliferation, and exposure to CSC will likely inhibit the ability to participate in the repairing process (Cantral et al., 1995).

Luppi et al. (2005) observed a dose-dependent increase in cell proliferation by exposure to low concentrations (0.25-1 AU/ml) of CSC for 24 hours by studying a human pulmonary muco-epidermoid carcinoma cell line. Concentration was expressed as arbitrary units (AU) per ml, and ten AU/ml corresponded to a mean of 5 % (vol/vol) CSC. Higher concentrations of CSC decreased cell proliferation. High concentrations of CSC can induce cell death because of the high concentrations of oxidants and other radicals produced during smoking and inflammation. CSC upregulates expression of genes encoding proinflammatory molecules. For example, CSC induces activation of NFκB (nuclear factor kappa-light-chain-enhancer of activated B cells), which is a protein complex that has a role in regulation of proinflammatory responses (Hellermann et al., 2002; Luppi et al., 2005).

Cell proliferation plays a role in epithelial wound closure in addition to cell migration, and CSC can also affect this. At higher concentrations (5 AU/ml) wound closure was totally inhibited in the above carcinoma cell line. However, at lower concentrations (1 AU/ml) a significant increase in wound closure was seen. By studying primary bronchial epithelial cells Luppi et al. obtained similarly results regarding wound closure. Conversely, it appears that cell proliferation does not contribute to wound closure in primary bronchial epithelial cells, in the same way as migration, due to that very few proliferating cells were present in the wound area. It has also been described that epithelial migration is inhibited by CSC (Luppi et al., 2005).

Finally, CSC is also known to decrease E-cadherin expression and promoter activity, and increase mesenchymal markers as N-cadherin, fibronectin and vimentin in both human lung adenocarcinoma and human bronchial epithelial lung. Hence, CSC appears to be contributing to EMT (Nagathihalli et al., 2012).

1.3 Epithelial-to-mesenchymal transition (EMT)

Epithelial layers are multicellular structures composed of closely associated and largely immobile cells. The structures are stabilized by E-cadherin, which will be discussed further down. By undergoing so-called epithelial-to-mesenchymal transition (EMT), epithelial cells acquire a mesenchymal phenotype that is characterised by loosely associated cells, which have the ability to move (Guarino et al., 2007).

EMT is a fundamental event in morphogenesis, due to its involvement in generation of tissues and organs during embryogenesis in both vertebrates and invertebrates. Essential features are disruption of intercellular contacts and enhancement of cell motility (figure 1.5). During this process, cells move around and switch between epithelial and mesenchymal states as a part of organ development. In adulthood, EMT is important during wound healing. In addition, EMT is also closely related to cancer progression, and it is observed in numerous types of epithelial cancer, as for example NSCLC (Byers et al., 2013). Transformed epithelial cells often acquire the abilities to invade other tissues, resist apoptosis and spread by acquiring the mesenchymal phenotype that is suitable for migration. This leads to reversible reprogramming of the cell, which is transcriptionally regulated. EMT-inducing transcription factors (EMT-TFs) are involved in migration and invasion, and also suppression of senescence and apoptosis and resistance to for example chemotherapy (Byers et al., 2013; De Craene and Berx, 2013; Guarino et al., 2007; Hanahan and Weinberg, 2011).

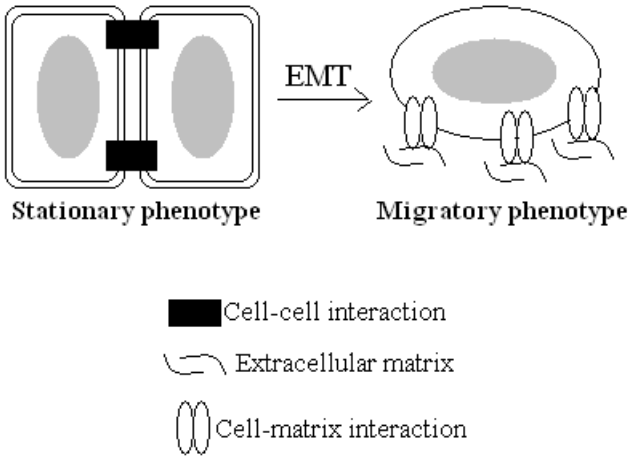

Figure 1.5: Epithelial-to-mesenchymal transition (EMT) involves change from stationary to migratory phenotype. Modified from Guarino et al. (2007).

Cells possessing invasive or metastatic properties have altered levels of proteins involved in tethering of cells to surrounding tissue, such as cell adhesion molecules (CAMs) and integrins. Members of immunoglobulin and calcium-dependent cadherin families are examples of the former, and the ladder includes proteins that link cells to the extracellular matrix (Hanahan and Weinberg, 2000; Hanahan and Weinberg, 2011). Cadherins belongs to a superfamily of proteins that functions in cell recognition, tissue morphogenesis and tumour

progression. E-cadherin is the prototypical cadherin, other classical cadherins include type I P-, N- and R-cadherins and type II cadherins (cadherins 5-12) (Hazan et al., 2004).

E-cadherin is encoded by the *CDH1* (cadherin-1) gene, which is defined as a tumour suppressor gene. Methylation of the CDH1 promoter is a part of EMT. E-cadherin forms adherens junctions between adjacent epithelial cells and mediates intercellular interactions and is thought to regulate gap junctions. The molecule is thought to be a premise for gap junctional intercellular communication (GJIC), which is important for cell growth, differentiation of tissues and homeostasis. Studies show that GJIC was inhibited by tumour promoting agents and alterations in GJIC may be involved in carcinogenesis. GJIC is dependent on cell-cell adhesion, and E-cadherin maintains intercellular adherence junctions in epithelial cells. Loss of E-cadherin expression is associated with a decrease in intercellular adhesion. Hence, E-cadherin helps assemble cells and maintain quiescence, and increased expression is therefore associated as an antagonist of cell invasion and metastasis (De Craene and Berx, 2013; Hanahan and Weinberg, 2011; Jinn et al., 1998). Alterations in E-cadherin are the most widely observed modifications in cell-to-environment interactions in cancer. E-cadherin function is lost in a majority of epithelial cancers. This can be due to mutational inactivation, repression of transcription by promoter DNA hypermethylation or proteolysis of the extracellular cadherin domain (Hanahan and Weinberg, 2000). Smokers also have low E-cadherin levels (Nagathihalli et al., 2012).

The neural cadherin (N-cadherin), encoded by the *CDH2* (cadherin-2) gene, is found primarily in neural tissue and fibroblasts. A less stable and more dynamic adhesion of cells characterises the linkages mediated by N-cadherin. N-cadherin undergoes a switch in expression and it is upregulated in invasive tumour cell lines. The protein is a potent inducer of invasion and metastasis, and cells expressing N-cadherin show a more efficient migration. Changes in cadherin expression can be referred to as the “cadherin switch”, and is a crucial event in tumour progression. By switching from E-cadherin to N-cadherin a signalling program is activated that promotes invasive, motility and survival capacities of tumour cells. Collaboration between tumour cells and the microenvironment is also important for tumour progression, and the cadherin switch encourages this. In breast tumour cells it has been observed that N-cadherin facilitates adhesion of cells to endothelial monolayers in blood vessels (Gravdal et al., 2007; Hazan et al., 2000; Hazan et al., 2004).

1.3.1 Forkhead-box (FOX) family proteins

FOX proteins are a family of transcription factors involved in regulation of cell growth, differentiation, embryogenesis and longevity. The FOX proteins bind DNA and are involved in transcriptional regulation and DNA repair. Mutations of FOX proteins are often associated with human diseases, due to its involvement in a variety of processes. They are involved in carcinogenesis as oncogenes or tumour suppressor genes. FOXA1 and FOXA2 proteins are expressed in lungs. Studies have shown that *FOXA1* gene may be amplified in lung cancer, and in some cases of lung cancer this might lead to overexpression of the gene. This may indicate an oncogenic role of this gene in carcinogenesis. FOXA1 binds within highly condensed chromatin regions, mainly in enhancer regions, and activates FOXA1-dependent enhancers, which is accompanied by demethylation of DNA (Katoh et al., 2013; Lin et al., 2002; Sérandour et al., 2011; Song et al., 2010; Wan et al., 2005).

A study indicates that FOXA2 has a positive correlation with epithelial phenotype and a negative correlation with mesenchymal phenotype, due to the fact that FOXA2 protein levels correlated with epithelial cell markers (Tang et al., 2011). Transforming-growth factor β (TGF-β) has been shown to induce EMT via autocrine or paracrine mechanisms and is one of the most important regulators of EMT. It also increases lung cancer cells ability for migration. Studies indicate that FOXA2 is a key target for TGF-β in regulation of EMT in human lung cancer cells. By overexpressing FOXA2, TGF-β-induced EMT was suppressed. FOXA2 might have a role as a tumour suppressor by repressing slug transcription through a conserved binding site in the slug promoter (figure 1.6). Slug is a transcription factor and a negative regulator of E-cadherin expression. Also, there is evidence of hypermethylation of FOXA2 promoter in NSCLC and epigenetic mechanisms are likely to cause the loss of *FOXA2* expression in lung cancer (Basseres et al., 2012; Tang et al., 2011).

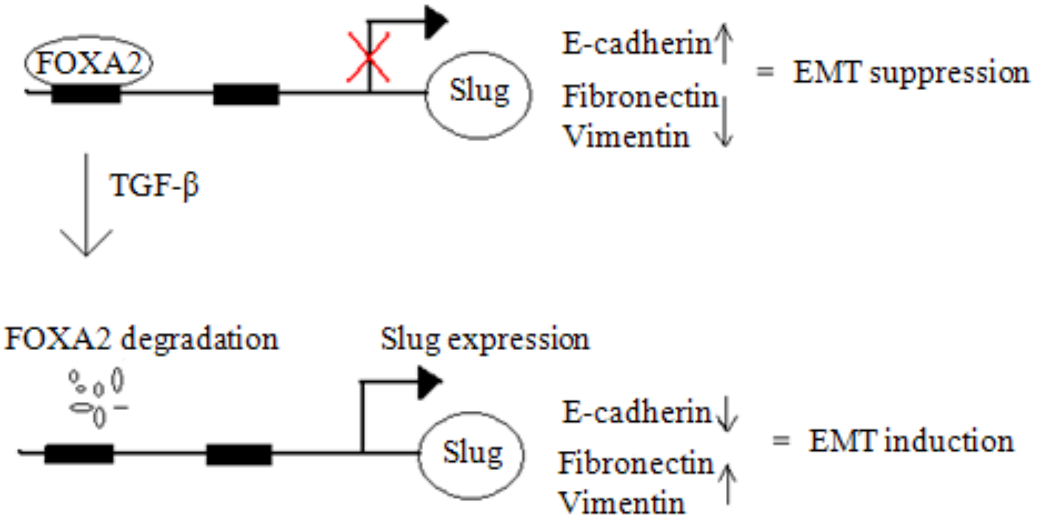

Figure 1.6: FOXA2 suppresses slug transcription, which again lead to EMT suppression. By treating A549 cells with TGF-β the FOXA2 protein was degraded, slug was actively transcribed and EMT was induced. Modified from Tang et al. (2011).

Studies have indicated that the downregulation of *FOXA1* and *FOXA2* genes is an essential step of EMT in progression of pancreatic cancer (Song et al., 2010).

1.4 Cell migration

Cell migration is an important mechanism for both unicellular and multicellular organisms (Glaß et al., 2012, Liang et al., 2007). Wound healing, immune responses and tissue formation during development all depend on movement of cells. During wound healing cells as neutrophils, macrophages and fibroblasts move to wound site and kill microorganisms and remodel damaged tissue (Ananthakrishnan and Ehrlicher, 2007; Glaß et al., 2012; Liang et al., 2007). Cell migration is a multistep process involved in cancer progression, arthritis and atherosclerosis (Ridley et al., 2003). Tumour cells have retained the same basic migration machinery for cell migration as normal, non-neoplastic cells. This includes integrins, matrix-degrading enzymes, CAM and cell-cell communication (Friedl and Wolf, 2003).

Mesenchymal cells have the ability to migrate, and they do so in a process of multiple steps, involving cell polarisation, protrusion extension, cell elongation and contraction. It is a continuous cycle of interdependent steps, which allows the cells to translocate. First, the cell is polarised and a pseudopod (temporarily, cylindrical finger-like protrusion) is formed at the leading edge of the cell, which becomes attached to the extracellular matrix for stabilisation. Integrins support the adhesion to the extracellular matrix. This is followed by contraction of

regions of the leading edge or the whole cell body. A traction force is generated that leads to forward gliding of the cell body (figure 1.7). Disassembly of adhesion is observed at the leading edge where it accompanies the formation of new protrusions, but also at the rear where it promotes the retraction of the cell.

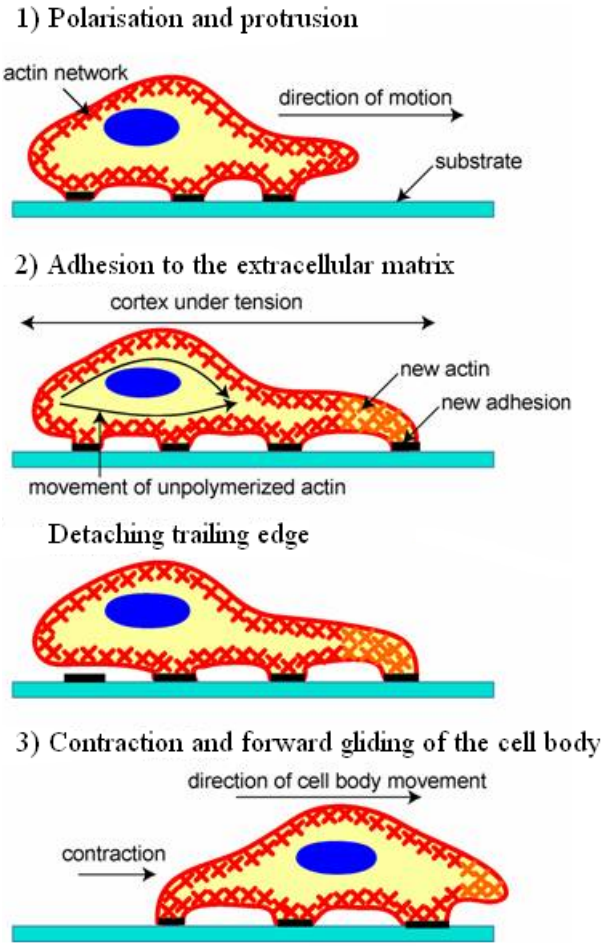

Figure 1.7: Schematic presentation of the process of cell migration. Modified from Ananthakrishnan and Ehrlicher (2007).

The cell protrusions vary in morphology and dynamics, but they all contain actin and a various set of structural and signalling proteins. Dynamic rearrangements of the actin cytoskeleton form protrusive structures and generate intracellular forces needed for cell translocation. Myosin motors pull the cell forward by a continuous repeated process of binding, power stroke and unbinding of actin filaments. This leads to generation of a contractile force known as acto-myosin contractile force and completion of the migration cycle (Ananthakrishnan and Ehrlicher, 2007; Debeir et al., 2008; Friedl and Wolf, 2003; Ridley et al., 2003; Yamaguchi et al., 2005). Migration can be either random or directed by external influences, as chemicals in the environment (Glaß et al., 2012).

Cancer kills patients mainly because of migratory properties of its cells. This is the process of metastasis, where cell migration is an important underlying mechanism (Debeir et al., 2008; Glaß et al., 2012; Yamaguchi et al., 2005). It is valuable to understand the essential mechanisms as it will accelerate the process towards effective therapeutic approaches for treatment (Ridley et al., 2003). Migration and invasion into tissues and intravasation into blood and lymphatic vessels are necessary for metastasis of cancer cells. These cells acquire a phenotype associated with increased expression of several genes involved in cell motility, as vimentin and epidermal growth factor receptor (Wang et al., 2005; Yamaguchi et al., 2005).

1.5 Epigenetic mechanisms

Epigenetic changes are heritable, reversible changes in expression of genes without leading to alterations in the DNA sequence itself. Processes involved in epigenetic modifications are DNA methylation, histone modification, nucleosome remodelling, and gene regulation by micro-RNAs (miRNAs). These modifications regulate accessibility and compactness of chromatin, which is the organisation of genetic information in the form of DNA within a cell. This again will influence activation or silencing of genes, which will create an "epigenetic landscape" that regulates how the mammalian genome reveals itself in different cell types, developmental stages and diseases. Epigenetic patterns serves as a guardian of cellular identity and determines for example cell fate and gene activity (Esteller, 2007; Kanwal and Gupta, 2010; Sharma et al., 2010).

DNA methylation is a post-replication modification, which is almost exclusively found on cytosines in the dinucleotide sequence CpG. In the genome there are CpG islands, which are regions rich in CpG dinucleotides preferentially located at the 5'end of genes. These regions span the 5' end region (promoter/enhancer, untranslated region and exon 1) of many genes. Approximately 10 % of the CpG dinucleotide methylation sites in the human genome are within gene promoters, where interaction with other chromatin factors facilitates gene silencing when cytosine is methylated. In normal cells, the 5' end region is often unmethylated. The modification is carried out by DNA methyltransferases (DNMTs). There are three main DNMTs: DNMT1, DNMT3a and DNMT3b. DNMT1 is the major maintenance enzyme and sustains existing methylation patterns. The enzyme does so by adding methyl groups to hemi-methylated CpG sites in DNA after replication. DNMT3a and DNMT3b are

de novo methyltransferases, and they target unmethylated CpG sites for initiation of methylation. They are highly expressed during embryogenesis, and minimally expressed in adult tissues. Methylation of cytosines is an essential mechanism during mammalian embryogenesis and development. Genome-wide de novo methylation is known to play a major role in establishing embryonic methylation pattern during early development. Studies show that early embryonic lethality occurs if DNMT3a and DNMT3b are inactivated. During tissue differentiation, de novo methylation also plays an important role in organising or compartmentalizing the genome to establish tissue-specific gene expression patterns (Aran et al., 2011; Kanwal and Gupta, 2010; Okano et al., 1999; Sharma et al., 2010; Tost and Gut, 2007).

CpG island methylation is also associated with X-chromosome inactivation during development, which is a mechanism to achieve dosage compensation of X-linked genes. Due to the fact that females have two X chromosomes compared to males that only have one X chromosome, this needs to be equalized. Methylation of the inactive X functions as a maintenance mechanism for X inactivation, where the promoter becomes methylated during development and leads to long-term transcriptional silencing (Avner and Heard, 2001; Okano et al., 1999; Sharma et al., 2010).

Histones comprise the nucleosome core, and they can undergo post-transcriptional modifications as methylation, acetylation and phosphorylation that may change the accessibility of chromatin or recruit other effector proteins. This can lead to either repression or activation of gene activity. Histone deacetylation may mediate downregulation of E-cadherin in NSCLC. Nucleosome remodelling may also regulate gene activity through changes in the chromatin structure, by altering accessibility of regulatory DNA sequences to transcription factors. Non-coding miRNAs also regulate gene activity, through posttranscriptional silencing. miRNAs consists of approximately 22 nucleotides. They base pair with 3'untranslated regions (UTR) of target messenger RNA (mRNA) and induce its degradation or inhibition of translation (Nagathihalli et al., 2012; Sharma et al., 2010). Any miRNA can bind to a broad spectrum of different mRNAs, as there are multiple conserved sites for a given miRNA in the same UTR of a gene. Hence, the miRNAs possess enormous and complex regulatory potential. In addition, the base pairing between mRNA and miRNA is localised to the 5'-proximal half of the miRNA (Ambros, 2004).

Changes in epigenetic modifications are common in many human diseases. Aberrant methylation of the promoter may lead to altered gene expression and this has been associated with cancer (Colella et al., 2003). Hypermethylation of tumour suppressor genes may lead to gene silencing and is a key feature of the pathogenesis of cancer. Oncogenes may be activated through hypomethylation, and this process may also increase genetic instability (Esteller, 2007; Sharma et al., 2010).

Epigenetic changes occur early during carcinogenesis and often underlie malignancy (Tost and Gut, 2007). In humans, methylation of cytosines within CpG dinucleotides is the most widely studied epigenetic modification, and it is considered to be a common hallmark of all types of human cancer (Esteller, 2007; van Eijk et al., 2012).

Cigarette smoke may trigger methylation of CpG islands in promoters and cause inhibition of gene expression, which has been demonstrated for many genes, highlighting the fact that environmental factors may alter cellular phenotypes through induction of epigenetic modifications (Tekpli et al., 2012; Word et al., 2013; Xu et al., 2007). The predominant model states that increased DNA methylation cause a decrease in gene expression, particularly in CpG islands and promoter regions. Nevertheless, recent studies indicate that relationship between genetic variation, DNA methylation and gene expression is much more complex. Positive correlations between DNA methylation in the gene body (transcribed portion of genes) and gene expression have been identified in *Arabidopsis thaliana* and in a variety of human cell lines. Gene bodies have been shown to be hypermethylated compared with other fractions of the genome and it is suggested that gene-body methylation may play yet unknown functions in multicellular organisms. Functions as for example protecting the gene body through methylation, regulate transcription elongation rates or control alternative promoter usage are suggested to depend on gene-body methylation (Aran et al., 2011; Jjingo et al., 2012; van Eijk et al., 2012).

1.6 Immortal human bronchial epithelial cell lines (HBECs)

Normal bronchial epithelial cells have a finite replicative potential. Transfecting specific genes into them has generated immortal HBECs that are valuable tools in studies of lung pathogenesis. In this thesis, HBECs that have been immortalized by insertion of cyclin-dependent kinase 4 (Cdk-4) and human telomerase reverse transcriptase (hTERT) were used

(Ramirez et al., 2004). Cdks are heterodimeric complexes composed of both catalytic (kinase) and regulatory (cyclin) subunits. They are divided into two groups depending on their roles in cell cycle progression or regulation of transcription. Cdk-4 is a member of the first group and is a core component of the cell cycle machinery. It phosphorylates retinoblastoma protein (Rb) and further facilitates G_1 to S (synthesis) transition in the cell cycle. In a hypophosphorylated state, Rb prevents cells to progress into S phase. Cyclin-dependent kinase inhibitor 2A (p16) is also a regulator of G_1 progression, and belongs to INK4 family of cell cycle inhibitors. They act as inhibitors of Cdk-4 and 6. As cells age, p16 accumulates and associates with Cdk-4 and 6 to induce release of D-type cyclins, and then further arrest cells in G_1. By overexpression of Cdk-4, this arrest is prevented and cells continue in the cell cycle (Ramirez et al., 2004; Shapiro, 2006).

Telomerase is an enzyme that adds DNA sequence repetitions at the ends of chromosomes; the telomeres, and by this prevents progressive shortening of the ends. The telomerase hypothesis suggests that this is the mitotic clock, which regulates senescence in somatic cells. By expression of hTERT, telomere-dependent senescence can be bypassed and in combination with overexpression of Cdk-4 continuously replicating, immortal cell lines is generated (Ramirez et al., 2004).

1.6.1 *In vitro* transformation model of HBECs

An *in vitro* premalignant transformation model had been established in our lab, where HBECs (table 1.2) were exposed to tobacco smoke carcinogens (B[*a*]P, CSC or MNU) for up to 15 weeks. Control cells were HBECs exposed to DMSO (table 1.3). The various doses of carcinogens were decided by toxicity tests of the cell lines, where the chosen doses should be as high as possible without causing too much toxicity (80 % or more of the cells should survive the dose given).

Table 1.2: Characteristics of the donor patients of the HBECs used in this thesis. NSCLC denotes non-small cell lung cancer

Cell line	Age	Gender	Diagnosis	Smoking history
HBEC-2KT	68	M	NSCLC	Smoker
HBEC-3KT	65	F	No cancer	Smoker
HBEC-12KT	55	F	NSCLC	Previous smoker

Table 1.3: HBECs used in this thesis and the treatment they received.

Cell lines	Treatment
HBEC-2KT control cells	HBEC-2KT cells exposed to DMSO
HBEC-2KT-CSC.L	HBEC-2KT cells exposed to a low dose of CSC (1 μg/ml)
HBEC-2KT-CSC.H	HBEC-2KT cells exposed to a high dose of CSC (3 μg/ml)
HBEC-12KT control cells	HBEC-12KT cells exposed to DMSO
HBEC-12KT-CSC.L-A	HBEC-12KT cells exposed to a low dose of CSC (1 μg/ml), isolated from colony A
HBEC-12KT-CSC.L-B	HBEC-12KT cells exposed to a low dose of CSC (1 μg/ml), isolated from colony B
HBEC-12KT-CSC.H	HBEC-12KT cells exposed to a high dose of CSC (3 μg/ml)
HBEC-12KT-B[*a*]P.L	HBEC-12KT cells exposed to a low dose of B[*a*]P (0.33 μM)
HBEC-12KT-B[*a*]P.H	HBEC-12KT cells exposed to a high dose of B[*a*]P (1 μM)
HBEC-12KT-MNU	HBEC-12KT cells exposed to MNU (0.5 μM)

During the transformation assay, cells were exposed to the treatments weekly; a control (DMSO) was also included. After 9, 12 and 15 weeks colony formation in soft agar was tested for the cell lines exposed to carcinogens. Transformation of cells leads to changes in phenotype, as for example anchorage independency. This capacity gives the cells abilities to form colonies in soft agar and these cells were defined as transformed. For the establishment of transformed cell lines, colonies from soft agar after 12 weeks exposure were chosen. One colony was chosen for all the cell lines, except for HBEC-12KT-CSC.L where two colonies were isolated (A and B). The colonies were isolated and seeded in soft agar a second time to ensure persistency of anchorage independent growth. Colonies were also formed after second time in soft agar. Four colonies were isolated from each treatment (2A, 2B, 2C and 2D) and seeded in single dishes to obtain clonal transformed cell lines (all cells originated from the same colony) (Sjøberg, 2012). The transformation model is depicted in figure 1.8, and the naming of the cells lines are explained in figure 1.9.

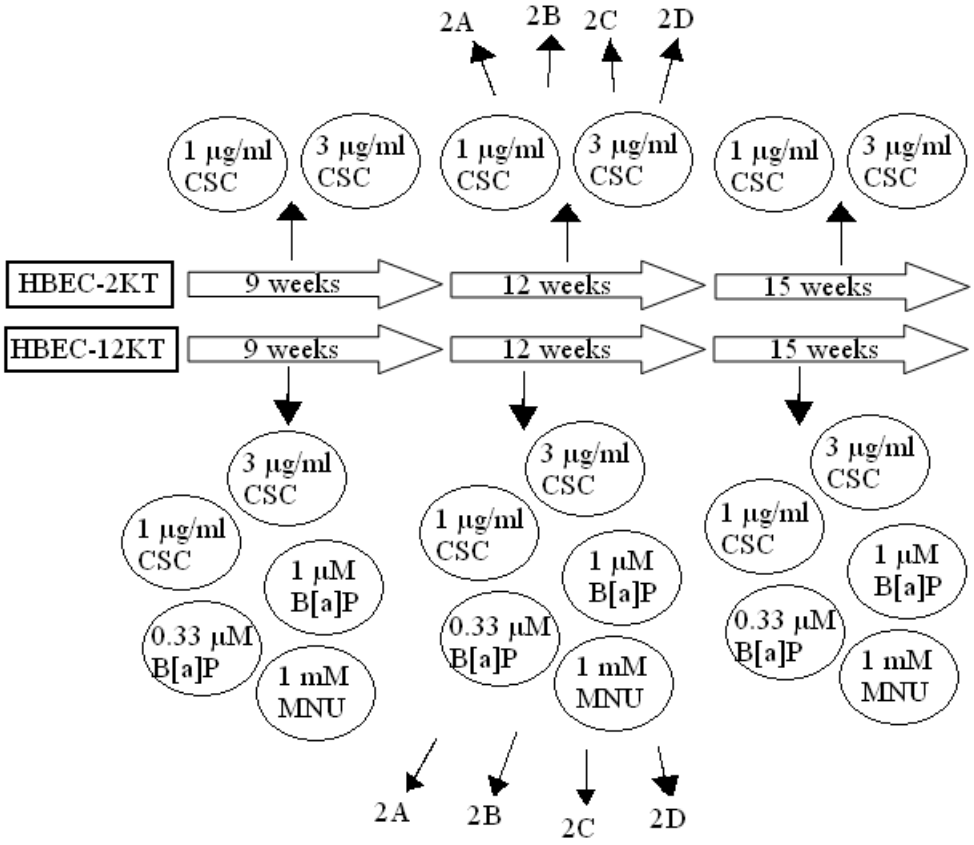

Figure 1.8: Colony formation of transformed HBEC-2KT and HBEC-12KT in soft agar after 9, 12 and 15 weeks. After 12 weeks, colonies were isolated and seeded into soft agar a second time to ensure anchorage independent growth. From second time in soft agar, four colonies from each treatment were isolated.

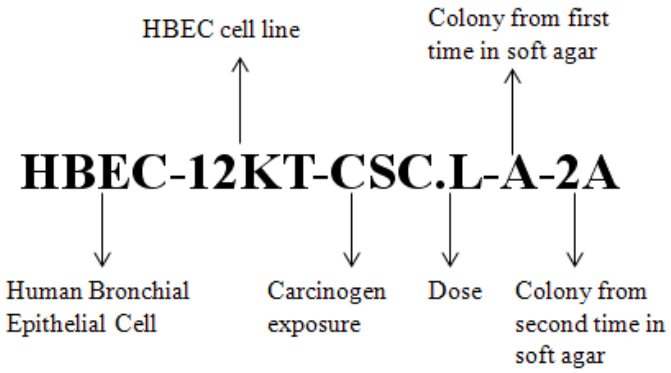

Figure 1.9: Naming of the cell lines used during this thesis.

When transformed, these cell lines were suitable models for further investigations of molecular changes involved in the process of transformation. Earlier studies indicate that transformation is associated with changes in cellular morphology, from an epithelial to a mesenchymal-like shape, and also changes in migration capability of the cells, which indicate activation of EMT (Sjøberg, 2012). Gene expression analyses (figure 1.10) showed reduced

expression of *FOXA1*, *FOXA2* and *CDH1* (E-cadherin) genes in HBEC-2KT and HBEC-12KT transformed cells compared to control cells (DMSO). *CDH2* (N-cadherin) gene had increased expression in all of the transformed cell lines of HBEC-2KT and HBEC-12KT compared to control cells (DMSO). These changes in the transformed cell lines are consistent with EMT. Audun Bersaas (staff engineer at STAMI) performed the gene expression analyses.

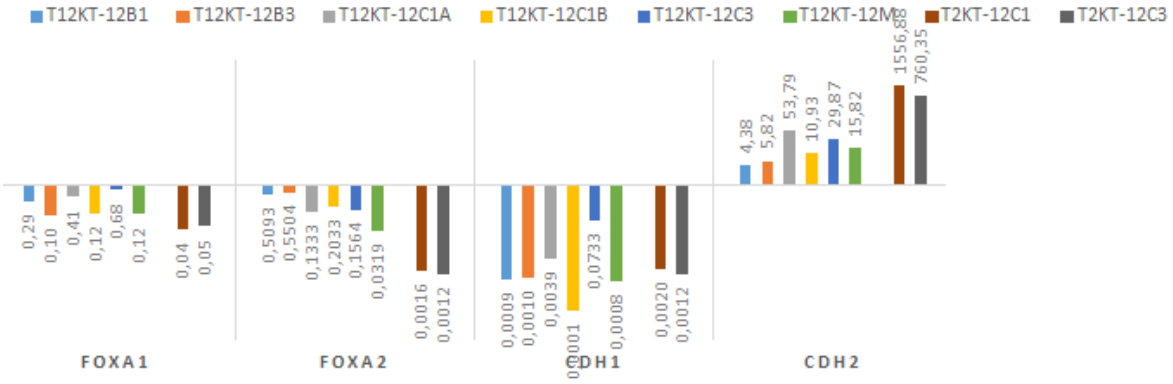

Figure 1.10: Fold change of gene expression of *FOXA1*, *FOXA2*, *CDH1* (E-cadherin) and *CDH2* (N-cadherin) genes in *in vitro* transformed HBEC-2KT and HBEC-12KT. Numbers (log-scale) denotes how much gene expression has decreased/increased compared to control cells (DMSO).

1.7 Aim of the study

The aim of this study was to investigate mechanisms involved in development of lung cancer. There was a special focus on epigenetic changes, which have proved to be important during the later years considering initiation and progression of cancer. HBECs were exposed to B[*a*]P, CSC and MNU in an already developed *in vitro* transformation model.

The first aim was to investigate how transformation affected cell migration, and relate this to previous gene expression analyses in EMT-related genes as *CDH1* and *CDH2*, and also *FOXA1* and *FOXA2* in transformed compared to non-transformed cells.

The second aim was to investigate whether downregulation of *FOXA1* and *FOXA2* gene expression in transformed versus non-transformed cell lines could be explained by DNA methylation.

2 Materials and methods

Various methods used during this thesis to study characteristics of transformed and non-transformed HBECs are presented in figure 2.1 below. The transformed cell lines used have been exposed to B[*a*]P, CSC and MNU for 12 weeks. Control cells have been exposed to DMSO for 7 weeks. Untreated HBECs have been included in the cell migration analyses.

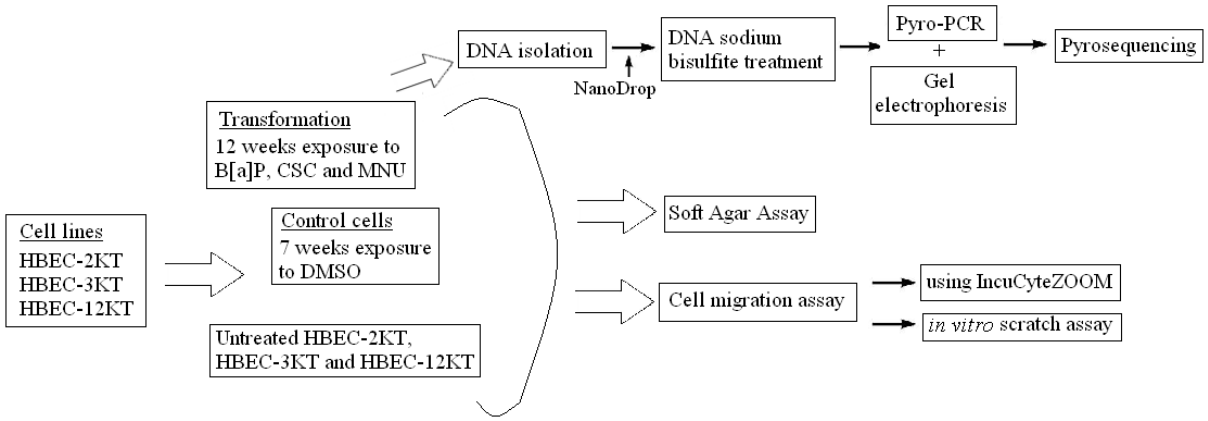

Figure 2.1: Overview of methods used.

2.1 General cell work

All cell work was performed with ventilation in OAS LAF benches under sterile conditions, with the use of Bunsen burners and plastic pipettes. Information regarding the materials used during this thesis can be found in appendix A. General cell culture work as thawing of cells, passaging cells and freezing of cells is described in appendix B. The cells were grown on collagen-coated dishes, either 96- and 6-well plates or 100 mm plates. Information regarding collagen coating is also described in appendix B. When the cells had reached about 80 % confluence they were passaged.

2.1.1 Cell lines and cell culture

Cells were taken from the liquid nitrogen cell bank at STAMI and cultured in an incubator (37 °C, 5% CO_2 atmosphere) until further experiments. It was always used the lowest possible passage number of the cells. Untreated HBEC cell lines were grown in LHC-9 medium, supplemented with penicillin and streptomycin (1 %). Transformed HBEC cell lines and control cells (DMSO) were grown in LHC-9 medium, supplemented with penicillin and

streptomycin (1 %) and foetal bovine serum (FBS) (10 %). Fresh medium was given approximately twice a week.

2.1.2 Seeding of cells for various experiments

This is a general description of the procedure. Volumes of different solutions and reagents varied according to the experiment performed, this is an example when using 100 mm petri dishes.

1. Starting material was always approximately 80 % confluent cell cultures.
2. The media over the cells was removed, and the dishes were washed twice with phosphate buffered saline (PBS) (10 ml).
3. Trypsin solution (1 ml) was added to the dishes.
4. The cells were incubated (37 °C) until detachment from the petri dish. This was monitored in the light microscope.
5. Medium (5 ml) was added and the cell suspensions were gently washed up and down a 10 ml pipette for separation of cells and washing of petri dish.
6. The cell suspension was transferred to a centrifuge tube and centrifuged (1000 rpm, 4 minutes).
7. The supernatant was discarded and the pellet was re-suspended in growth medium (5 ml).
8. Cell suspension (10 μl) was mixed with trypan blue stain (10 μl) in an eppendorf tube, and 10 μl of this mix was added to a cell counting chamber slide.
9. Cells were counted using Countess Automated Cell Counter.
10. The cells were then added growth medium to obtain the appropriate density of the cells.
11. Cells were seeded on appropriate plates.
12. Plates were incubated (37 °C) for further use.

2.2 Soft agar assay

Growth in soft agar is an indication of cell transformation (anchorage independent growth). Tumour cell line A549 was used as a positive control in this assay. The soft agar assay is based on a top- and base-layer, where the base-layer (0.7 % agar) is made first. When the base-layer has congealed, a top-layer is added. The top-layer is made of a lower agar

concentration (0.35 %) where a specific number of cells are added. Two parallels were made for each cell line. To make the soft agar, the 3 % agar solution was kept in a water bath at 50 ℃ and when cells were added to the lower agar concentration the solutions were kept in a water bath at 40 ℃. It was important to work rapid and efficiently, due to the rapid solidification of agar solutions and in order to keep the cell at temperatures above 37 ℃ for as short time as possible.

1. 1 g Difco Agar Noble was mixed with 33.3 ml PBS to obtain a stock agar solution of 3 %.
2. The agar solution was autoclaved on the program for liquids.
3. Agar stock solution (3 %) was mixed with growth medium to obtain an concentration of 0.7 %, which formed the base-layer.
4. 0.7 % agar solution (1.5 ml) was added to each well on 6-well plates and this was left to gel at 4 ℃ (30 minutes).
5. Cells were trypsinised and counted. The cell suspension was diluted in medium to obtain $4x10^4$ cells/ml.
6. The diluted cell suspension was mixed with an equal volume of the 0.7 % agar solution to obtain a top-layer of 0.35 % agar. This layer would then have $2x10^4$ cells/ml.
7. The top-layer (1 ml) was added over the base-layer.
8. The plates were left to gel at 4 ℃ (30 minutes).
9. The plates were then incubated at 37 ℃ for 3-4 weeks to evaluate appearance of colonies.
10. After two days, 500 μl fresh medium was added, and this was repeated once a week.

2.2.1 Visualisation of colonies by crystal violet staining

Crystal violet was used to visualise colonies in soft agar. When dissolved in water, crystal violet has a blue violet colour. The substance colours cell walls, and makes the cells easy to visualise in a light microscope.

1. A crystal violet solution (0.05 %) was diluted 10x with autoclaved water to make a solution of 0.005 %.
2. The 0.005 % crystal violet solution was added (500 μl) to the soft agar plates, which were then incubated for 30 minutes (37 ℃).

3. Colonies were visualised in the light microscope and images were taken.

2.3 DNA Isolation

DNA was isolated using Wizard® Genomic DNA Purification Kit (Promega). This kit is designed for isolation of genomic DNA from various tissues and cells, one of them being cell cultures. The purification procedure includes four steps. The first step is lysis of cells and nuclei, followed by an RNase digestion step. The third step is salt precipitation, where cellular proteins are precipitated and leave high molecular weight genomic DNA in solution. The last step includes concentration and desalting of DNA by isopropanol precipitation (Wizard® Genomic DNA Purification Kit, Promega, 2010).

1. Tissue culture cells grown on 100 mm dishes were trypsinised and counted. The cell suspension was diluted in medium to obtain a concentration of $3x10^6$ cells.
2. The solution was centrifuged at 16 000 g for 10 seconds, or 1000 rpm for 4 minutes if the volume was above 1.5 ml, at room temperature.
3. The supernatant was removed and the pellet was washed with PBS (200 μl)
4. The solution was centrifuged as above.
5. The supernatant was removed until there was 10-15 μl left in the tube.
6. Nuclei Lysis Solution (600 μl) was added to lyse the cells. Lysate was transferred to eppendorf tubes if volume was above 1.5 ml.
7. RNase Solution (3 μl) was added to the nuclear lysate and the tube was mixed by inversion 2-5 times.
8. The mixture was incubated at 37 ℃ for 30 minutes, and left at room temperature for 5 minutes to cool down.
9. Protein Precipitation Solution (200 μl) was added to the mixture, which was then vortexed for 20 seconds. The sample was left on ice for 5 minutes.
10. The tube was centrifuged at 16 000 g for 10 minutes at 4 ℃.
11. The supernatant was transferred to an eppendorf tube with 600 μl room tempered isopropanol.
12. The solution was inverted until DNA formed a visible mass.
13. The tube was centrifuged at 16 000 g for 1 minute at room temperature.
14. The supernatant was discarded.
15. Ethanol (70 %, room tempered) was added and the tube was inverted to wash DNA.

16. The tube was centrifuged at 16 000 g for 1 minute at room temperature.
17. Ethanol was carefully removed from the tube containing DNA.
18. The tube was inverted on a paper, and the pellet was left to dry for 10-20 minutes.
19. DNA Rehydration Solution (50 μl) was added.
20. The tube was incubated at 65 ℃ for an hour, and the solution was gently mixed every 15 minutes.

DNA was stored at 4 ℃, until further applications as PCR amplification, bisulfite treatment and pyrosequencing.

2.3.1 Quality and quantity of DNA

NanoDrop spectrophotometer was used to assess the quality and quantity of DNA. NanoDrop utilizes a retention technology. A beam of light is passed through a droplet of sample and measures the intensity of light that is transmitted through it (NanoDrop 8000 Spectrophotometer, V2.2 User Manual, Thermo Scientific). Absorption maximum of nucleic acids is 260 nm. The ratio OD_{260}/OD_{280} can be calculated to assess purity of the solution. For DNA a ratio of 1.8 indicates that it is pure. A low ratio can be due to contamination by proteins or phenols. The ratio 260/230 is a secondary measure of nucleic acid purity. 260/230 is usually in the range between 1.8 and 2.2, and if lower this can be an indication of the presence of co-purified contaminants (Barbas et al., 2007).

2.4 Agarose gel electrophoresis

Agarose gel electrophoresis separates DNA fragments of different size in an electric field. Smaller fragments migrate faster than larger ones (Reece, 2004). In this thesis, agarose gel electrophoresis was used to test if PCR products had the correct length and if there was only one product. It was also used to check quality and quantity of PCR products before carrying out the pyrosequencing.

A DNA standard ladder was run alongside the samples during gel electrophoresis to estimate the size of unknown DNA samples and identify the band of interest. Different ladders were used, as for example 100 bp DNA ladder and ϕX174 DNA/HaeIII marker, which was used in this thesis.

1. 50X TAE buffer was diluted to 1X TAE buffer:
    a. 8 ml 50X TAE + 392 ml dH_2O to make a small gel.
    b. 24 ml 50X TAE + 1176 ml dH_2O to make a large gel.
2. Agarose powder was weighed:
    a. 2.4 g SeaKem GTG Agarose in 120 ml 1xTAE buffer to make a 2 % gel for testing of PCR products for pyrosequencing.
    b. 1.5 g NuSieve 3-1 Agarose in 50 ml 1xTAE buffer to make a 3 % gel for genomic DNA testing.
3. The mixture was heated in a microwave to make a clear solution.
4. GelRed (7 µl for large and 2.5 µl for small gels) was added for staining of DNA.
5. The solution was poured into a gel former containing a comb to form wells and left to set.
6. The comb was removed, the gel was placed in aqueous buffer and DNA was loaded in the wells:
    a. PCR products for pyrosequencing: 1 µl sample. PCR products for pyrosequencing contained a CoralLoad Concentrate, so no loading buffer was necessary.
    b. Genomic DNA: 3 µl sample + 1 µl loading buffer.
7. Large gels were run at 120 V and small gels at 100 V, both for about 1.5 hours.
8. The gels were examined under UV-light to see the localisation of DNA bands.

2.5 Cell migration assay

Two methods were used to study cell migration. Both assays are based on observations that when a scratch is made in a cell monolayer, the cells at the edge of the newly formed opening will move towards it and close the wound (Glaß et al., 2012; Liang et al., 2007; Rodriguez et al., 2005). Using IncuCyte ZOOM, from Essen Biosciences, the method of studying cell migration was mainly automated. The other method used was the manual *in vitro* scratch assay.

2.5.1 IncuCyte ZOOM

The migration assay from Essen BioSciences can be used to assess the 2D migration potential of various cells. The IncuCyte ZOOM instrument was only in the house for a demo for three

weeks. A 96-well WoundMaker was used to create a cell-free zone in a monolayer, without disrupting the coating of the wells. ImageLock plates (Essen Biosciences) were used for this purpose. These plates had markers on the bottom of the plate that serve as a reference point for accurate picturing. After wounding fresh media was added to the wells and the 96-well plate was put in the IncuCyte ZOOM instrument to be monitored for a chosen time course. Usually for 24 hours. The instrument can automatically acquire images at a chosen interval during the experiment. When the assay was completed, images were analysed using IncuCyte's integrated software, which provides ways to quantify both migration and invasion. The whole process is outlined in figure 2.2.

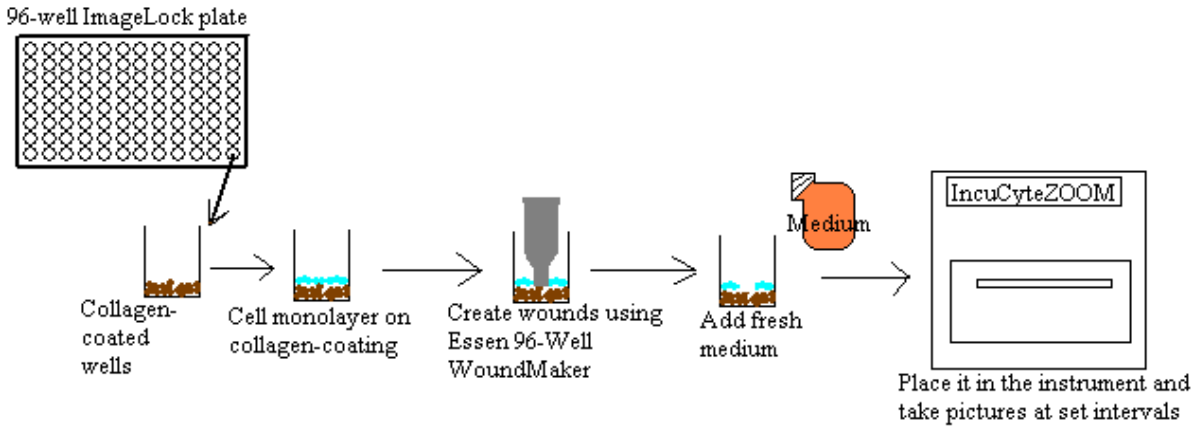

Figure 2.2: The process of making wounds using the Essen 96-Well WoundMaker for migration assay with IncuCyte ZOOM. Modified from Roddy et al. (Roddy et al., s.a.).

1. 25 000 cells/well were plated on 96-Well ImageLock plates, which were left in the incubator to form a confluent monolayer (37 ℃, 1 day).
2. Wounds were made using the 96-pin WoundMaker.
3. Plates were washed twice with PBS (2*200 µl/well).
4. Fresh media (100 µl) was added to the wells and the plate was placed in the IncuCyte ZOOM instrument inside the incubator.
5. The plates were allowed to equilibrate within the instrument for minimum 15 minutes before the first scan. The software was set to take images every hour for 24 hours with "Scratch Wound" as the experimental type.

Analysis of results

For processing of the data an image collection was created using a representative number (three to five) of images. A Processing Definition was used to analyse the data, via a

Processing Software Package in the instrument. The data from the migration assay was analysed using the metric Relative Wound Density (RWD), which is an algorithm that is a part of the IncuCyte software tool. It is robust across multiple cell lines. This algorithm measures cell density in the wound area relative to the cell density outside the wound area at every set time point. At t=0, the RWD is set to be zero. When the cell density inside the wound is the same as the cell density outside the initial wound the RWD is 100 % (Roddy et al., s.a.). Graphs were made using the software.

2.5.2 *In vitro* scratch assay

The manual *in vitro* scratch assay involved creating a scratch in the cell monolayer using a pipette tip, capturing images at regular intervals during the cell migration process and analysis of images to quantify percentage methylation.

CellProfiler was used for analysis of the results. Different modules in the software process the cell images. The modules are placed in a sequential order to create a "pipeline", typically starting with image processing, followed by object identification and at last, measurements. The modules are mostly automatic, but some of them are interactive, where the user can optimize for particular cell types and experimental conditions. The different modules can be mixed and matched for a specific usage and each of the modules settings can be changed according to the purpose (Carpenter et al., 2006).

1. $5x10^5$ cells/well were plated on 6-well plates, which were left to form a confluent monolayer (37 ℃, 3-4 days).
2. Scratches were made in the cell monolayer with a yellow pipette tip, as shown in figure 2.3. The plates were marked on the bottom side according to figure 2.4 to ensure that the images were taken on the same place. The cells were washed once with PBS and fresh medium (2 ml) was added.

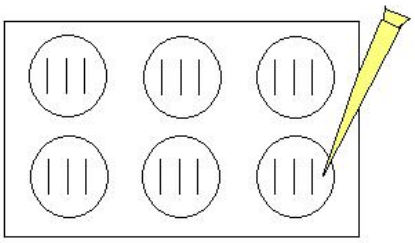

Figure 2.3: Schematic presentation of scratch making with a pipette tip in 6-well plates for the cell migration assay.

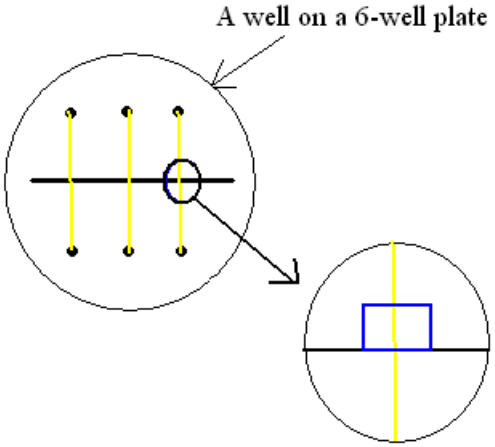

Figure 2.4: How the plates were marked on the bottom side to ensure that images were taken at the same spot. Black lines denote the marking, yellow the scratching and a blue square where the images were taken.

3. An initial light microscope image of each scratch wound was taken (0 hours).
4. Plates were placed in an incubator.
5. Another light microscope image was taken after 12 hours.
6. The images were analysed using CellProfiler.

Analysis of results

Light microscope images of scratch wounds were analysed using CellProfiler. An example pipeline for wound healing at the CellProfiler web page was used as basis. By testing different combinations of the different algorithms we developed a pipeline suited for this study. Appendix C presents the development of the pipeline. Calculation of percentage migration was done using the formula:

$$\frac{U_0 - U_{12}}{U_0} * 100$$

U_0 = total area - occupied area at 0 hours

U_{12} = total area - occupied area after 12 hours

2.6 DNA sodium bisulfite treatment

Sodium bisulfite treatment of DNA is used to convert unmethylated cytosines to uracil through the process of deamination. Methylated cytosines will remain unchanged, and this allows cytosine to be distinguished from 5-methylcytosine. Methylation status of DNA is represented by a ratio of cytosine and thymine, as thymine will be incorporated in place of uracil during PCR (Dupont et al., 2004; Yang et al., 2004).

1. The following solutions were prepared freshly:
    a. 6.07 g sodium metabisulfite in 12 ml dH_2O
    b. 110 mg hydroquinone in 5 ml dH_2O
2. Solutions were mixed on an agitator until dissolved.
3. A 6.3 M solution of sodium hydroxide (NaOH) was prepared freshly:
    1.26 g NaOH in 5 ml dH_2O.
4. The pH of sodium metabisulfite was adjusted to 5 by adding 750 µl NaOH.
5. Hydroquinone (450 µl) was added to the sodium metabisulfite, and the solution was heated to 55 °C.
6. DNA (1 µg in 20 µl TE-buffer) was spun down (30 sec, 3000 rpm) and the sample was denatured on a thermomixer at 95 °C, 400 rpm for 23 minutes.
7. The sample was spun down at 3500 rpm for 30 seconds and added 2 µl NaOH, mixed and spun down (3000 rpm, 30 seconds). The sample was then incubated for 10 minutes at 39 °C.
8. Pre-warmed bisulfite/hydroquinone solution (416 µl) was added to the DNA sample, which was mixed well and spun down quickly.
9. A cyclic reaction was run according to table 2.1:

Table 2.1: Setup for bisulfite treatment of DNA by cycling reaction

Temperature (°C)	Time (min)	
58	15	15 cycles
95	1	

10. 4 sets of eppendorf tubes were prepared:
    a. 2 sets of tubes without lids, 1.5 ml.
    b. 2 sets of tubes with lids, 1.5 ml.
11. DNA was cleaned using Promega Wizzard DNA Clean Up Kit. The Resin bottle was mixed well before use, and 1 ml Resin was added to one set of eppendorf tubes with lids. The bisulfite treated DNA was added to each tube, which was mixed by inversion.
12. The filter and 10 ml syringe were linked together and attached to the vacuum pump station. The DNA/Resin mix was added to each syringe, vacuum was applied and the liquid was allowed to pass through the filter. Then, 2 ml 80 % isopropanol was added to each syringe, and DNA was now desalted in the filter. The syringes were discarded.
13. The filters were transferred to clean 1.5 ml eppendorf tubes without lids and centrifuged (10 000 g, 2 minutes, room temperature).
14. Again, the filters were transferred to clean eppendorf tubes without lids. 50 µl TE-buffer (55 °C) was added directly to the filter and incubated 1 minute at room temperature.
15. Filters were centrifuged at 10 000 g for 30 seconds and 12 000 g for 30 seconds to elute the DNA. The filters were discarded.
16. NaOH (2.5 µl) was added. The sample was mixed and spun down. The samples were incubated at 42 °C for 20 minutes at 400 rpm on a thermomixer. This was the desulphonation step.
17. Ammonium acetate (NH_4OAc) (22.5 µl) and acrylamide (5 µl, 0.25 %) were added to an eppendorf tube with lid. The DNA was added to the mixture, mixed and spun down.
18. Ice-cold (-80 °C) 96 % ethanol (1 ml) was added and the tubes were inverted 4x. The tubes were then incubated at -20 °C for 10 minutes.
19. The tubes were centrifuged at 20 000 g for 15 minutes at -4 °C.

20. The supernatant was removed and cold (-20 °C) 70 % ethanol (1 ml) was added. The mixture was vortexed and spun down at 20 000 g for 15 minutes at -4 °C. The supernatant was removed and the washing step was repeated.
21. The DNA was left to dry after final removal of supernatant.
22. DNA was resuspended in elution buffer (25 µl) and incubated at 60 °C for 1-2 minutes. The tubes were cooled down on ice, spun down and stored at -20 °C for later use.

2.7 PCR using PyroMark PCR kit

By using a thermal cycler, segments of DNA are amplified via the principle of PCR. Repetitive cycles of heating and cooling will amplify the DNA sequence flanked by two primers. There are three steps in each PCR cycle: denaturation, annealing and extension. Denaturation is the use of heating to separate two DNA strands. The temperature is lowered and the two primers bind to the target DNA in a process named annealing. Finally, DNA polymerase binds to the free 3'-end of the primers and start extending the DNA sequence (Reece, 2004). In this thesis, PCR was used to amplify desired segments of bisulfite treated DNA for further analysis by pyrosequencing. It was important that one primer was biotinylated for further isolation of PCR products by Sepharose beads.

A challenge arises when amplifying bisulfite treated DNA, due to the presence of uracil and DNA mainly consisting of three bases: adenine, thymine and guanine. Due to the reduced complexity there is an increased risk of mispriming and nonspecific product can be formed. Qiagen has overcome this by a unique mastermix that ensures specific primer binding, prevents mispriming and minimizes the production of artefacts and redundant biotinylated primer, which can interefere with pyrosequencing. HotStarTaq DNA polymerase requires a 15-minute activation step, which prevents formation of primer-dimers and misprimed products at low temperatures. The PyroMark PCR buffer has a unique combination of salts that ensures a high ratio of specific-to-nonspecific primer binding. CoralLoad Concentrate was added to ensure specific PCR and high yields of the amplified DNA. Q-solution facilitates amplification of templates high in secondary structures and GC content. The solution modifies the melting behaviour of DNA. Magnesium stabilizes DNA and raises the melting temperature (PyroMark PCR Handbook, 2009, Qiagen).

PyroMark Assay Design 2.0 was used to design primers. The software generates primer set that includes both PCR and sequencing primers and each set is given a quality score based on several parameters specific for the Pyrosequencing procedure. For this thesis four sets of primers were designed, Audun Bersaas (staff engineer at STAMI) did help with this. Two assays for the *FOXA1* gene, named FOXA1_pyro1 and FOXA1_pyro2, and two assays for the *FOXA2* gene, named FOXA2_cpg1 and FOXA2_TSS (their positioning is depicted in section 3.4.1). Information regarding the different primers can be seen in table 2.2. The reverse primers had a biotinylated 5'-end.

Table 2.2: Primers used for PyroMark PCR.

Primers	Position, 5'-3'	Length (bp)	% GC	T_m (°C)	Amplicon (bp)
FOXA1_pyro1 (forward)	120-140	21	42.9	59.7	
FOXA1_pyro1 (reverse)	383-361	23	43.5	59.4	264
FOXA1_pyro2 (forward)	1201-1228	28	39.3	61.4	
FOXA1_pyro2 (reverse)	1346-1326	21	42.9	59.1	146
FOXA2_cpg1 (forward)	9-29	21	42.9	55.7	
FOXA2_cpg1 (reverse)	259-234	26	50.0	60.0	251
FOXA2_TSS (forward)	1216-1245	30	23.3	56.7	
FOXA2_TSS (reverse)	1552-1525	28	32.1	58.8	337

1. A mastermix was made for each primer assay. Table 2.3 shows the setup for the different mastermixes and table 2.4 contains information regarding the different optimized conditions for the PCR reaction.

Table 2.3: PyroMark PCR-setup for the different FOXA pyrosequencing assays

Reagents	Volume/sample (µl): FOXA1_pyro1	Volume/sample (µl): FOXA2_cpg1	Volume/sample (µl): FOXA1_pyro2, FOXA2_TSS
dH_2O	6	3.75	5
PyroMark PCR Master Mix, 2X	12.5	12.5	12.5
CoralLoad	2.5	2.5	2.5
Q-Solution	0	2	0
$MgCl_2$, 25 mM	0	0	1
Primer up, 10 pmol/µl	0.5	0.75	0.5
Primer up, 10 pmol/µl	0.5	0.5	0.5
Template DNA	3	3	3
Total volume	25	25	25

Table 2.4: PyroMark PCR-setup. For FOXA1_pyro1 and FOXA2_cpg1 the annealing step is at 60 °C, whereas for FOXA1_pyro2 and FOXA2_TSS the temperature is 58.5 °C.

Step	Temperature (°C)	Time	
Activation	95	15 min	
Denaturation	94	30 sec	47 cycles
Annealing	60/58.5	30 sec	
Extension	72	30 sec	
Final extension	72	10 min	
	4	∞	

2. Template-DNA was added.
3. After completion of the PCR, 1 µl of the PCR products were used for agarose gel electrophoresis on a 2 % gel.
4. The products were kept at -20 °C for further use.

2.8 Pyrosequencing

Pyrosequencing is a based on a real-time sequencing-by-synthesis technology, and it relies on detection of pyrophosphate release when a nucleotide is incorporated during synthesis (Langaee and Ronaghi, 2005). The released pyrophosphate is converted to adenosine-5'-triphosphate (ATP) by sulfurylase, which is sensed by the enzyme luciferase that converts ATP to light. The principle is illustrated in figure 2.5.

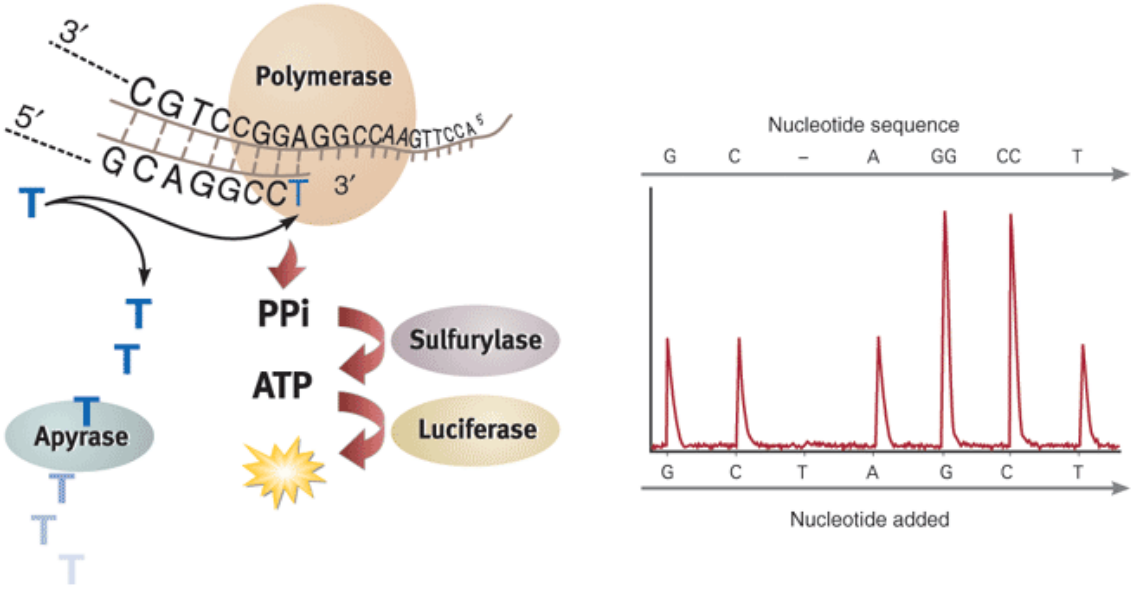

Figure 2.5: When a nucleotide is incorporated by polymerase during synthesis a pyrophosphate is released. This molecule is further converted to ATP by sulfurylase, and luciferase further produces light. This is detected as peaks in the pyrogram. A double peak indicates incorporation of two nucleotides. Apyrase then removes the nucleotides (England and Pettersson, 2005).

The pyrosequencing software generated a dispensation order according to the known DNA sequence, and only one of the four bases (adenine, thymine, cytosine and guanine) was added at a time in terms of the dispensation order. Since the DNA sequence is already known, it is performed a re-sequencing of the DNA to determine the ratio of cytosine and thymine in CpG sites. From these results the software can decide the methylation percentage in each CpG site.

The intensity of the light is proportional to the number of bases incorporated. Deoxyadenosine alpha-thio triphosphate (dATPαS) is added instead of deoxy-ATP (dATP), as it recognized by DNA polymerase but not luciferase. Before another nucleotide is added the previous one is degraded by apyrase. The process is repeated until the DNA sequence is determined (Dupont et al., 2004; Langaee and Ronaghi, 2005).

In this thesis, pyrosequencing was used to determine the number of methylated cytosines in various CpG sites in isolated DNA. A summary of the procedure for this thesis is shown in figure 2.6 and the sequences to be analysed are presented in table 2.5.

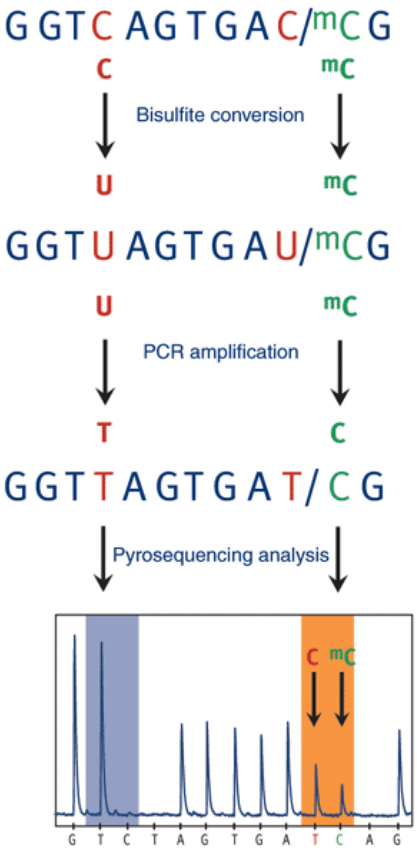

Figure 2.6: During bisulfite treatment unmethylated cytosine is converted to uracil, whereas methylated cytosine remains unchanged. PCR incorporated thymine in the place of uracil, and during pyrosequencing thymine will represent unmethylated cytosine. Methylated cytosine will remain cytosine through the whole procedure (England and Pettersson, 2005).

Table 2.5: Sequences to be analysed by pyrosequencing. Y stands for C/T, where levels of methylation are to be determined

Assay	Sequence to analyse
FOXA1_pyro1	YGYGGGTATT TYGGGTAGTY GTTAGYGGAG GAAGYGGTTT YGTTTTTTTY GGAAGTTGTT TTTGTTATAT TYGTGGGGTT TGTTTTYGGY GTAGTTTYGT AGTATTTGAG
FOXA1_pyro2	TYGTAGGYGT TTTYGGGGAG TATYGTTAGG YGATATTGGA TTGAATTTYG TAYGTATTTT AGTTAGGGAT TTAGGTTT
FOXA2_cpg1	YGTTTTTTGT YGGTYGTTAG GTTYGYGGGA TYGATTYGAG TTTTTATTTA TTTT
FOXA2_TSS	YGGAAYGGTT TYGGGAGAAG YGYGGGGYGT AYGGTTTGGT YGTTTYGGTT TTTYGATTTT TTAGATATYG GTYGTTAGGG ATTYGTAGTG GGGYGGTYGG YGTTTGGYGT AAGTAGTTTT TTTAGTAGYG GTYGAYGGTT GGGAGGTTGA GATTTGTTTT TG

The process of pyrosequencing consists of several steps:

a. Testing the PyroMark Q24 Vacuum Work Station.
b. Immobilization of PCR products on Streptavidin Sepharose beads.
c. Separation of DNA strands and isolation of DNA strand to be sequenced.
d. Attachment of samples to the sequencing primers, information in table 2.6.
e. Preparation of PyroMark Q24 Gold Reagents and pyrosequencing.

Table 2.6: Sequencing primers for pyrosequencing

Sequencing primers	Sequence, 5'-3'	Length (bp)	% GC	T_m (°C)
FOXA_pyro1	GAG GAT TGT AGG GTG	15	53.3	45.9
FOXA1_pyro2	AGG GAA AGT TGA ATT TTT	18	27.8	44.2
FOXA2_cpg1	GGG TTT TTA TAG TGA TAG GG	20	40.0	47.0
FOXA2_TSS	GTT TTT TTT TGT TAT AGT TTA GAT T	25	16.0	42.9

2.8.1 Testing the PyroMark Q24 Vacuum Work Station

1. A container on the PyroMark Q24 Work Station was added 70 ml dH_2O and the vacuum pump was started.
2. The filter tips were lowered in the water and after 20 seconds the water should be absorbed.
3. A 24-well PCR plate was added dH_2O (100 µl) in each well. The filter tips were lowered in the plate and left there for 10 seconds. Proper absorption of water from all the wells was inspected.
4. The procedure was repeated if there was any trouble during the absorption. If problems persisted the filters were changed.

2.8.2 Immobilization of PCR products to Streptavidin Sepharose beads

1. The bottle of Streptavidin Sepharose beads was carefully mixed to obtain a homogenous solution.
2. A mastermix was made:

Streptavidin Sepharose High Performance	2 µl per sample
Binding buffer	40 µl per sample
dH_2O	14 µl per sample
	56 µl per sample

3. Mastermix (56 µl) was added to each well on the PCR plate.
4. PCR products were added to the mixture. Figure 2.7 summarises this.
5. The plate was sealed with a lid and incubated for 10 minutes at 20 °C and 1500 rpm on a thermomixer.
6. Sepharose beads sedimented rapidly and the absorption by vacuum filters was done quickly after incubation (section 2.10.3, point 6).

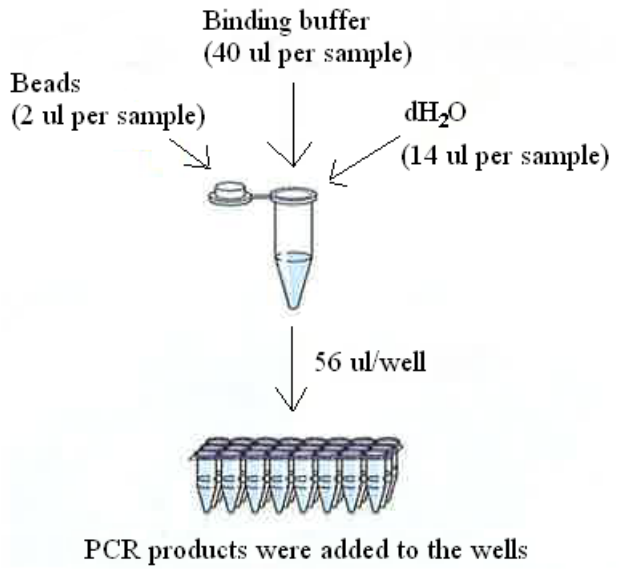

Figure 2.7: Immobilization of PCR products to Streptavidin Sepharose beads (PyroMark Q24 User Guide).

2.8.3 Separation of DNA strands and clearing of samples in the PyroMark Q24 plate

1. A mastermix per sequencing primer was made:

Annealing buffer	24.25 µl per sample
Sequencing primer (10 pmol/µl)	0.75 µl per sample
	25 µl per sample

2. Mastermix (25 µl) was added to wells on the PyroMark Q24 plate.
3. The plate was placed properly in the vacuum work station (depicted in figure 2.8).

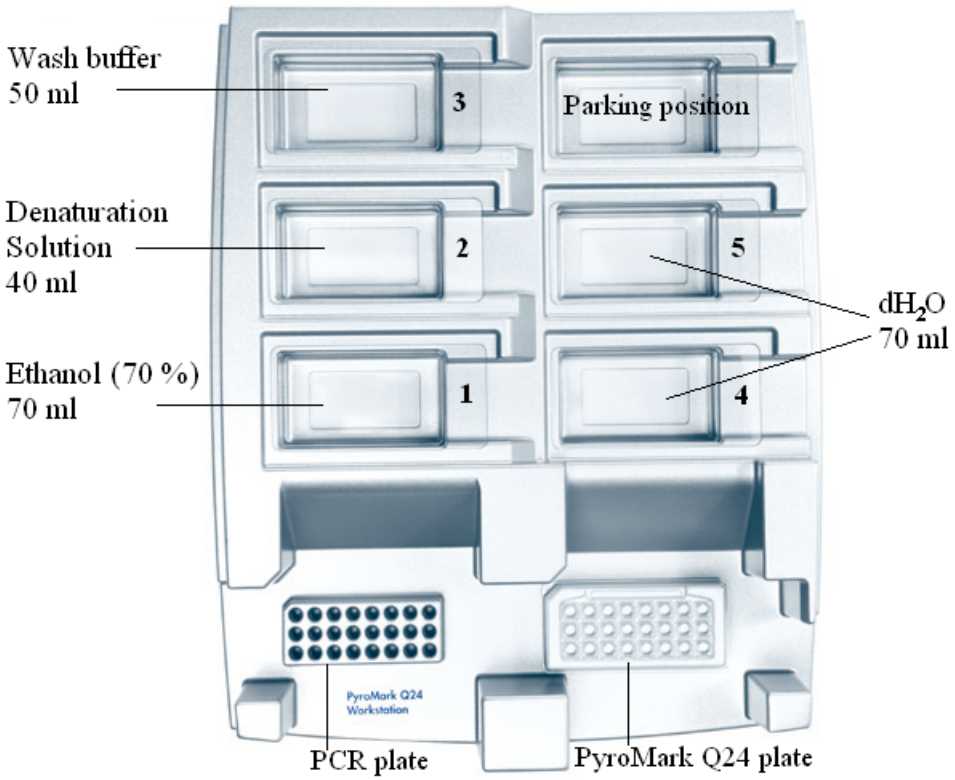

Figure 2.8: Filling of the work station containers (PyroMark Q24 User Guide).

4. In the five containers on the PyroMark Q24 vacuum station different solutions were added:
    1. 70 % ethanol (70 ml).
    2. Denaturation solution (40 ml).
    3. 1x Washing Buffer (50 ml).
    4. dH_2O (70 ml).
    5. dH_2O (70 ml).
5. The filter tips were washed in container 5, and 70 ml dH_2O was added again
6. The PCR plate was placed in the vacuum workstation and the filter tips were slowly lowered into the plate to catch the beads with immobilized template. The filter tip holder was left there for 15 seconds.
7. The filters were washed in:
    a. 70 % ethanol for 7 seconds.
    b. Denaturation solution for 7 seconds.
    c. Washing buffer for 16 seconds.
8. It was important to ensure that the Sepharose beads were attached to the filters after washing. This was done by inspection by eye.

9. The filters were held above the PyroMark plate while the vacuum was turned off. The filters were then lowered onto the plate and the tool was shaken for 30 seconds to release the beads.
10. The tool was placed in container 4 and shaken for 10 seconds.
11. The vacuum was turned on and the tool was washed twice with dH_2O (70 ml).
12. When finished, the tool was placed in the parking position.

2.8.4 Attachment of sequencing primers to the samples

1. The PyroMark Q24 plate was incubated for 2 minutes at 80 °C.
2. The samples were left to cool down for 5 minutes at room temperature.

2.8.5 Preparation of PyroMark Q24 Gold Reagents and pyrosequencing

1. The freeze-dried enzyme and substrate (PyroMark Q24 Gold Reagents) were added filtrated water (620 µl) and left to dissolve for at least 10 minutes.
2. Enzyme, substrate and nucleotides were added to the PyroMark Q24 cartridge according to the Pre Run Information report.
3. The cartridge was then placed in the PyroMark Q24 sequencing instrument, along with the PyroMark Q24 plate.
4. The run file was uploaded and the sequencing procedure was initiated.
5. After the run the container was cleaned thoroughly and a pressure-test was performed to ensure that the needles in the bottom were not blocked.

The pyrosequencing procedure is presented by the manufacturer in this video: http://www.labtube.tv/channel.aspx?v=137486&u=QIAGEN.

2.8.6 Analysis of results

The results were presented as pyrograms in PyroMark Q24 2.0.6.20 (figure 2.9). The software calculated the methylation percentage for each CpG site in the four different assays. The light signal is proportional to each incorporated nucleotide. Percentage methylation in CpG sites is calculated as the ratio of the signal height for methylated cytosine divided by the sum of the signal height of methylated and unmethylated cytosines. The methylation percentages were given a colour code based on the quality assessments for the variable position. According to

the PyroMark Q24, blue represent approved, yellow indicates approved, but under doubt and red indicates not approved. The instrument do the assessments based on how well the signals corresponds to the average signal from the reference sequence. We have chosen to present all data, with reservations that red coloured data points need to be inspected carefully. Blue and yellow are both considered reliable, and red are not considered in the analysis. Data from the pyrograms are represented as a graph where the methylation percentage is shown.

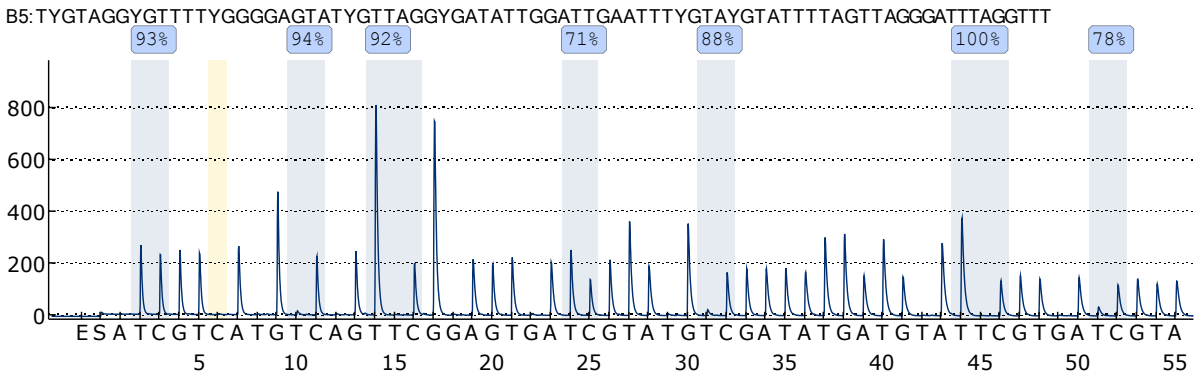

Figure 2.9: A pyrogram represented in PyroMark Q24 2.0.6.20. This is the result from FOXA1_pyro2 assay with DNA from HBEC-2KT-CSC.L. Peak height relates to the number of nucleotides incorporated Y represents C/T ratio. The analysis results are shown above each CpG site (blue background colour) and the colour around the percentage represents the quality of the analysis. Blue denotes approved. The sequence to be analysed is shown at the top. The bisulfite treatment controls are marked with yellow background colour.

2.9 Statistical Methods

Statistical analysis was done using SigmaPlot 12.3 and $p<0.05$ was accepted as statistically significant. Comparison of multiple groups was performed using one-way ANOVA followed by post-hoc tests to identify which groups that differed from each other. One-way ANOVA followed by Holm-Sidak test was used on normal distributed data, and data that were not normal distributed was analysed using one-way ANOVA on Ranks followed by Dunn's test.

3 Results

3.1 Transformed cell lines

The cell lines used for this study are HBEC derived cell lines exposed to various components present in cigarette smoke (B[*a*]P, CSC and MNU) for 12 weeks and selected two times in soft agar. HBECs exposed to DMSO for 7 weeks were used as control, as these were the only available control cells. HBEC control cells were also exposed to DMSO for 12 weeks followed by isolation of RNA and DNA and subsequent testing in soft agar, which resulted in no growth. Unfortunately, these control cells were not preserved for further experiments. An overview of the cell lines is presented in table 1.3.

3.2 Soft agar assay

HBEC-12KT control cells (DMSO) and untreated HBEC-12KT were tested for colony formation in soft agar. No anchorage-independent growth was observed for either cell lines. Colony formation was observed for the positive control (tumour cell line A549) (figure 3.1).

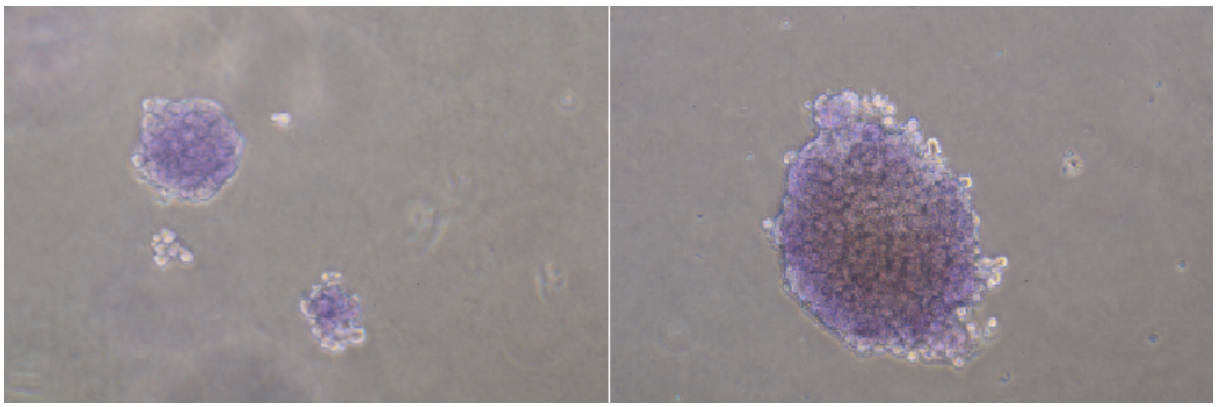

Figure 3.1: A549 colonies in soft agar stained with crystal violet.

3.3 Cell migration assay

Cell migration is an important process for all living cells, especially during development and wound healing. This process is also essential for progression and metastasis of cancer cells.

Two methods for studying cell migration were used in this thesis. Both involved the same basic procedure; make a wound in the cell monolayer, monitor wound-healing progression by

light microscope and capture images after a chosen time course. This was followed by calculation of migration capacity. The first method included the use of IncuCyte ZOOM, and is a semi-automated approach. Images were acquired on an hourly basis. The second method was an *in vitro* scratch assay that was performed manually. Images were obtained after 0 and 12 hours. Following, the images and graphs are presented and at the end the migration data from both *in vitro* scratch assay and IncuCyte ZOOM are summarised (table 3.1).

3.3.1 Cell migration analysis by IncuCyte ZOOM

IncuCyte ZOOM is a light microscope instrument that acquires images automatically and can be placed in an incubator at the laboratory. By using specific ImageLock plates for the purpose of migration, images are taken at the exact same spot each time, as the plates have reference markers at the bottom, providing points to accurately locate the images. Scratch wounds were made using a special tool that ensured uniform wounds in the cell monolayer. Cells were seeded at a density of 25 000 cells per well in 96-well plates and grown to confluence in the incubator, which usually took about 24 hours.

In the following sections are representative results of the IncuCyte migration assay presented by images taken 0, 12 and 24 hours after wounding. Only parallel A from second time in soft agar (2A) was used during experiments with IncuCyte ZOOM. Representative videos of HBEC-2KT control cells (DMSO), HBEC-2KT-CSC.L, HBEC-12KT control cells (DMSO) and HBEC-12KT-CSC.L-B can be found here: http://youtu.be/iZey1Fdq0z8, http://youtu.be/cs7vksAyk9E, http://youtu.be/KzgaZ6sQXVA, http://youtu.be/vpqJbVO5X7E respectively. Appendix D presents images from all cell lines analysed by IncuCyte ZOOM.

Figure 3.2 represents the cell migration of HBEC-2KT control cells (DMSO) during 24 hours. A clean-cut scratch wound (time point 0 hours) was made, by Essen 96-well WoundMaker, in the confluent cell monolayer. After 12 hours, HBEC-2KT control cells (DMSO) had almost closed the wound and only a few open spaces were seen where the wound originally was made. After 24 hours the cells had migrated to a confluent monolayer again.

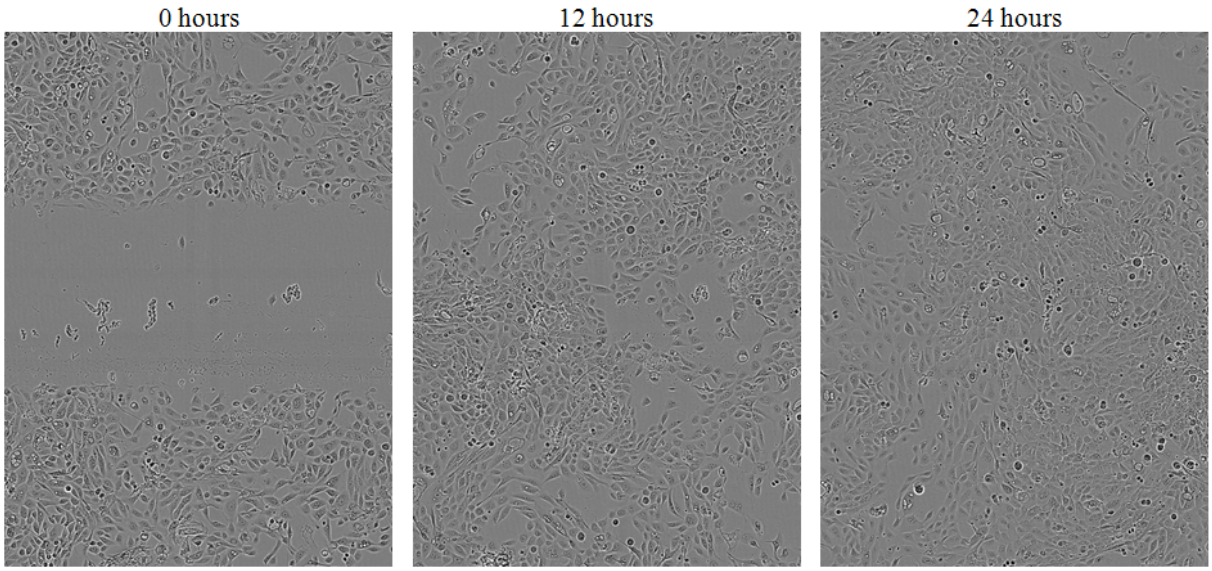

Figure 3.2: Migration of HBEC-2KT control cells (DMSO) 0, 12 and 24 hours after wounding.

HBEC-2KT-CSC.L showed slower migration than their control cells (DMSO). This is illustrated in figure 3.3. Some migration of the cells after 12 hours could be observed. After 24 hours the cells had practically closed the wound, but the initial location of the wound was still noticeable.

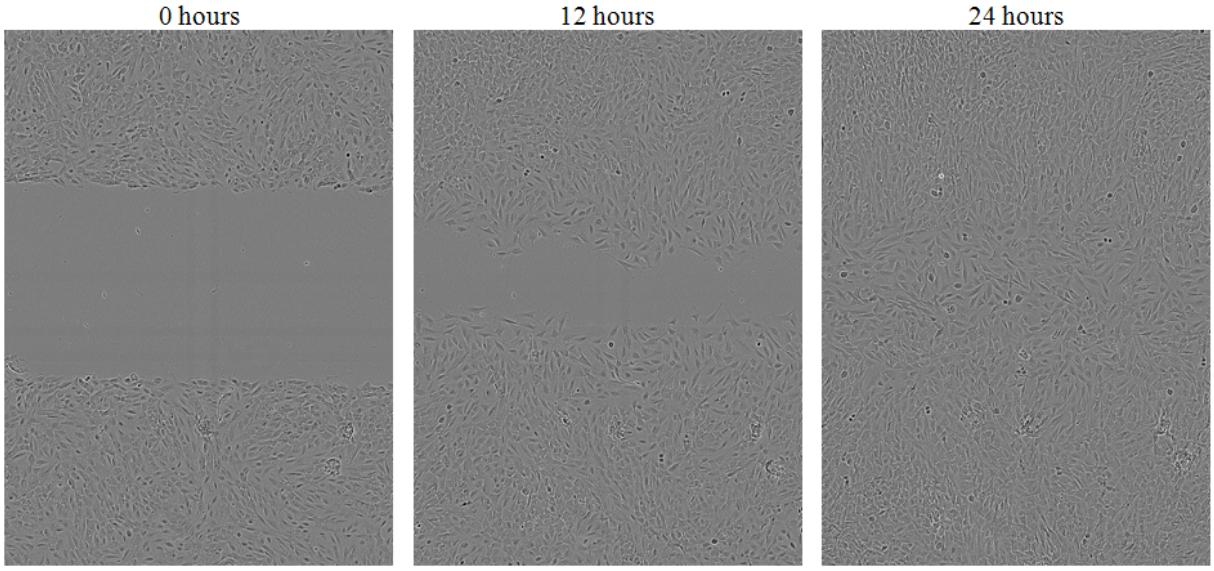

Figure 3.3: Migration of HBEC-2KT-CSC.L 0, 12 and 24 hours after wounding.

Figure 3.4 illustrates migration of HBEC-12KT control cells (DMSO). Here, the wound was closed after 12 hours. At this time point, it seems as these cells had migrated to such a high extend that they "overpopulated" the wound; it looks like the cells migrated on top of each other. After 24 hours the cells were evenly distributed.

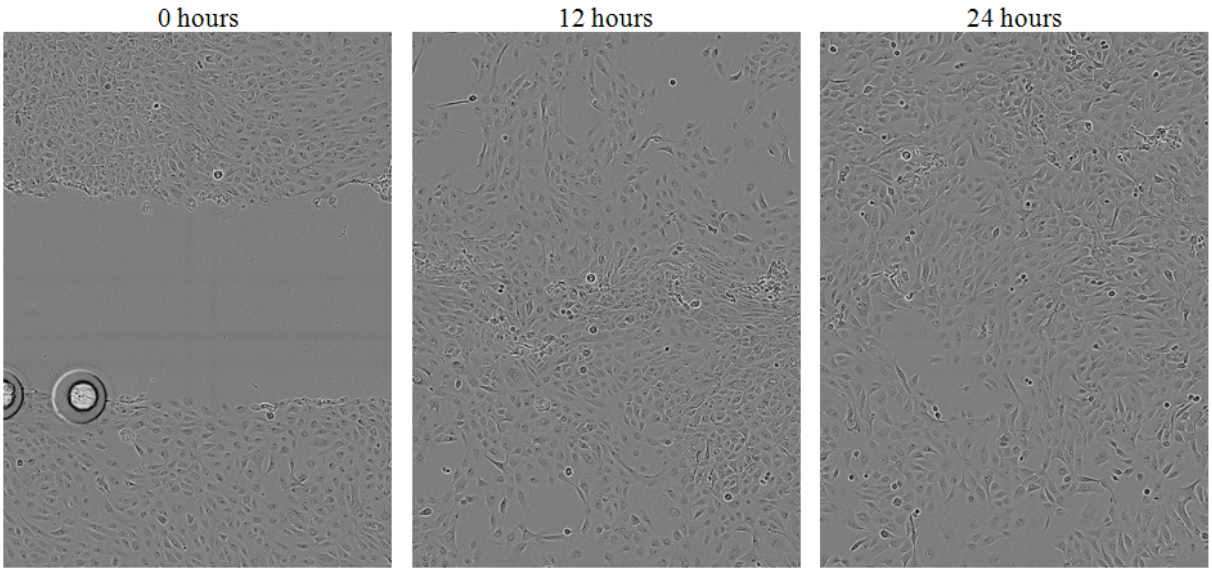

Figure 3.4: Migration of HBEC-12KT control cells (DMSO) 0, 12 and 24 hours after wounding.

Figure 3.5 illustrates migration of HBEC-12KT-CSC.L-B. These cells migrated slower compared to their control cells (DMSO). After 12 hours the wounding area was reduced in size. After 24 hours the wound was still not completely closed.

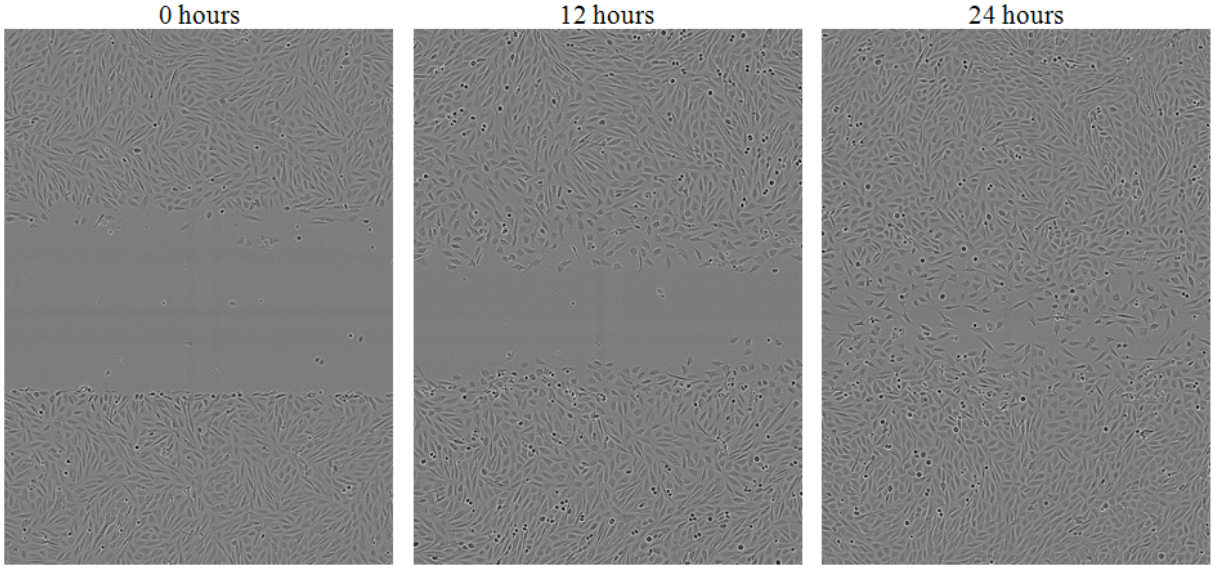

Figure 3.5: Migration of HBEC-12KT-CSC.L-B 0 hours, 12 hours and 24 hours after wounding.

Migration assay using IncuCyte ZOOM was repeated three times for the majority of the cell lines, except for untreated HBECs that were only analysed once. HBEC-12KT-CSC.L-A was examined four times. Number of parallels for each experiment is variable. The number of experiments and parallels depended on the limited availability of instrument usage, as well as errors during the procedure, as for example imperfect wounds and bubbles disrupting the calculations done by the instrument, which led to insecure data. All of the experiments for each cell line are represented in appendix E and a high degree of consistency can be observed

between the independent experiments. One representative was chosen for each cell line in the following presentations. Visual inspection of the overall trend of the data was used to decide which parallels were to be included in analyses. An example of this process is shown in appendix F.

In figure 3.6, migration percentage during 24 hours is represented as relative wound density as a function of time (0-24 hours). Untreated HBEC-3KT closed the wound significantly faster than HBEC-2KT and HBEC-12KT 12 hours after wounding ($p<0.050$, one-way ANOVA with Holm-Sidak post test). Untreated HBEC-2KT and HBEC-12KT showed similar migration values.

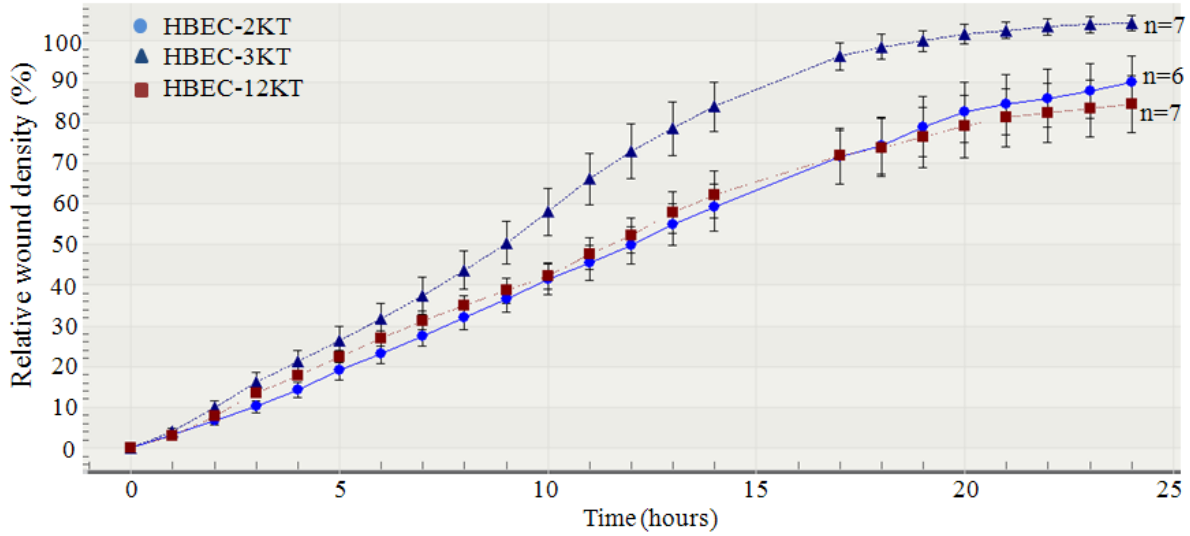

Figure 3.6: Relative wound density (%) of untreated HBEC-2KT, HBEC-3KT and HBEC-12KT over a time course of 24 hours. HBEC-2KT is denoted by blue circles, HBEC-3KT by blue triangles and HBEC-12KT by red squares. During the time period between 15 and 16 hours after initiation of the experiment the instrument had to reboot and hence lack of data points. Number of parallels (n) is denoted at the end of each curve. Error bars denote SD for each data point.

When comparing time courses for HBEC-2KT derived cell lines from the *in vitro* transformation experiment, the control cells (DMSO) migrated above 100 % from 13 to 24 hours (figure 3.7). This was due to the calculation method used and is further explained in section 4.1.1. Untreated HBEC-2KT, HBEC-2KT-CSC.L and HBEC-2KT-CSC.H showed similar time courses and all had a significantly slower migration compared to control cells (DMSO) 12 hours after wounding ($p<0.05$, one-way ANOVA with Holm-Sidak post test).

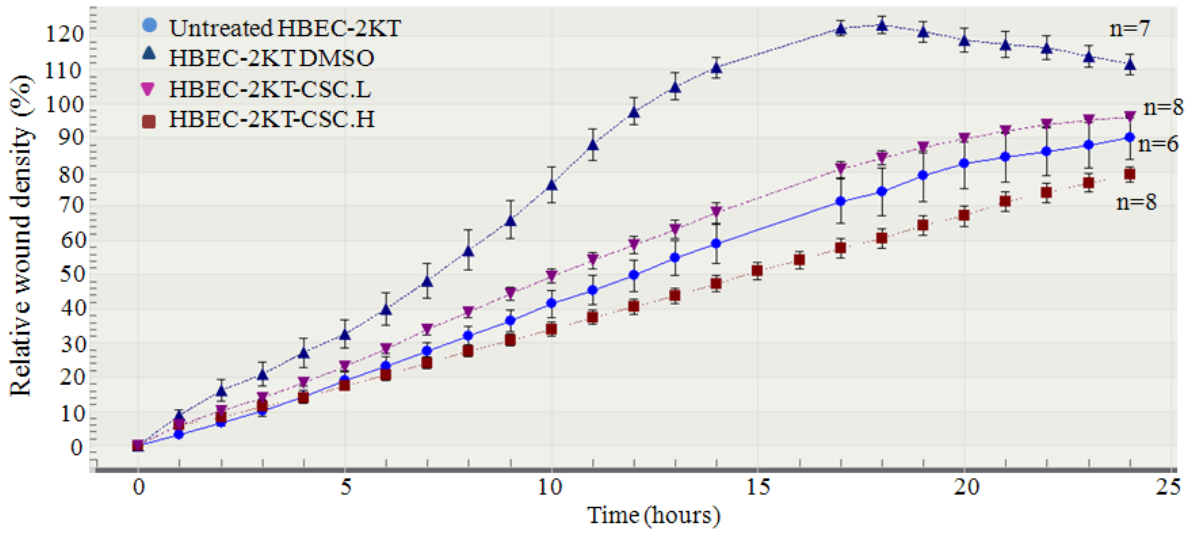

Figure 3.7: Relative wound density (%) of HBEC-2KT and its transformed cell lines over a time course of 24 hours. Blue circles denote untreated cells and blue triangles denote control cells (DMSO). Transformed cell lines are denoted by pink triangles and red squares, low dose CSC and high dose CSC respectively. During the time period between 15 and 16 hours after initiation of the experiment the instrument had to reboot and hence lack of data points. Number of parallels (n) is denoted at the end of each curve. Error bars denote SD for each data point.

HBEC-12KT control cells (DMSO) showed a significantly faster migration compared to some of the transformed cells (B[*a*]P.L, B[*a*]P.H, CSC.L-A and CSC.L-B) 12 hours after wounding ($p<0.05$, one-way ANOVA on Ranks with Dunn's post test). However, control cells (DMSO) did not show a significantly faster migration compared to HBEC-12KT-CSC.H, HBEC-12KT-MNU and untreated HBEC-12KT 12 hours after wounding (figure 3.8). All of the transformed cell lines displayed similar migration patterns, but the figure may indicate somewhat faster wound closure of for example HBEC-12KT-CSC.H compared to HBEC-12KT-CSC.L.

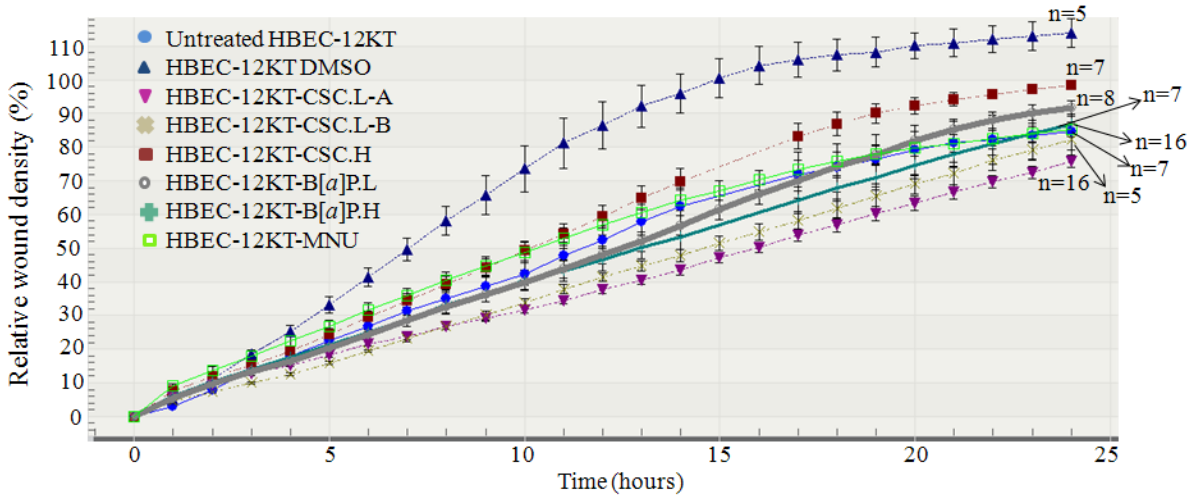

Figure 3.8: Relative wound density (%) of HBEC-12KT and its transformed cell lines over a time course of 24 hours. Blue circles denote untreated cells and blue triangles denote control cells (DMSO). Transformed cell lines are denoted by pink triangles, beige crosses, red squares, grey circles, blue green crosses and green squares; low dose CSC colony A and B, high dose CSC, low dose and high doses B[*a*]P and MNU respectively. During the time period between 15 and 16 hours after initiation of the experiment the instrument had to reboot and hence lack of data points. Number of parallels (n) is denoted at the end of each curve. Error bars denote SD for each data point.

3.3.2 *In vitro* scratch assay

Cells were seeded at a density of $5x10^5$ cells/well in 6-well plates for the manually *in vitro* scratch assay and incubated for two till three days until a confluent monolayer was formed. The majority of cell lines were seeded in three wells within each experiment and three scratches were made in each well (a total of nine scratches). Six scratches were included in the calculations (n=6), due to errors during the experiment, as open spaces in the monolayer and debris in the wounding area. Cells originating from HBEC-2KT-CSC.H-2D and HBEC-12KT-CSC.L-B were seeded in only one well (n=3). This was one of the first experiments performed (where cells were only seeded in one well), and as they showed an overall consistency they were not repeated. Light microscopy images were acquired at time point 0 hours (immediately after the wounds were made) and after 12 hours incubation. The migration data were analysed and representative results are depicted below.

HBEC-2KT control cells (DMSO) showed some migration 12 hours after wounding (figure 3.9). HBEC-2KT-CSC.L (figure 3.10) migrated faster than its control cells (DMSO) during 12 hours incubation.

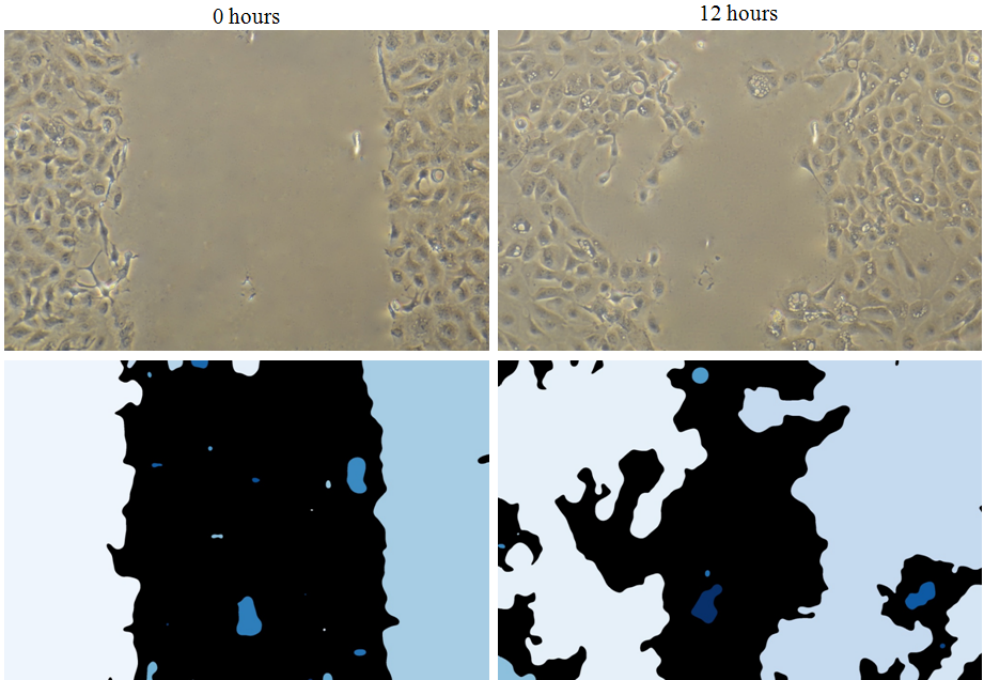

Figure 3.9: Migration of HBEC-2KT control (DMSO) cells 0 and 12 hours after wounding. At the top are images acquired with a light microscope (10x magnification) and at the bottom are results from the software CellProfiler. Different blue colours represent areas covered by cells and black corresponds to open spaces.

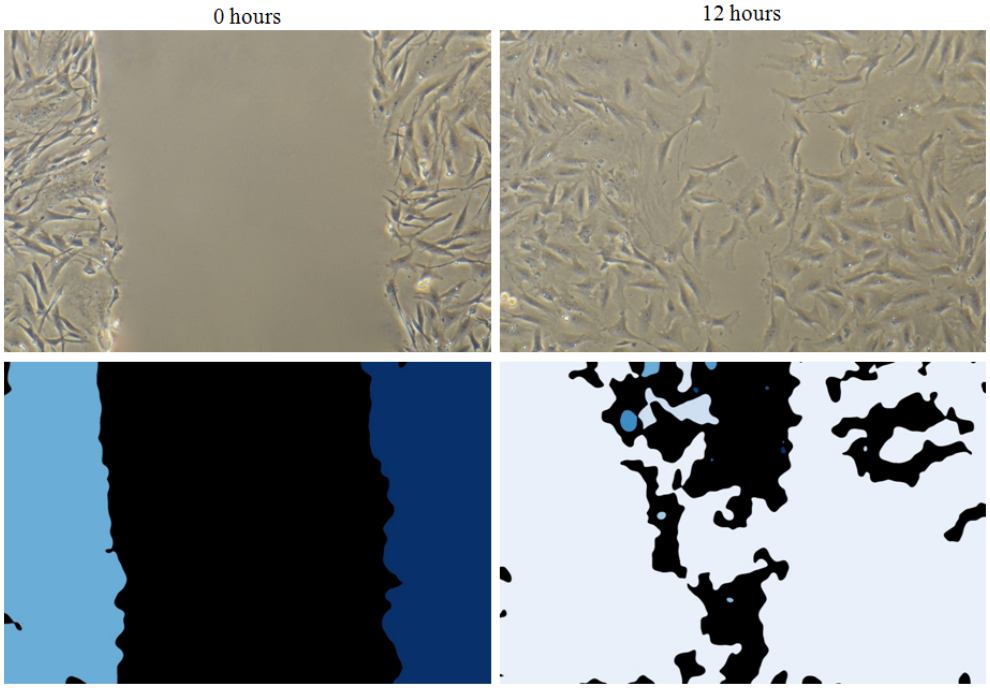

Figure 3.10: Migration of HBEC-2KT-CSC.L 0 and 12 hours after wounding. At the top are images acquired with a light microscope (10x magnification) and at the bottom are results from the software CellProfiler. Different blue colours represent areas covered by cells and black corresponds to open spaces.

HBEC-12KT control cells (DMSO) had entirely closed the wound 12 hours after wounding, and the wounding area appeared clearly oversaturated (figure 3.11). A monolayer of cells outside the wounding area could clearly be observed, but the CellProfiler software mistakenly analysed it as no cells; hence it became black. Thus, by visual inspection of the images it was concluded that HBEC-12KT control cells (DMSO) had completely closed the wound 12 hours after wounding. HBEC-12KT-CSC.L-B apparently migrated at a slower rate compared to its control cells (DMSO). There was some evidence of migration, as figure 3.12 shows, but not complete closure of the wound during the 12-hour duration of the experiment.

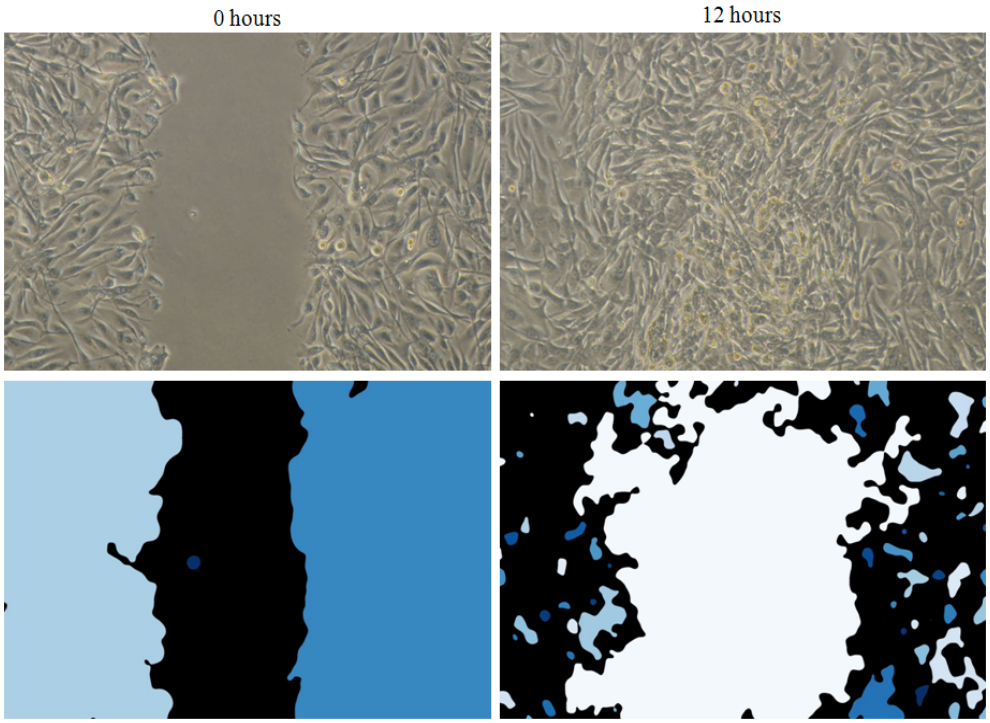

Figure 3.11: Migration of HBEC-12KT control cells (DMSO) 0 and 12 hours after wounding. At the top are images acquired with a light microscope (10x magnification) and at the bottom are results from the software CellProfiler. Different blue colours represent areas covered by cells and black corresponds to open spaces.

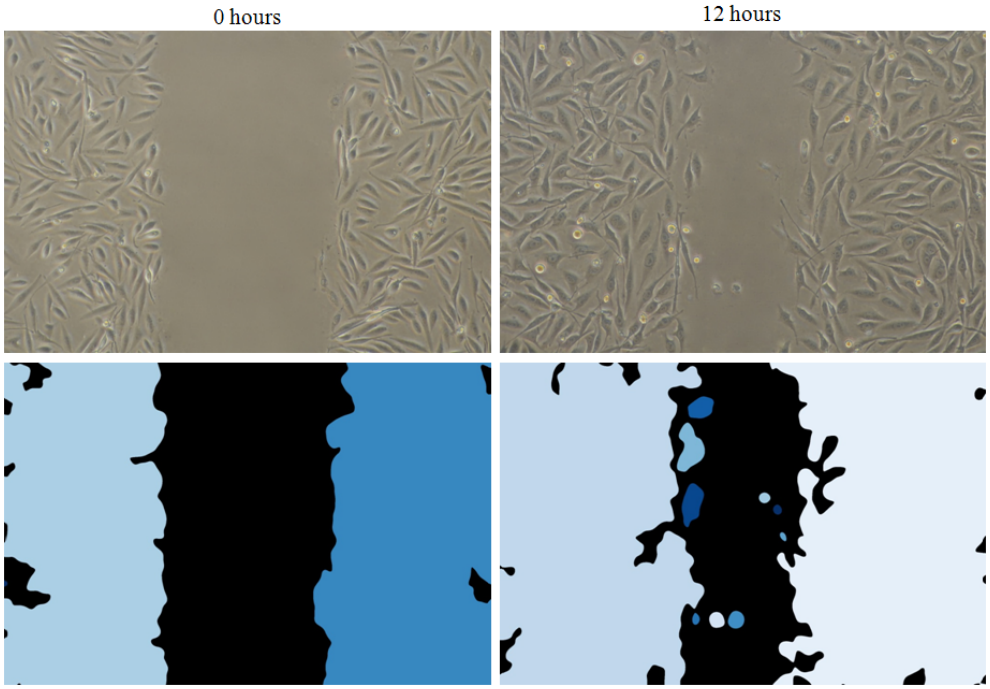

Figure 3.12: Migration of HBEC-12KT-CSC.L_B 0 and 12 hours after wounding. At the top are images acquired with a light microscope (10x magnification) and at the bottom are results from the software CellProfiler. Different blue colours represent areas covered by cells and black corresponds to open spaces.

Migration percentages were calculated from data obtained by CellProfiler according to the formula in section 2.7.2. Area occupied by cells was subtracted from total area (area occupied by cells and area not occupied by cells) to obtain uncovered area, at 0 hours and 12 hours after wounding. By using the wound area at 0 hours as a reference, the migration percentage for each cell line was determined by calculating the percentage cell coverage in the wounding area 12 hours after wounding.

Figure 3.13 shows that untreated HBEC-2KT showed a significantly higher migration percentage than both untreated HBEC-3KT and HBEC-12KT 12 hours after wounding ($p<0.05$, one-way ANOVA with Holm-Sidak post test). Untreated HBEC-12KT also showed a significantly higher migration percentage than untreated HBEC-3KT 12 hours after wounding ($p<0.05$, one-way ANOVA with Holm-Sidak post test).

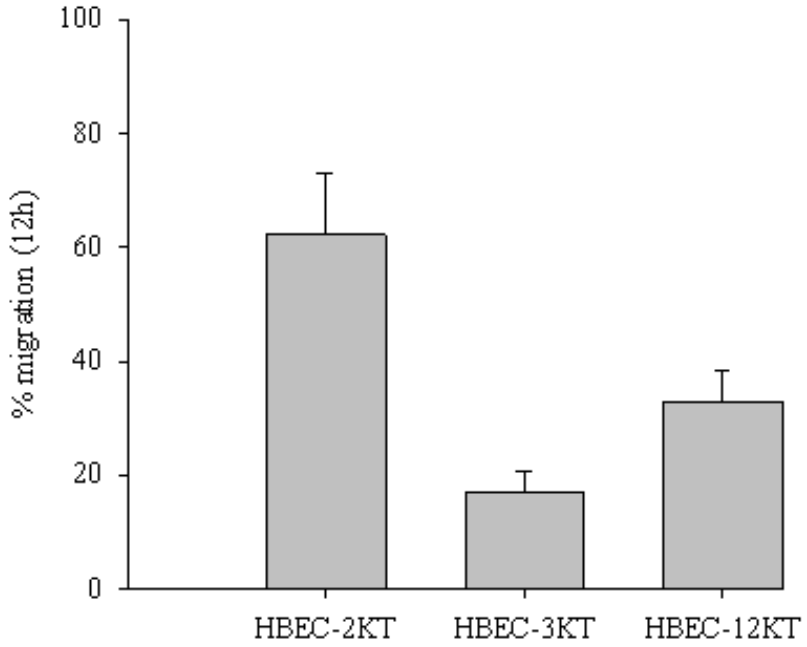

Figure 3.13: Percentage migration of untreated HBEC-2KT, HBEC-3KT and HBEC-12KT 12 hours after wounding. Standard deviation is shown above the bars. Number of parallels is 6 for HBEC-2KT and HBEC-12KT, and 4 for HBEC-3KT. One-way ANOVA with Holm-Sidak post test was performed ($p<0.05$).

Four colonies of each of the transformed cell lines were analysed by *in vitro* scratch assay (2A, 2B, 2C and 2D). These represent four different colonies after the second selection in soft agar. In this case, when analysing results from the *in vitro* scratch assay the mean migration percentage was calculated for each of the colonies (2A-2D), resulting in one value for each colony. This gives four values used to represent the percentage migration of that transformed cell line.

Untreated HBEC-2KT and its transformed cells had similar percentage migration 12 hours after wounding. In contrast, HBEC-2KT control cells (DMSO) showed a significantly slower migration 12 hours after wounding than the transformed cells ($p<0.05$, one-way ANOVA with Holm-Sidak post test) (figure 3.14). This is in contradictory to results obtained from IncuCyte ZOOM. Cells transformed with low dose CSC showed about 35 % increased migration, and those transformed with high dose of CSC about 20 % when analysed by *in vitro* scratch assay.

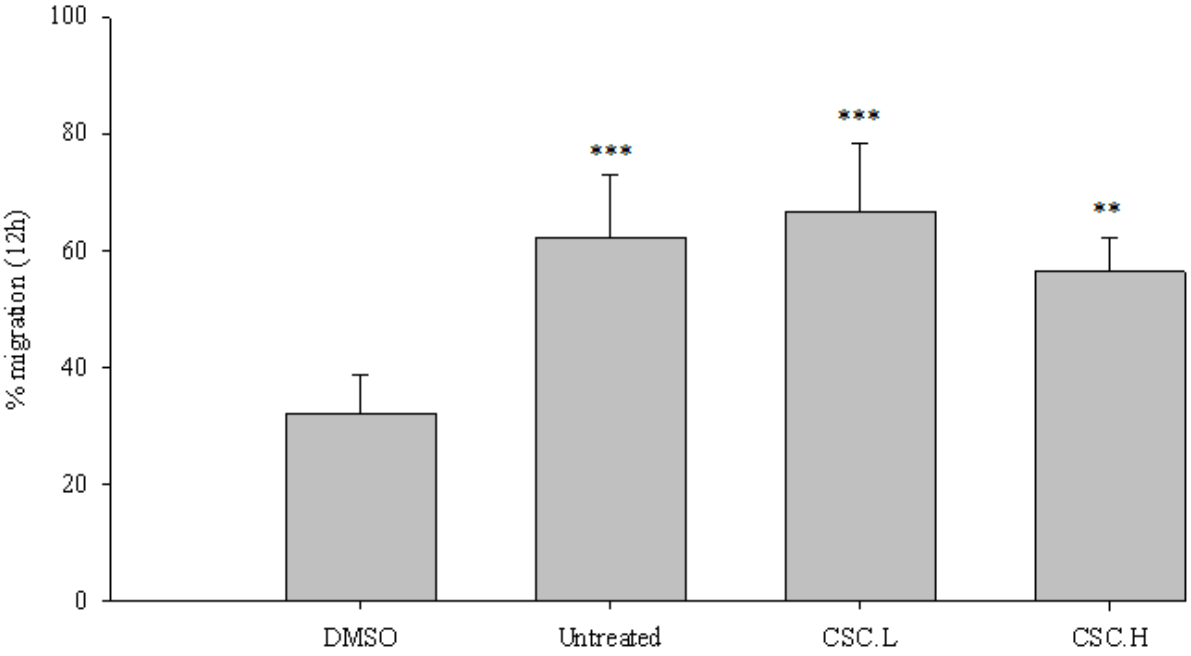

Figure 3.14: Percentage migration of HBEC-2KT control cells (DMSO), untreated cells and its transformed cells (CSC.L and CSC.H) 12 hours after wounding. Standard deviation is shown above the bars. Number of parallels is 6 for DMSO and untreated cells, and 4 for transformed cell lines. One-way ANOVA with Holm-Sidak post test was performed and the following p-values are marked: $p<0.05$=*, $p<0.01$=**, $p<0.001$=***.

In figure 3.15 it can be seen that by transforming HBEC-12KT with various doses of CSC, B[*a*]P and MNU the migration capacity decreased significant to varying degrees compared with the control cells (DMSO) 12 hours after wounding ($p<0.05$, one-way ANOVA with Holm-Sidak post test). High doses B[*a*]P repressed the migration significantly (approximately 90 %) compared with the other transformed cells. Low dose of CSC reduced migration with approximately 40 % as observed in colony A and approximately 70 % as observed in colony B. High dose of CSC and MNU repressed the migration with near 50 %, and low dose B[*a*]P reduced the migration with approximately 40 %. Untreated HBEC-12KT migrated close to 30 % after 12 hours.

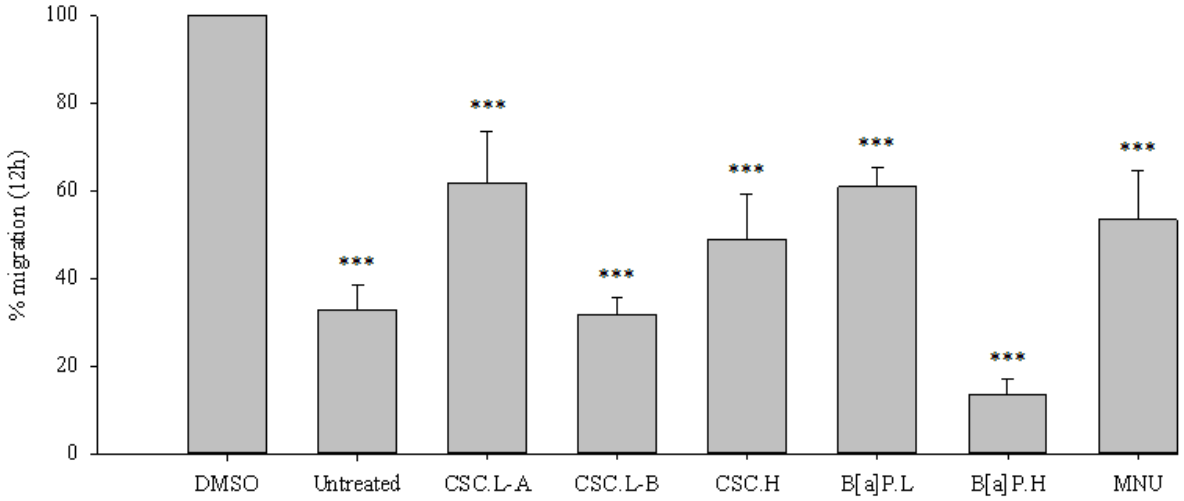

Figure 3.15: Percentage migration of HBEC-12KT control cells (DMSO), untreated cells and its transformed cells (CSC.L-A , CSC.L-B, CSC.H, B[*a*]P.L, B[*a*]P.H and MNU) 12 hours after wounding. Standard deviation is shown above the bars. Number of parallels is 3 for DMSO, 6 for untreated cells, and 4 for transformed cell lines. One-way ANOVA with Holm-Sidak post test was performed and the following p-values are marked: $p<0.05$=*, $p<0.01$=**, $p<0.001$=***.

Table 3.1 summarises the migration data acquired from both *in vitro* scratch assay and IncuCyte ZOOM. The migration percentages analysed by *in vitro* scratch assay is represented after 12 hours, whereas results from the migration analysis by IncuCyte ZOOM are represented after both 12 and 24 hours. In the comparisons of the two methods, the focus is on 12 hours after initial wounding. As mentioned above, migration percentages from *in vitro* scratch assay were calculated from the mean of the four colonies (2A-2D) after second selection in soft agar. However, migration results from IncuCyte ZOOM only include colony 2A. The *in vitro* scratch assay showed an overall similar migration percentage for all the colonies within each exposure group, and therefore colony 2A was chosen to represent the transformed cell lines during experiments with IncuCyte ZOOM. This was done due to the large amount of data that would be obtained and the time given to work with the instrument.

Overall, great consistency was observed between migration percentages analysed by the two different methods (table 3.1). Untreated HBEC-2KT and transformed cells displayed in general similar migration percentages. However, regarding HBEC-2KT control cells (DMSO) there was a clear difference in migration percentage measured across the methods, from 32 % migration obtained by *in vitro* scratch assay and CellProfiler till 98 % migration calculated by

the integrated software in IncuCyte ZOOM. Untreated HBEC-3KT also varied in migration percentage; 17 % migration was obtained by *in vitro* scratch assay and CellProfiler versus 74 % measured by IncuCyte ZOOM's integrated software. Among HBEC-12KT derived cells the migration percentages for untreated cells and two of the transformed cells (CSC.L-A and B[*a*]P.H) varied most between the two methods. Regarding the other transformed cells, there was an overall consistency.

Table 3.1: Migration (%) of the HBEC control cells (DMSO), untreated cells and their transformed cells. Results from *in vitro* scratch assay 12 hours after wounding and migration assay using IncuCyte ZOOM 12 and 24 hours after wounding.

Cell lines	Migration (%)		
	In vitro scratch assay	IncuCyte ZOOM	
	12h	12h	24h
Untreated HBEC-2KT	62	50	90
HBEC-2KT control cells (DMSO)	32	98	100
HBEC-2KT-CSC.L	67	60	88
HBEC-2KT-CSC.H	53	41	80
Untreated HBEC-3KT	17	74	100
Untreated HBEC-12KT	33	52	85
HBEC-12KT control cells (DMSO)	100	86	100
HBEC-12KT-CSC.L-A	62	39	76
HBEC-12KT-CSC.L-B	32	42	82
HBEC-12KT-CSC.H	49	60	99
HBEC-12KT-B[*a*]P.L	61	49	91
HBEC-12KT-B[*a*]P.H	13	48	86
HBEC-12KT-MNU	53	58	85

The width of the wounds for the *in vitro* scratch assay varied from 1.5-3.3 mm. Results from the migration images obtained by IncuCyte ZOOM showed a wound width of approximately 0.7 mm.

3.4 DNA methylation assay

DNA methylation is essential in normal development in mammals. It is an epigenetic modification, and changes may alter the expression of genes and this has been associated with cancer. Pyrosequencing is a quantitative method of DNA sequencing and was used to examine DNA methylation levels in this thesis. Previous studies showed that expression of the *FOXA1* and *FOXA2* genes was significantly downregulated in transformed cell lines of

both HBEC-2KT and HBEC-12KT. The subject for this part of the thesis was to examine if altered *FOXA* expression could be explained by changes in DNA methylation of the genes.

3.4.1 Assay design

A total of four assays were used during the pyrosequencing procedure, designed by Audun Bersaas; engineer at STAMI. Two assays in the *FOXA1* gene (FOXA1_pyro1 and FOXA2_pyro2) and two assays in the *FOXA2* gene (FOXA2_cpg1 and FOXA2_TSS) were designed. Figure 3.16 shows the localisation of the assays in the genes, along with promoter, exons, CpG islands, primer pairs and position of transcription start site. Details about the assay designs are discussed in section 4.1.3.

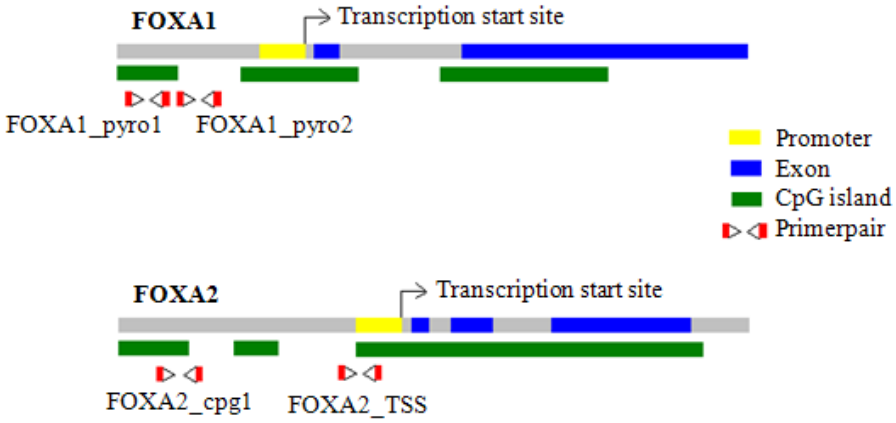

Figure 3.16: Localisation of assays on the *FOXA1* and *FOXA2* genes, along with promoter, exons, CpG islands, primer pairs and position of transcription start site.

The number of CpG sites examined by the different assays was: FOXA1_pyro1; 12 CpG sites, FOXA1_pyro2 and FOXA2_cpg1; 7 CpG sites and FOXA2_TSS; 20 CpG sites.

3.4.2 Pyrosequencing

The bisulfite treatment and pyrosequencing procedure was repeated twice for the majority of the cell lines with the exception of methylase-treated DNA that was only performed once, and HBEC-2KT-CSC.L-2C (FOXA2_cpg1 and FOXA2_TSS) that was repeated three times. There was observed an overall good consistency between the independent experiments.

In the following section, results of the pyrosequencing analysis are presented. Data points are represented by colour codes as determined by the PyroMark Q24 software. Blue data points characterise approved data, but is in this study represented by individual colours on the graphs (purple, green or black) to differentiate between experiments. Yellow points represent that percentage methylation of the specific CpG site was approved under doubt and red points when not approved by the software. The software does the quality assessment based on how well the signals correspond to the average signal from the reference sequence. In this thesis, all data are included in the graphs. Unless otherwise stated red points were left out of the analysis, whereas blue and yellow were both considered approved and reliable. This is based on previous experiences with pyrosequencing analysis at STAMI.

Pyrosequencing results from methylase-treated DNA

DNA treated with the enzyme methylase was used as a positive control for the procedure (figure 3.17). DNA isolated from HBEC-2KT-CSC.L-2A was treated with methylase and included in the pyrosequencing experiments (this was the same positive control used by a fellow master student performing methyl-DNA immunoprecipitation (MeDIP)). There was observed an overall trend of high methylation, ranging from 90-100 %, at the different CpG sites, except for CpG 11 (44 %) in FOXA1_pyro1 (red point) and CpG 7 (80 %) in FOXA1_pyro2 (red point) assays. Also, in both FOXA2 assays there was observed an overall trend of high methylation percentages at the different CpG sites, except for some, which are considerably lower. In FOXA2_cpg1 assay CpG 3 (28 %) was remarkably lower than the other CpG sites. In FOXA2_TSS assay CpG's 1, 2, 10 and 15-17 were below 50 % and lower than the other CpG sites examined in this assay. This experiment has only been performed once, and should be repeated to confirm the results. In FOXA1_pyro1 at CpG 11 the software informs that the signals do not correspond to the reference sequence. For FOXA2_TSS, the same reasons were given for the red points, and in addition, the CpG's from 15-20 have high sum deviation in the variable positions. FOXA1_pyro2 and FOXA2_cpg1 assay was unsuccessful due to a notation of failed bisulfite conversion.

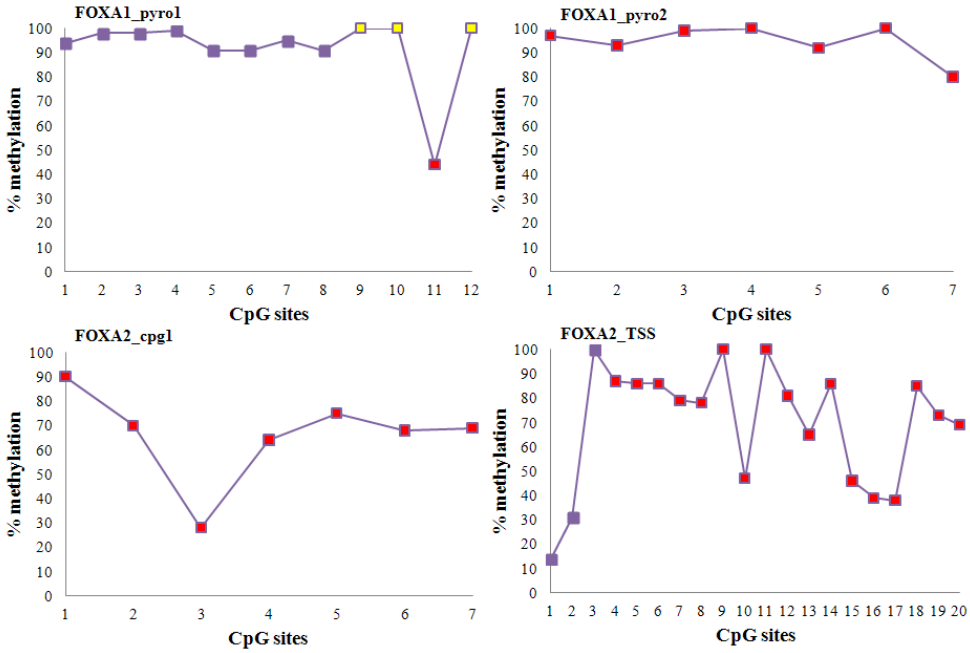

Figure 3.17: Methylation percentage in CpG sites in methylase-treated DNA (from HBEC-2KT-CSC.L-2A), across *FOXA1* (top) and *FOXA2* (bottom) genes. The location of the different assays is depicted in figure 3.16. PyroMark Q24 defines yellow squares as approved under doubt and red means the data is not approved. Blue is defined as approved and is here represented as the colour of the graph: purple.

Pyrosequencing results from HBEC-2KT derived cell lines

HBEC-2KT control cells (DMSO) (figure 3.18) showed an overall high methylation in all of the CpG sites in FOXA1_pyro1 assay ranging from 70-100 %, with the same decrease at CpG 11 as methylase-treated DNA. This particular site is not reliable due to red points in two repeated measurements. HBEC-2KT cells exposed to a low dose CSC (figures 3.19-3.22) showed varying degrees of methylation across the FOXA1_pyro1 CpG sites examined. Overall, the majority of the methylation percentages ranged between 35-90 %. There was a tendency towards lower methylation at CpG 4 (10-15 %) and 9 (15-25 %, except parallel 2A), and partly 8 (10-20 %) in 2B and 2D. These cells also showed lower methylation at CpG 11 compared with CpG sites close by. CpG 11 was a red data point for some of the parallels, as in many of the later analysis. HBEC-2KT exposed to a high dose CSC (figure 3.23) showed a general methylation percentage ranging from 70-100 % at CpG sites 1-5, 7 and 12 in FOXA1_pyro1 and 50 % methylation and below at CpG's 6 and 8-11.

In the FOXA1_pyro2 assay HBEC-2KT control cells (DMSO) (figure 3.18) and its transformed cells (figures 3.19-3.23) showed an overall high degree of methylation ranging from 80-100 %. All showed a tendency toward lower methylation in CpG 7 compared to

adjacent CpG sites. This was considered reliable in 9 out of 12 experiments with HBEC-2KT derived cell lines. HBEC-2KT-CSC.L showed methylation of approximately 70 % in CpG 4. CpG's 1 and 3 in HBEC-2KT-CSC.H also showed a trace of decreased methylation percentage in the range of 70-75 %. They were all considered reliable.

FOXA2_cpg1 assay showed an overall methylation below 10 % for transformed HBEC-2KT cell lines (figures 3.19-3.23) and the control cells (figure 3.18). There was a tendency toward increased methylation at CpG 6 to varying degrees compared with the overall methylation degree in the assay, expect one of the experiments with HBEC-2KT-CSC.H. The indicated increased methylation was considered reliable in 9 of 11 experiments. In HBEC-2KT-CSC.L-2D all of the sites were marked red and interpreted by PyroMark Q24 software as failed bisulfite conversion.

In the FOXA2_TSS assay there was an overall very low methylation percentage among HBEC-2KT control cells (DMSO) (figure 3.18) and transformed cells (figures 3.19-3.23), ranging from 0-30 % for control cells (DMSO) and cells exposed to low dose CSC. In contrast, cells exposed to high dose CSC had methylation varying from 0-50 %. Control cells (DMSO) showed a tendency to increased migration at the last CpG sites, but this cannot be considered valid due to red data points (CpG's 13-20) (some signals do not correlate with the references and also in some CpG sites there is high sum deviation in the variable position). Thus, in all of the following analysis, only the CpG's 1-12 were considered reliable in the analysis of FOXA2_TSS CpG sites. HBEC-2KT-CSC.L-2A showed a methylation of approximately 15 % at CpG 5 compared to methylation below 10 % for adjacent CpG's. CpG 6 in HBEC-2KT-CSC.L-2C showed a methylation of 26 %, but this is not considered reliable due to that two repeated experiments show 1-3 % methylation in the same CpG site. HBEC-2KT-CSC.H showed methylation varying from 0-36 % across the FOXA2_TSS assay. In CpG's 2 and 7 an increased methylation compared to adjacent CpG's was shown.

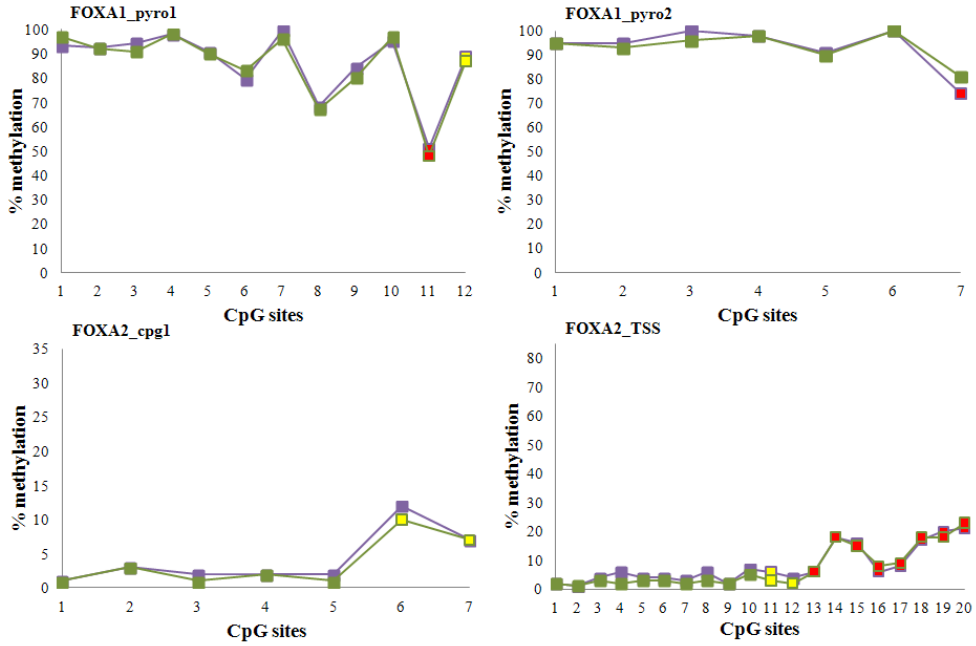

Figure 3.18: Methylation percentage in CpG sites in HBEC-2KT control cells (DMSO) across *FOXA1* (top) and *FOXA2* (bottom) genes. The location of the different assays is depicted in figure 3.16. The green and purple lines represent two independent bisulfite/pyrosequencing experiments on the same DNA sample. Yellow squares mean that the data from pyrosequencing are approved under doubt and red means the data is not approved. Blue is defined as approved and is here represented as the colour of the graphs: green and purple.

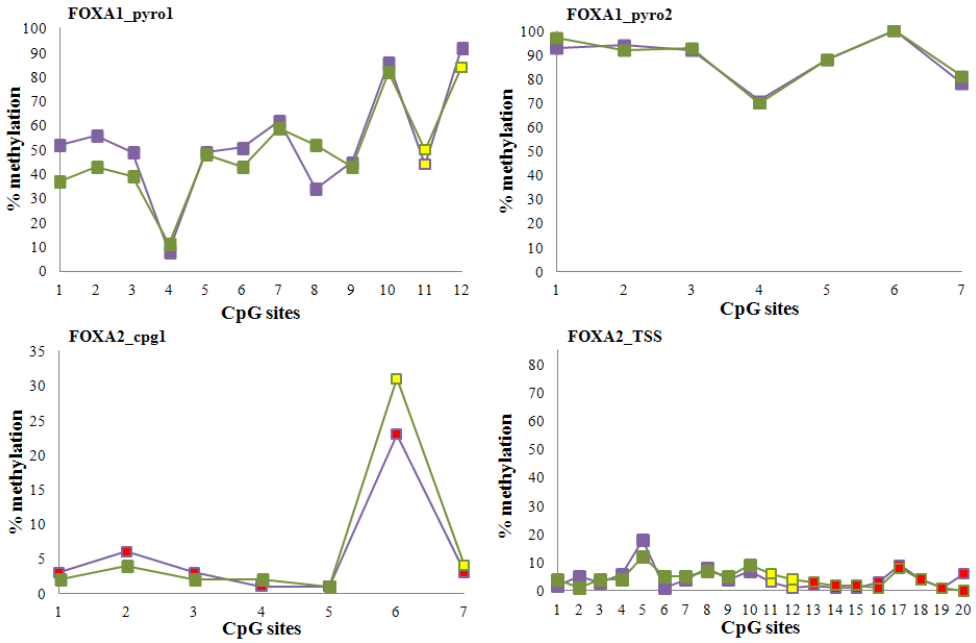

Figure 3.19: Methylation percentage in CpG sites in HBEC-2KT-CSC.L-2A across *FOXA1* (top) and *FOXA2* (bottom) genes. The location of the different assays is depicted in figure 3.16. The green and purple lines represent two independent bisulfite/pyrosequencing experiments on the same DNA sample. Yellow squares mean that the data from pyrosequencing are approved under doubt and red means the data is not approved. Blue is defined as approved and is here represented as the colour of the graphs: green and purple.

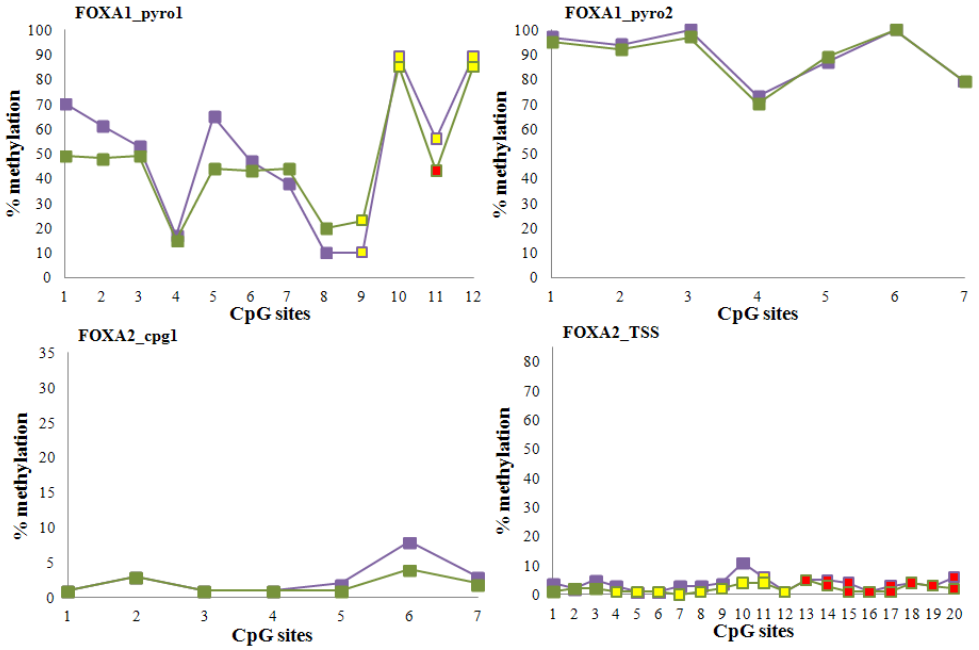

Figure 3.20: Methylation percentage in CpG sites in HBEC-2KT-CSC.L-2B across *FOXA1* (top) and *FOXA2* (bottom) genes. The location of the different assays is depicted in figure 3.16. The green and purple lines represent two independent bisulfite/pyrosequencing experiments on the same DNA sample. Yellow squares mean that the data from pyrosequencing are approved under doubt and red means the data is not approved. Blue is defined as approved and is here represented as the colour of the graphs: green and purple.

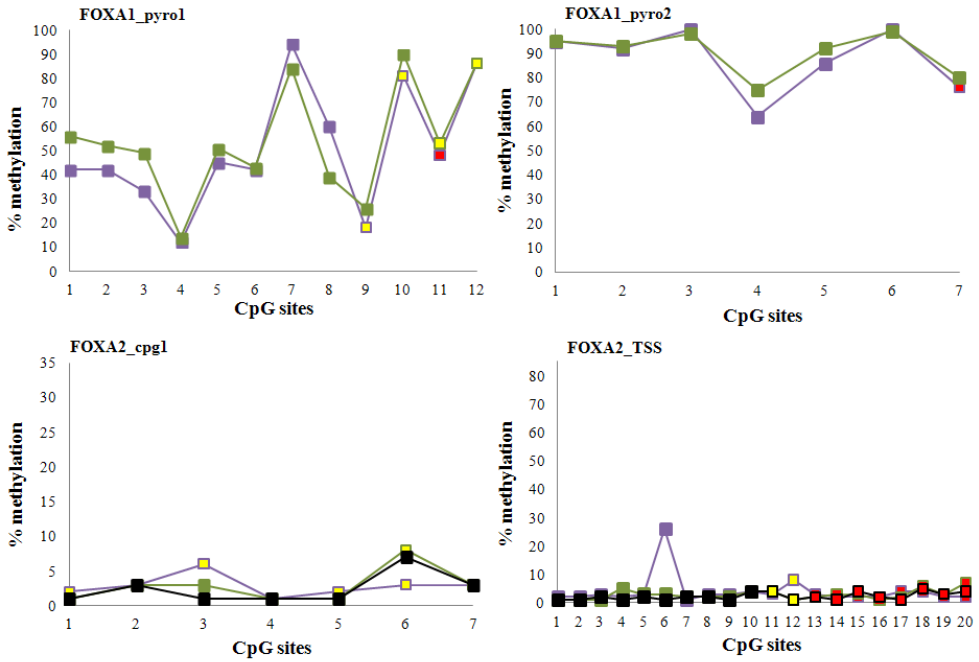

Figure 3.21: Methylation percentage in CpG sites in HBEC-2KT-CSC.L-2C across *FOXA1* (top) and *FOXA2* (bottom) genes. The location of the different assays is depicted in figure 3.16. The green, purple and black lines represent two independent bisulfite/pyrosequencing experiments on the same DNA sample. Yellow squares mean that the data from pyrosequencing are approved under doubt and red means the data is not approved. Blue is defined as approved and is here represented as the colour of the graphs: green, purple and black.

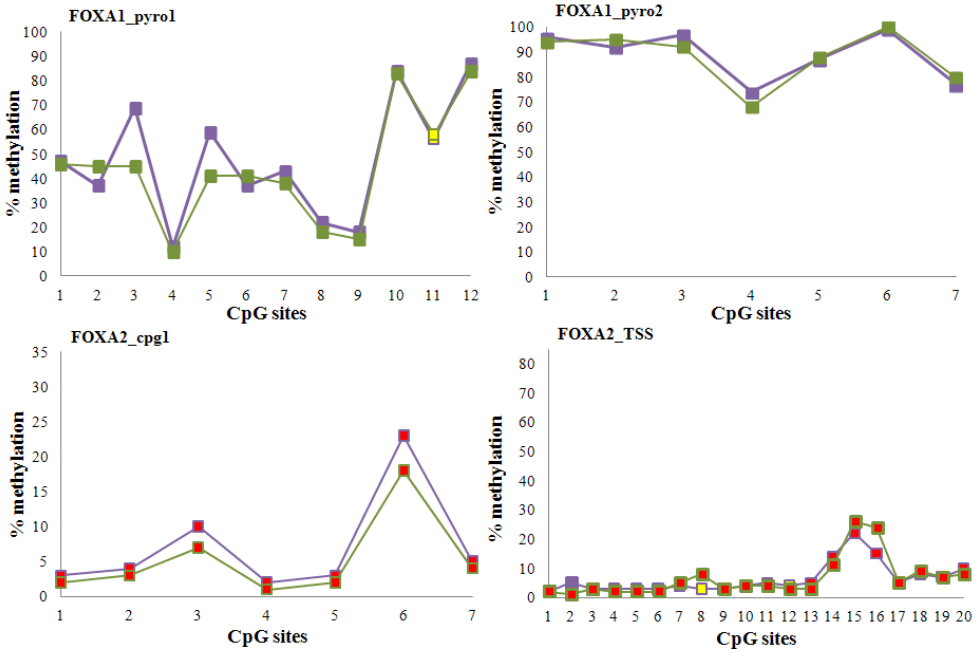

Figure 3.22: Methylation percentage in CpG sites in HBEC-2KT-CSC.L-2D across *FOXA1* (top) and *FOXA2* (bottom) genes. The location of the different assays is depicted in figure 3.16. The green and purple lines represent two independent bisulfite/pyrosequencing experiments on the same DNA sample. Yellow squares mean that the data from pyrosequencing are approved under doubt and red means the data is not approved. Blue is defined as approved and is here represented as the colour of the graphs: green and purple.

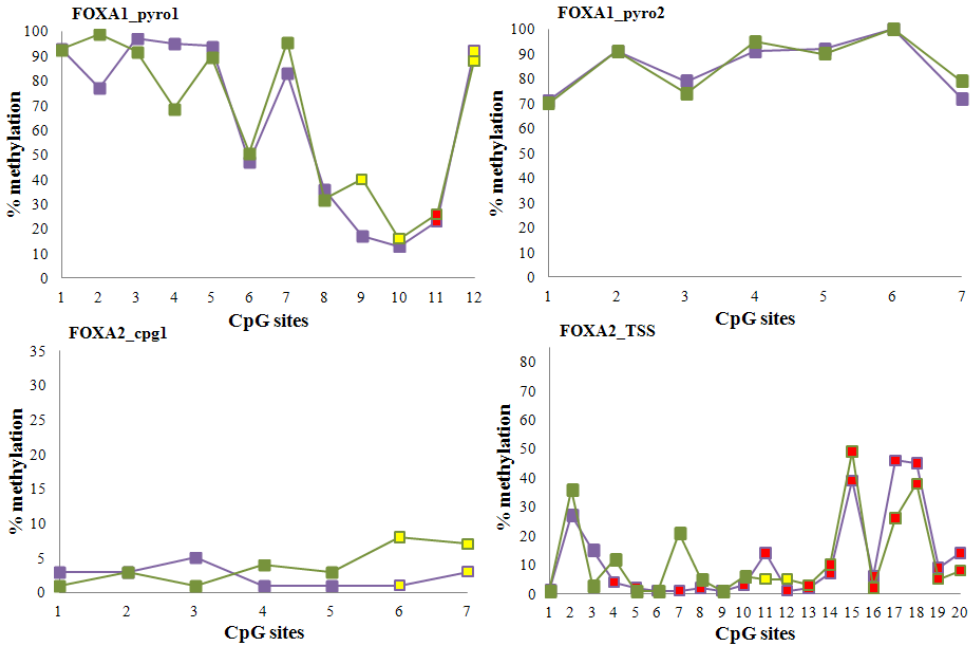

Figure 3.23: Methylation percentage in CpG sites in HBEC-2KT-CSC.H across *FOXA1* (top) and *FOXA2* (bottom) genes. The location of the different assays is depicted in figure 3.16. The green and purple lines represent two independent bisulfite/pyrosequencing experiments on the same DNA sample. Yellow squares mean that the data from pyrosequencing are approved under doubt and red means the data is not approved. Blue is defined as approved and is here represented as the colour of the graphs: green and purple.

Pyrosequencing results from HBEC-12KT derived cell lines

HBEC-12KT control cells (DMSO) (figure 3.24) and transformed cells (figures 3.25-3.33) also showed a high methylation percentage in the FOXA1_pyro1 assay, ranging from 70-100 %, except in HBEC-12KT-B[*a*]P.L where one of the experiments showed overall lower migration percentages than the other experiments. As for HBEC-2KT derived cell lines, all of the HBEC-12KT derived cell lines also show a lower methylation of about 50-55 % at CpG 11 (red point). HBEC-12KT control cells (DMSO), HBEC-12KT-CSC.L-A (figure 3.25), HBEC-12KT-CSC.H (figure 3.30), HBEC-12KT-B[*a*]P.L (figure 3.31) and HBEC-12KT-B[*a*]P.H (figure 3.32) all showed a tendency of decreased methylation at CpG 9. This is considered a valid data point as set by the PyroMark Q24 software.

FOXA1_pyro2 assay showed an overall methylation of 90-100 % in all of the transformed HBEC-12KT cell lines and their control cells (DMSO). At CpG 7 there was a tendency of decreased methylation to about 70-75 % for both control cells (DMSO) and transformed cells.

There was observed low levels of DNA methylation of all the transformed HBEC-12KT cell lines and their control cells (DMSO) in the FOXA2_cpg1 assay, ranging from 0-6 %. In addition, there was a tendency toward higher methylation in some of the sites, as CpG 3 in control cells (DMSO), CpG 6 in HBEC-12KT-CSC.L-B (3.26-3.29), HBEC-12KT-B[*a*]P.H and HBEC-12KT-MNU (one of the experiments), and CpG 2 in HBEC-12KT-CSC.H (though not valid in one of the parallels). These represented only a minor increase compared with the overall methylation.

The FOXA2_TSS assay showed fluctuating methylation across the CpG sites studied in HBEC-12KT control cells (DMSO) and their transformed cells. As for HBEC-2KT derived cell lines, there were also red data points at CpG's 13-20 in this assay for HBEC-12KT derived cell lines. Thus, in all of the following analysis of HBEC-12KT derived cell lines, only the CpG's 1-12 were considered in the analysis. The majority of the HBEC-12KT transformed cells lied at the same level as the control cells (DMSO), ranging from 20-50 % methylation. CpG 11 analysed in HBEC-12KT-CSC.L-B-2A, -2B and -2D showed above 70 % methylation. The same cell line's parallels 2A, 2B and 2C show methylation below 10 % at the first three CpG sites, and also CpG 4 in parallel 2A. Parallel 2D showed below 10 % methylation at CpG 3. HBEC-12KT-CSC.H also showed methylation below 10 % at CpG's 1,

2, 4 and 5. HBEC-12KT-B[*a*]P.L showed methylation below 10 % at CpG's 1, 2, 4 and one experiment in CpG 11, and HBEC-12KT-B[*a*]P.H at CpG's 1-4.

HBEC-12KT transformed with MNU (figure 3.34) showed different overall methylation percentage from the two independent experiments in the FOXA2_TSS assay; the results from the first experiment indicated about 20 % overall methylation, however there was red points at CpG's 4-12 due to that signals did not correlate with the reference. Results from the second experiment ranged from 30-45 % methylation. There seemed to be a tendency towards lower methylation at CpG's 1, 2 (in the first experiment), 3, 9, 11 and 12 compared to the other CpG's.

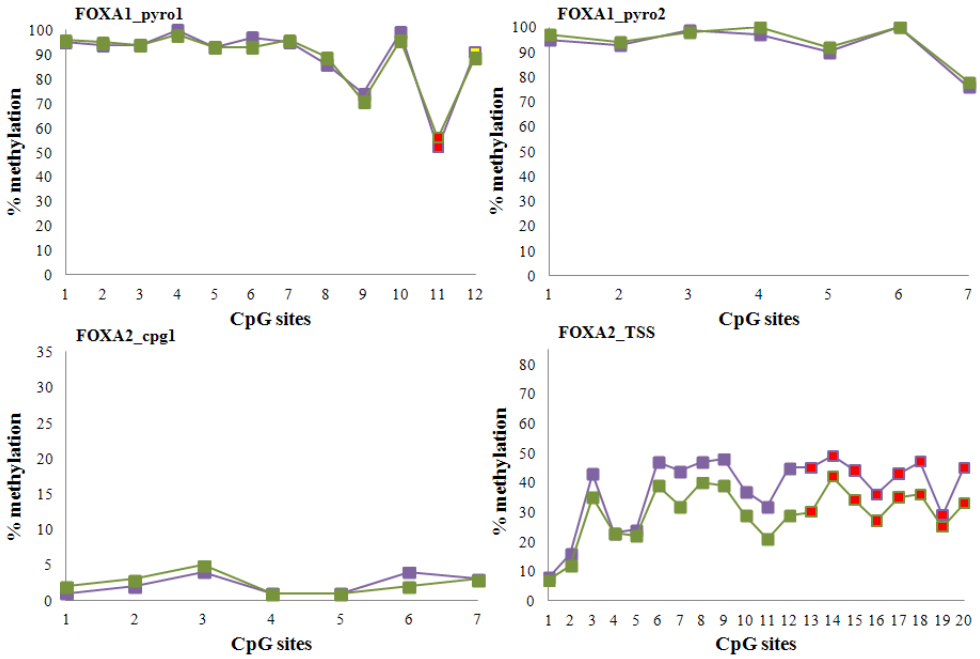

Figure 3.24: Methylation percentage in CpG sites in HBEC-12KT control cells (DMSO) across *FOXA1* (top) and *FOXA2* (bottom) genes. The location of the different assays is depicted in figure 3.16. The green and purple lines represent two independent bisulfite/pyrosequencing experiments on the same DNA sample. Yellow squares mean that the data from pyrosequencing are approved under doubt and red means the data is not approved. Blue is defined as approved and is here represented as the colour of the graphs: green and purple.

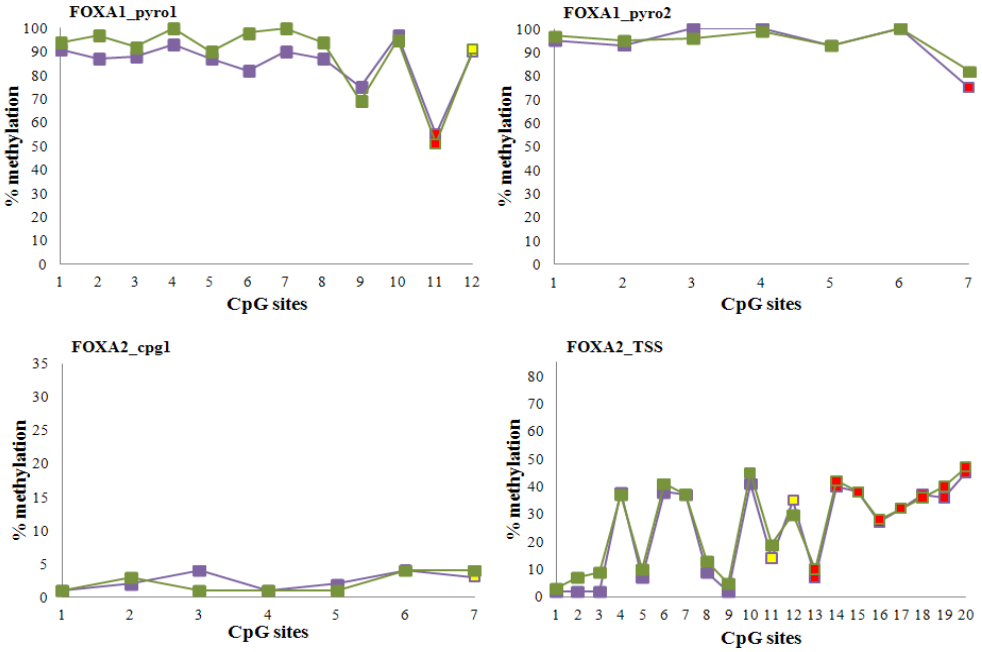

Figure 3.25: Methylation percentage in CpG sites in HBEC-12KT-CSC.L-A across *FOXA1* (top) and *FOXA2* (bottom) genes. The location of the different assays is depicted in figure 3.16. The green and purple lines represent two independent bisulfite/pyrosequencing experiments on the same DNA sample. Yellow squares mean that the data from pyrosequencing are approved under doubt and red means the data is not approved. Blue is defined as approved and is here represented as the colour of the graphs: green and purple.

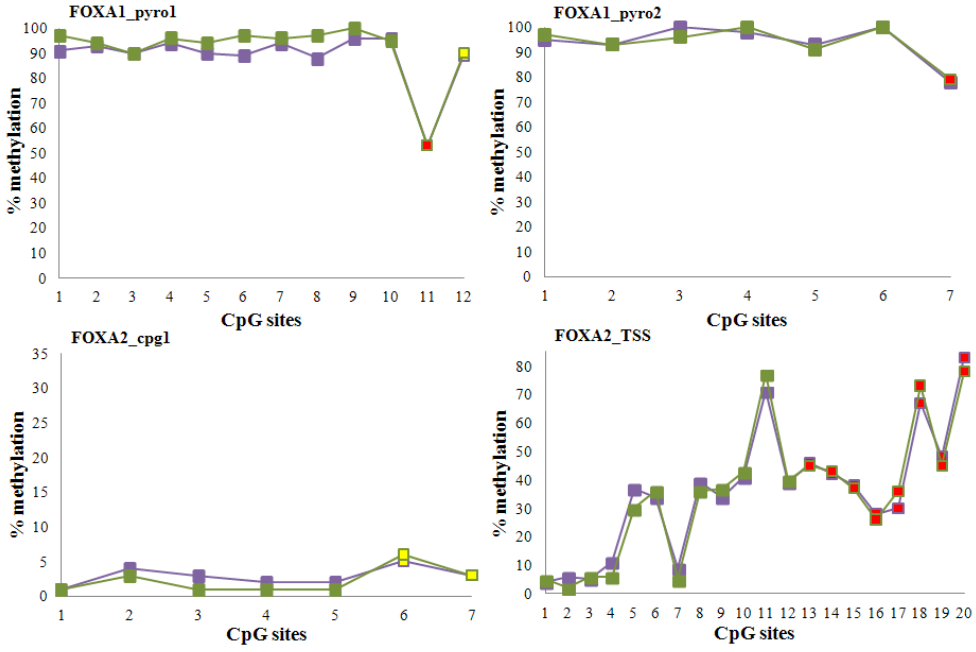

Figure 3.26: Methylation percentage in CpG sites in HBEC-12KT-CSC.L-B-2A across *FOXA1* (top) and *FOXA2* (bottom) genes. The location of the different assays is depicted in figure 3.16. The green and purple lines represent two independent bisulfite/pyrosequencing experiments on the same DNA sample. Yellow squares mean that the data from pyrosequencing are approved under doubt and red means the data is not approved. Blue is defined as approved and is here represented as the colour of the graphs: green and purple.

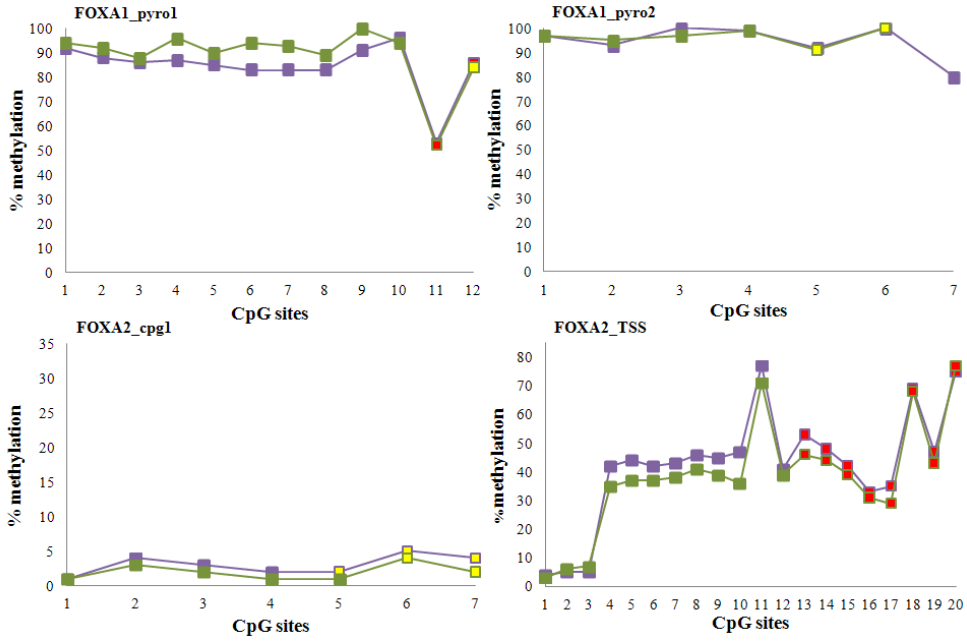

Figure 3.27: Methylation percentage in CpG sites in HBEC-12KT-CSC.L-B-2B across *FOXA1* (top) and *FOXA2* (bottom) genes. The location of the different assays is depicted in figure 3.16. The green and purple lines represent two independent bisulfite/pyrosequencing experiments on the same DNA sample. Yellow squares mean that the data from pyrosequencing are approved under doubt and red means the data is not approved. Blue is defined as approved and is here represented as the colour of the graphs: green and purple.

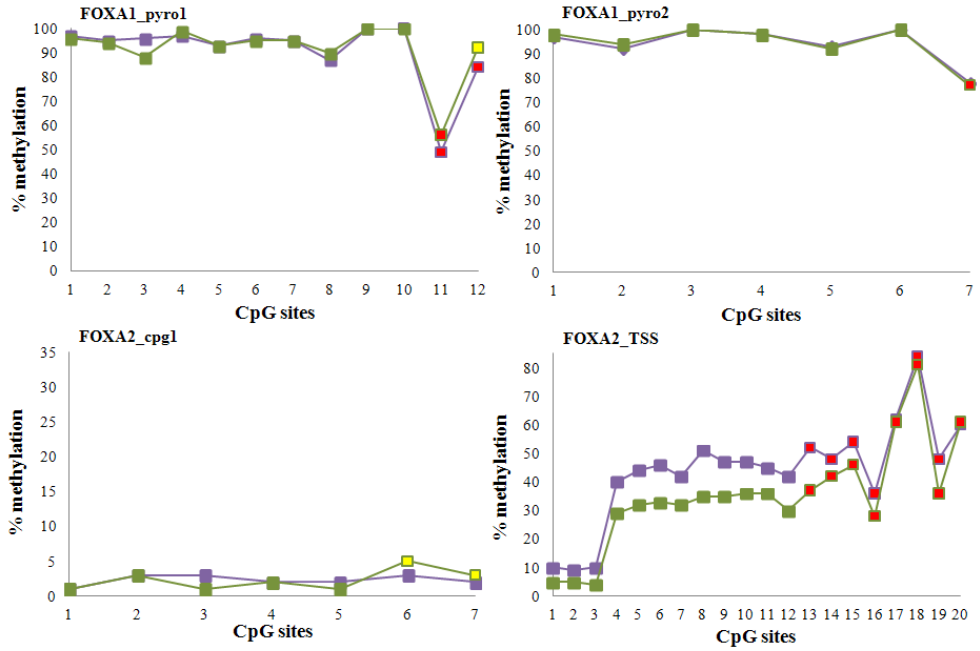

Figure 3.28: Methylation percentage in CpG sites in HBEC-12KT-CSC.L-B-2C across *FOXA1* (top) and *FOXA2* (bottom) genes. The location of the different assays is depicted in figure 3.16. The green and purple lines represent two independent bisulfite/pyrosequencing experiments on the same DNA sample. Yellow squares mean that the data from pyrosequencing are approved under doubt and red means the data is not approved. Blue is defined as approved and is here represented as the colour of the graphs: green and purple.

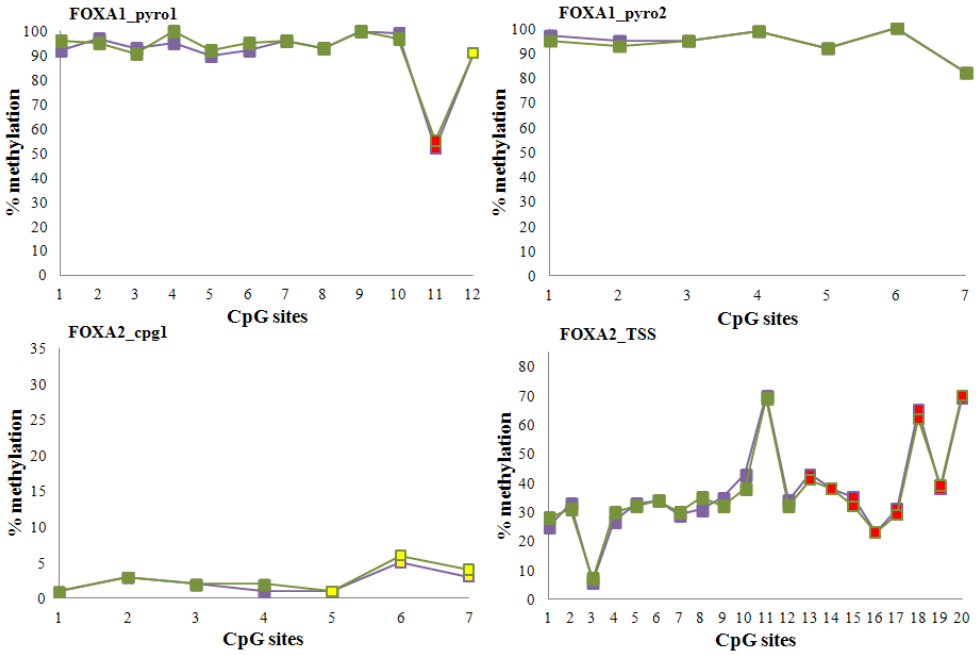

Figure 3.29: Methylation percentage in CpG sites in HBEC-12KT-CSC.L-B-2D across *FOXA1* (top) and *FOXA2* (bottom) genes. The location of the different assays is depicted in figure 3.16. The green and purple lines represent two independent bisulfite/pyrosequencing experiments on the same DNA sample. Yellow squares mean that the data from pyrosequencing are approved under doubt and red means the data is not approved. Blue is defined as approved and is here represented as the colour of the graphs: green and purple.

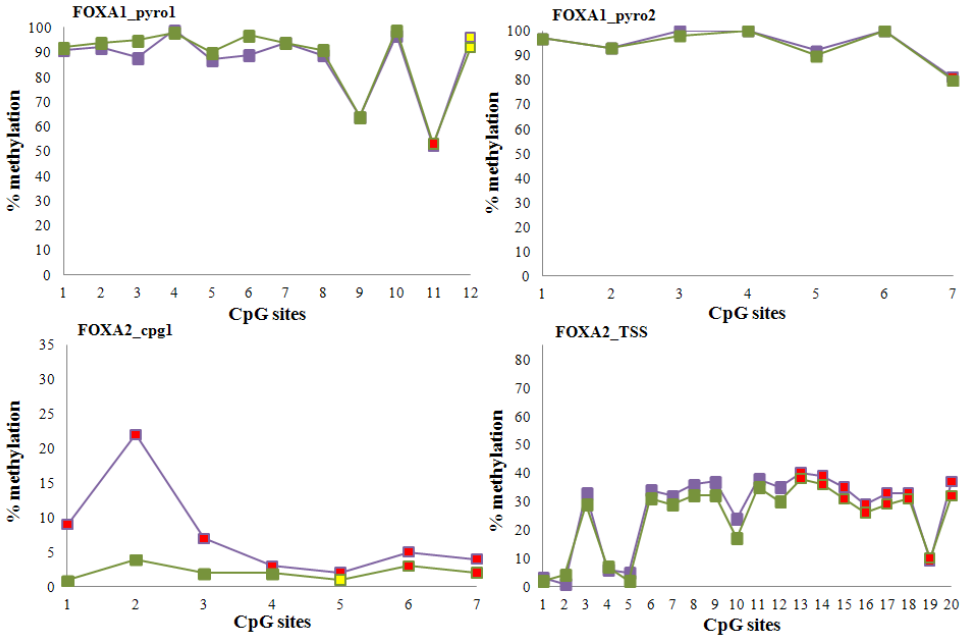

Figure 3.30: Methylation percentage in CpG sites in HBEC-12KT-CSC.H across *FOXA1* (top) and *FOXA2* (bottom) genes. The location of the different assays is depicted in figure 3.16. The green and purple lines represent two independent bisulfite/pyrosequencing experiments on the same DNA sample. Yellow squares mean that the data from pyrosequencing are approved under doubt and red means the data is not approved. Blue is defined as approved and is here represented as the colour of the graphs: green and purple.

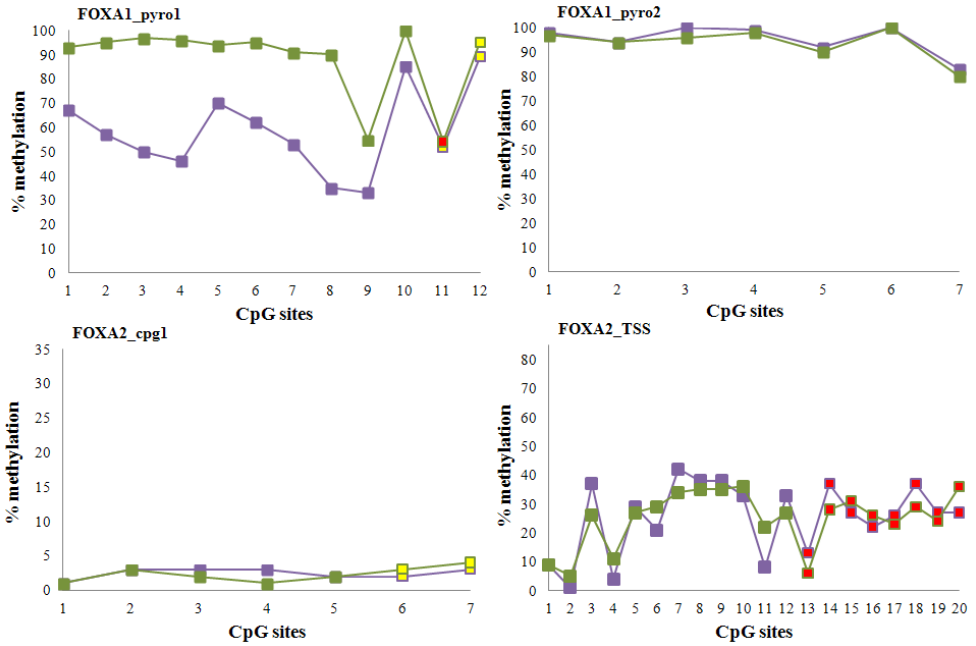

Figure 3.31: Methylation percentage in CpG sites in HBEC-12KT-B[*a*]P.L across *FOXA1* (top) and *FOXA2* (bottom) genes. The location of the different assays is depicted in figure 3.16. The green and purple lines represent two independent bisulfite/pyrosequencing experiments on the same DNA sample. Yellow squares mean that the data from pyrosequencing are approved under doubt and red means the data is not approved. Blue is defined as approved and is here represented as the colour of the graphs: green and purple.

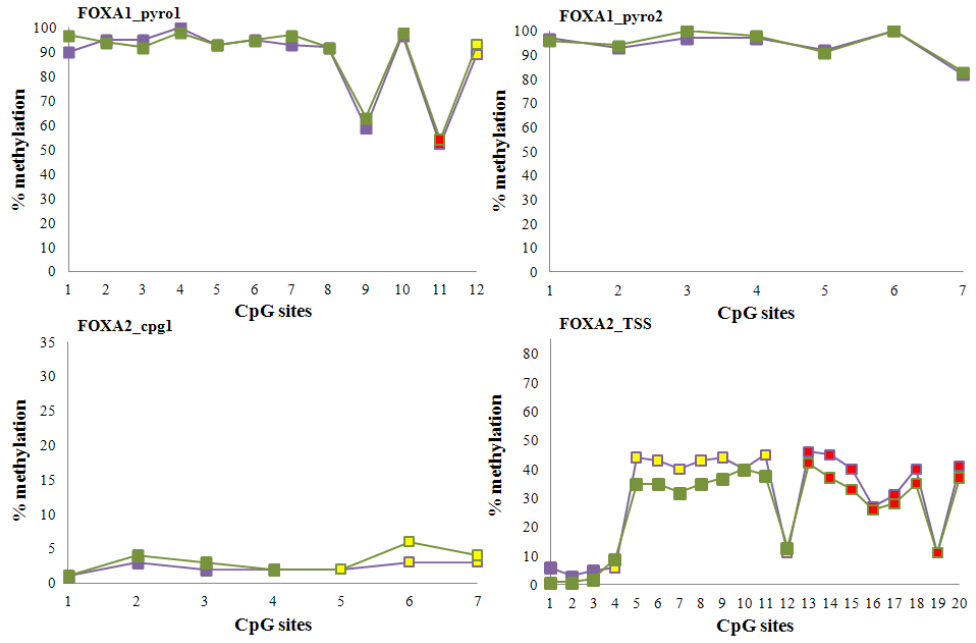

Figure 3.32: Methylation percentage in CpG sites in HBEC-12KT-B[*a*]P.H across *FOXA1* (top) and *FOXA2* (bottom) genes. The location of the different assays is depicted in figure 3.16. The green and purple lines represent two independent bisulfite/pyrosequencing experiments on the same DNA sample. Yellow squares mean that the data from pyrosequencing are approved under doubt and red means the data is not approved. Blue is defined as approved and is here represented as the colour of the graphs: green and purple.

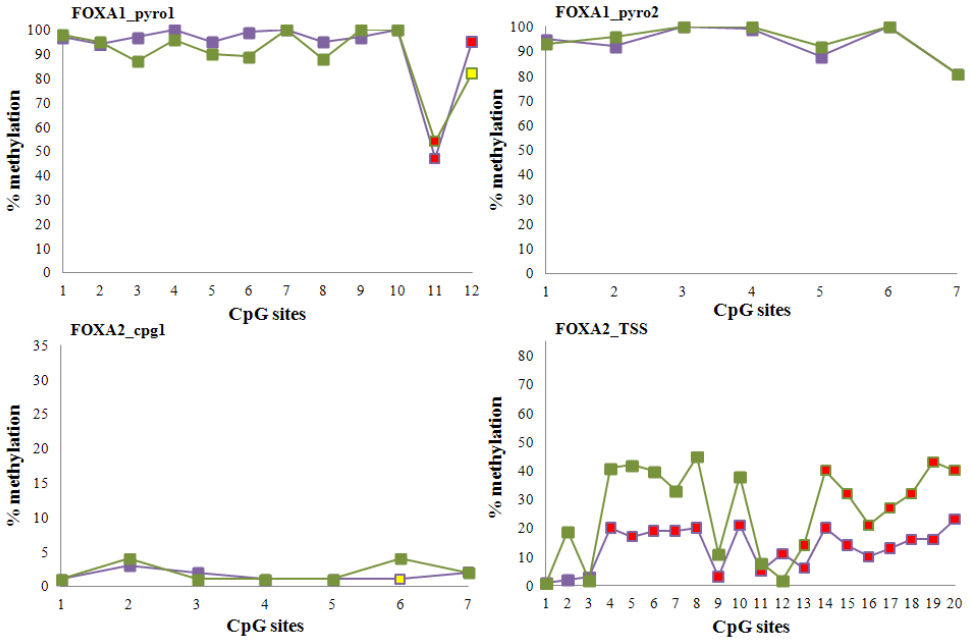

Figure 3.33: Methylation percentage in CpG sites in HBEC-12KT-MNU across *FOXA1* (top) and *FOXA2* (bottom) genes. The location of the different assays is depicted in figure 3.16. The green and purple lines represent two independent bisulfite/pyrosequencing experiments on the same DNA sample. Yellow squares mean that the data from pyrosequencing are approved under doubt and red means the data is not approved. Blue is defined as approved and is here represented as the colour of the graphs: green and purple.

To summarise the results, CpG 11 in FOXA1_pyro1 showed generally lower percentage methylation compared with the other CpG sites in that assay. However, CpG 11 in FOXA1_pyro1 was in general a red point, so according to PyroMark Q24 this was not valid. Further, FOXA1_pyro1 showed generally higher percentage methylation in both HBEC-12KT control cells (DMSO) and transformed cells, compared to HBEC-2KT derived cells where it was more fluctuating in methylation percentages. FOXA1_pyro2 assay generally showed a high degree of DNA methylation for all of the cell lines studied. In the CpG sites of FOXA2_cpg1 assay there was an overall low degree of DNA methylation in all the transformed HBEC-2KT and transformed HBEC-12KT, and their control cells (DMSO). This also applied to FOXA2_TSS in HBEC-2KT control cells (DMSO) and transformed cells. HBEC-12KT control cells (DMSO) and transformed cells showed more fluctuating methylation percentages in CpG sites in the FOXA2_TSS assay. Thus, no outstanding changes in DNA methylation were observed between non-transformed and transformed cell lines in the CpG sites studied.

4 Discussion

The aim of this study was to investigate characteristics of *in vitro* transformed HBEC derived cell lines to look into how various carcinogens can affect the cells migration capability and if methylation of CpG islands in the *FOXA1* and *FOXA2* genes might be able to explain their observed downregulation.

Immortalized HBEC derived cell lines used during this study are valuable tools for studying the multistage pathogenesis of lung cancer, and they offer several advantages. Especially the ability to genetically modify the cell lines, and study genetic and epigenetic alterations in lung cancer is invaluable. Also, immortalized cell lines do not have a finite replication potential as normal cells, due to shortening of telomeres, senescence and cell cycle arrest. The immortalized cells do not exhibit independent growth in soft agar, as studies show in section 3.2. In addition, the HBECs maintain an intact p53 checkpoint and stability of the genome is preserved (Gazdar et al., 2010; Ramirez et al., 2004).

However, there are limitations to using cell line models. It is important to keep in mind that genetic instability, selective growth advantages and lack of interaction with non-tumour components might influence the cell lines. Nevertheless, if cell lines with unlimited lifespan were not available, the knowledge of lung cancer would be much less advanced. It is important to keep in mind factors affecting the model, such as how well it resembles the original tumour, driver mutations and acquired differentiated properties during long term passage. Then, data can be interpreted from *in vitro* studies concerning lung pathogenesis (Gazdar et al., 2010).

4.1 Discussion of methods

4.1.1 Cell migration

Two methods have been used to study cell migration in this thesis: the manual *in vitro* scratch assay and a semi-automated technique using IncuCyte ZOOM. *In vitro* scratch assay is commonly chosen as method for cell migration analysis, due to its advantages: easy set-up and materials needed are available in any laboratory performing cell culturing. In addition the method does to some extend mimic the migration of cells *in vivo* (Liang et al., 2007). Here,

cells were seeded at a density of $5x10^5$ cells per well in a 6-well plate until a confluent layer of cells was formed. The wound was made using a pipette tip, and it was ensured that images were obtained from the exact same spot at 0 and 12 hours after wounding. Manually wounding with a pipette tip makes it challenging to ensure the same width of the wounds in every trial. Width of the wounds varied from approximately 1.3-3.3 mm. After images were achieved they were retouched to eliminate debris in the wound area. There are no indications that variations in wound width affected the results, as some cells with a wider wound in the cell monolayer showed higher migration percentages than some cells with a narrower wound, and conversely.

The CellProfiler software was used to analyse cell migration data acquired from the manual *in vitro* scratch assay. To develop a suitable pipeline for the purpose of the study, different algorithms were tested by trial and error approach. The fully developed pipeline is presented in appendix C. After image analysis and data processing the results obtained were inspected by eye to ensure the functioning of the pipeline. For example, migration percentages from HBEC-12KT control cells (DMSO) were ambiguous. A confluent layer of cells could be observed from the cell images (figure 3.11), but the software analysed some of it as no cells. An oversaturation of cells in the wound area appears to have occurred showing a higher cell density in the middle, which contributes to a higher intensity. As speckles (areas of increased intensity in relation to its immediate neighbourhood) were chosen as the features to identify in the CellProfiler software, the area surrounding the oversaturated wound was not included as "features", as it had lower intensity.

The assay could be improved by the use of alternative softwares for data processing, as CellProfiler mainly relies on image brightness (Glaß et al., 2012).

Cell migration was also analysed using the instrument IncuCyte ZOOM, which represents a semi-automated migration analysis. The method used is an extension and improvement of the scratch wound assay (Nelson et al., s.a.). One advantage of this method is the 96-well WoundMaker that creates smooth wounds of equal size. In addition there are markers at the ImageLock plates from Essen Biosciences, ensuring accurate imaging. Another advantage is that there is no need for retouching of images in the same way as with the *in vitro* scratch assay. Furthermore, the instrument automatically acquires images at set time intervals and

IncuCyte's integrated software enables quantification of the migration percentage straight after images have been acquired and gives opportunities for on-going analysis.

Migration above 100 % was observed for some cell lines. This might be due to the calculation method used. As mentioned in section 2.7.1, when using RWD, cell density in the wound area is measured relative to the cell density outside the wound area. But some cell lines, as for example HBEC-2KT control cells (DMSO), oversaturation of cells were observed in the wound area, together with small open spaces in the cell monolayer outside the wound area. Hence, the cell density inside the wound was greater than the cell density outside the wound, and hence migration percentages above 100 % were calculated.

Disadvantages with the use of IncuCyte ZOOM that might cause downstream errors in the results were experiences. Instrumental errors, such as rebooting of the instrument for various reasons caused lack of data points. Also, during wound making, the WoundMaker sometimes introduced errors by imperfect wounds. Care had to be taken to avoid air bubbles during washing procedures and addition of fresh media, as they were difficult to remove and might have affected the results in a negative way.

4.1.2 DNA methylation analysis

Existing methods for analysis of DNA methylation have advantages and disadvantages. For example, the desired precision (quantitative versus qualitative data), screening or in depth analysis, number of samples and DNA quality and quantity will influence the choice of technique. The methods vary in accuracy, sensitivity, reproducibility and types of bias (Dahl and Guldberg, 2003; Laird, 2010).

In this study, bisulfite treatment of DNA followed by pyrosequencing was the method of choice. Bisulfite sequencing has been rendered the most trustworthy method when it comes to identification of methylated cytosines in any sequence (Laird, 2010). Methods involving bisulfite treatment of DNA tends to be fairly accurate and reproducible. Compared with analyses using restriction endonucleases, methods relying on bisulphite treatment possess several advantages. Most importantly, the methylation status can be determined of virtually any CpG site in the genome. However, some sources of error exist, as incomplete bisulfite conversion of unmethylated cytosine to uracil, which may arise from incomplete denaturation

before bisulfite treatment or reannealing during conversion. To reduce the risk of reannealing the bisulfite reaction can be done in a thermocycler with repeated steps of heating. Besides that, overtreatment with bisulfite may degrade DNA, due to partial acid-catalysed depurination, and also lead to increased incidence of methylated cytosines converted to uracil. This will result in under-reporting of the methylation percentage. The incubation time also influences damage to template sequences. Four hour incubation with bisulfite has been reported to be sufficient for complete conversion (Dahl and Guldberg, 2003; Laird, 2010).

Bisulfite-treated DNA can be used directly in a standard PCR reaction and further sequence-analysed by for example pyrosequencing. Uracil (represent unmethylated cytosine) and thymine will be amplified as thymine, whereas 5'-methylcytosine will be amplified as cytosine (Dahl and Guldberg, 2003). The PCR procedure can be improved in various ways; one approach is by increasing the annealing temperature of the PCR reaction. After DNA has been bisulfite-treated, methylated DNA has a higher content of guanine and cytosine than unmethylated DNA, and this can favour secondary structures as hairpins (Shen et al., 2007). Sequence analysis of PCR products after bisulfite treatment is considered the gold standard for gene-specific methylation providing information about the methylation status of every cytosine within the target sequence (Dahl and Guldberg, 2003). Pyrosequencing can be used for quantitative determination of both global DNA methylation and gene-specific analyses.

Restriction endonucleases, with different sensitivity to cytosine methylation, can be used to study methylation changes within their recognition site. Methylation of specific cytosines will render the DNA sequence insensitive to cleavage by one enzyme, but not the other. Usually the enzymes *Hpa*II/*Msp*I are used, where both enzymes cleave CCGG sites, but only *Msp*I cleaves if internal cytosine is methylated. This makes these enzymes valuable tools for rapid DNA methylation analyses. When amplifying by PCR only the methylated sequence will result in PCR products. This method is suitable for a large number of samples, due to its simplicity, low cost and ease of interpretation. Limitations might be that this method only provides information about CpG's within the cleavage site, furthermore, there is a risk of false positives due to incomplete digestion (Dahl and Guldberg, 2003; Oakeley, 1999). Several techniques have now been developed whose strategy is to interact directly with methylated DNA. A simple approach based on direct immunoprecipitation of methylated DNA has been developed (MeDIP) where monoclonal antibodies against 5'-methylcytosine are used to purify methylated DNA. The methylation status can be further studied by the use of specific

primers for the desired gene section followed by PCR. This method of analysis is excellent when there are regions with high CpG density, as in CpG islands. In contrast, when analysing promoters low in CpG dinucleotides this technique may not be suitable (Jacinto et al., 2008).

Methylation-specific PCR takes benefit of the bisulfite-induced sequence difference in bisulfite-treated DNA. It is a widely used technique to investigate methylation status in specific CpG sites. Nevertheless, information obtained from this technique should be further validated by quantitative methods, and therefore methylation-specific PCR is best suited as a rapid technique to initially screen samples for methylation of specific genes (Dahl and Guldberg, 2003).

In the future, nanopore sequencing might be the next revolution in high-throughput DNA methylation analysis, and will eliminate the need for bisulfite treatment by offering a potential for direct sequencing of 5'-methylcytosine in DNA (Laird, 2010).

4.1.3 Assay design for pyrosequencing

Two assays in both the *FOXA1* gene (FOXA1_pyro1 and FOXA2_pyro2, figure 3.16) and the *FOXA2* gene (FOXA2_cpg1 and FOXA2_TSS, figure 3.16) were designed for this study. The regions were chosen in accordance with ENCODE, taken into account especially results from earlier methylation studies in various cell lines and the binding of transcription factors (figure 4.1 and 4.2). Further, a fellow master student at STAMI worked with MeDIP in a parallel thesis and we wanted the pyrosequencing assay to lie in the same areas so that the two approaches of examining DNA methylation could be compared. This was obtained for FOXA1_pyro1 and both FOXA2 assays. It was important to optimize the PCR conditions to ensure specific PCR products, especially the annealing temperature. For FOXA1_pyro1 and FOXA2_cpg1 the annealing step was set to 60 °C, whereas for FOXA1_pyro2 and FOXA2_TSS the temperature was 58.5 °C. The assays for the *FOXA1* gene are located upstream of the gene, possibly in an enhancer region (figure 4.1).

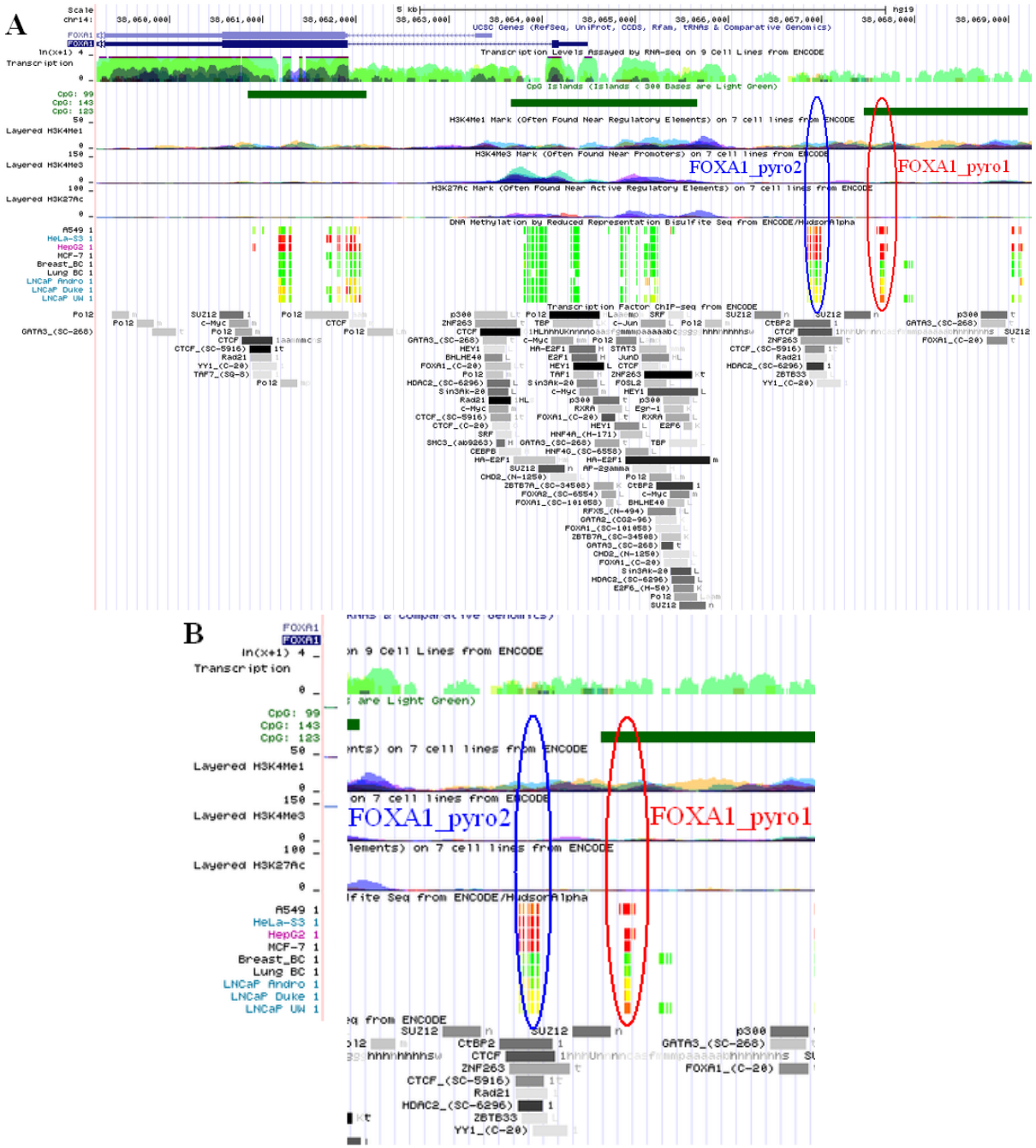

Figure 4.1: Localisation of FOXA1_pyro1 (red oval) and FOXA1_pyro2 (blue oval) assays represented by data from ENCODE (the gene, transcription levels, CpG islands (dark green lines), histone methylations, histone acetylation, methylation levels and transcription factor binding sites (grey)) is shown in A. In B there are zoomed in on the localisations of the assays. Both assays are located upstream of the gene. FOXA1_pyro1 is localized in a CpG island, whereas FOXA1_pyro2 is not. DNA methylation is represented by red (100 % of molecule sequences are methylated), yellow (50 %) or green (0 %).

FOXA1_pyro1 is located within a CpG island and there is proof of methylation in this area in A549 (human lung adenocarcinoma epithelial cell line), HepG2 (liver hepatocellular

carcinoma cells), MCF-7 (human breast adenocarcinoma cells) and LNCaP (lymph node carcinoma of the prostate). Thus, we wanted to examine this area in HBEC derived cell lines as well. FOXA1_pyro2 is not located in a CpG island, but by considering data from ENCODE, hypermethylation in this region has been reported for the cell lines A549, HeLa-S3 (human epithelial carcinoma cell line), HepG2 and MCF-7. Also, results indicate some methylation in LNCaP. Further, several transcription factor binding sites are shown to be located in this area via chromatin immunoprecipitation (ChIP) analyses. In both of the areas where the assays are located, normal breast and lung cells show no methylation, indicating that there might be a difference between cancer cells and normal cells.

Assays for the *FOXA2* gene also lie upstream of the gene (figure 4.2). FOXA2_cpg1 is located in a CpG island and there is several transcription factor binding sites in this area according to ENCODE data (figure 4.2). No methylation analyses are represented here in ENCODE. FOXA2_TSS is located immediately upstream of the gene in the promoter and is in a CpG island. According to ENCODE there is some indication of methylation in MCF-7 and many transcription factor binding sites (ChIP analyses). For the FOXA2_TSS assay, data from Basseres et al. (2012) was also considered. Results from this study indicated methylated CpG dinucleotides in various lung cancer cell lines in CpG's located in the area of the promoter.

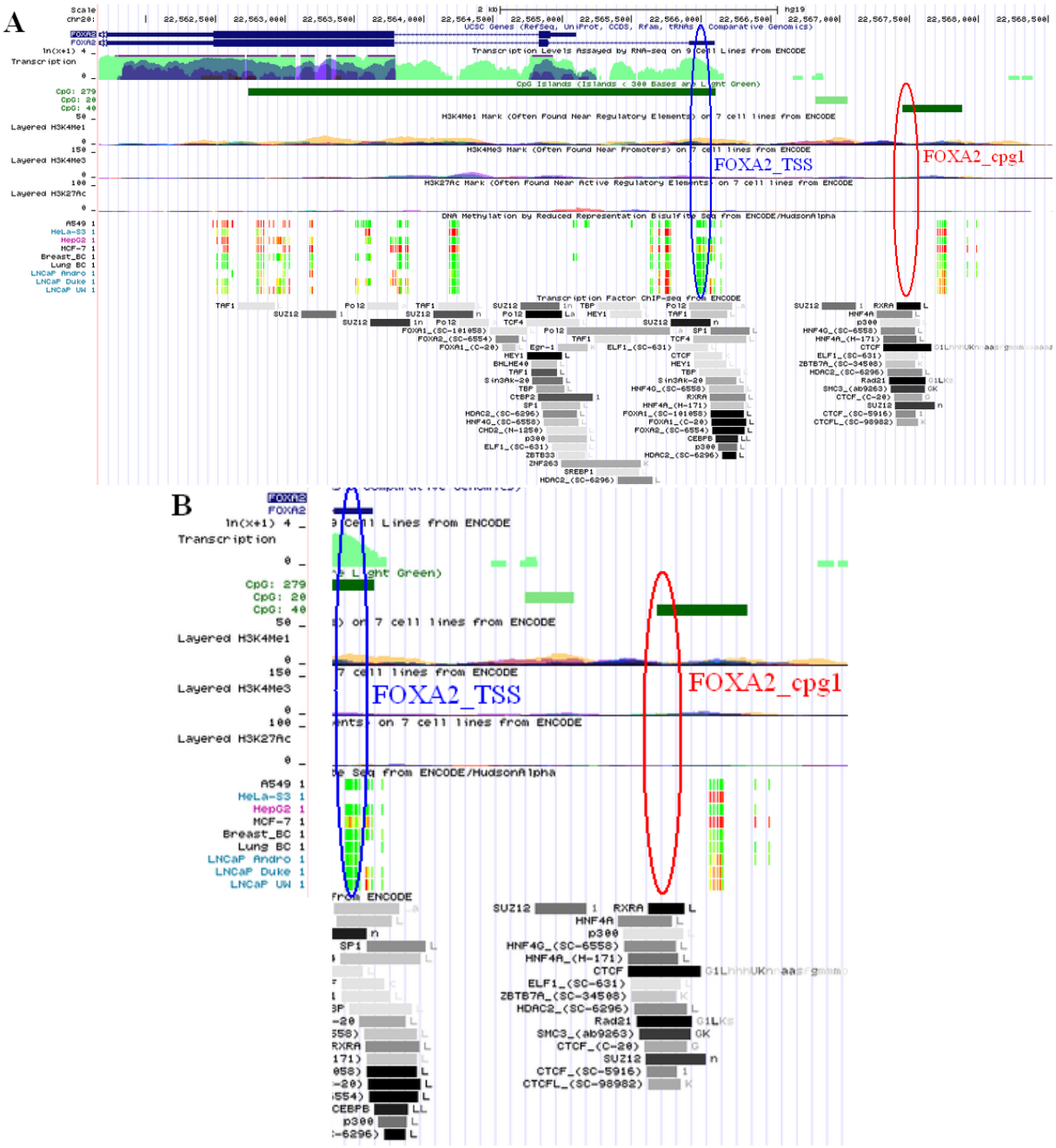

Figure 4.2: Localisation of FOXA2_cpg1 (red oval) and FOXA2_TSS (blue oval) assays represented by data from ENCODE (the gene, transcription levels, CpG islands (dark green lines), histone methylations, histone acetylation, methylation levels and transcription factor binding sites (grey)) is shown in A. In B there are zoomed in on the localisations of the assays. FOXA2_cpg1 is located upstream of the gene in a CpG island, whereas FOXA2_TSS lies around the promoter and also within a CpG island. DNA methylation is represented by red (100 % of molecule sequences are methylated), yellow (50 %) or green (0 %).

4.2 Discussion of results

Transformed cell lines (two from HBEC-2KT and six from HBEC-12KT) were established prior to this study. The cells had been exposed to various carcinogens over a time course of up to 15 weeks, followed by selection of colonies in soft agar. Hence, observed effects are results of earlier exposures that might have led to development of new, stable phenotypes. In addition, gene expression differences are expected to occur, which might be at least partly due to epigenetic mechanisms. Thus, methylation studies were conducted to investigate whether DNA methylation had a role in altered expression of the *FOXA1* and *FOXA2* genes in transformed cell lines.

Anchorage independent growth is an indication of carcinogen-induced transformation, and is confirmed by growth in soft agar. HBEC-12KT control cells (DMSO) and untreated HBEC-12KT did not form colonies in soft agar, which was also expected from earlier tests in our laboratory. HBEC-2KT control cells (DMSO) and untreated HBEC-2KT did not form colonies in soft agar either, as confirmed by earlier experiments (Damiani et al., 2008; Sjøberg, 2012). The soft agar assay selects for cells with acquired heritable changes, which would facilitate growth in the absence of attachment to a surface on the petri dish or flask (Freshney, 1987).

4.2.1 Cell migration

Cell migration is an important mechanism for tumour cells. By studying *in vitro* wound healing of transformed cells versus non-transformed cells one can get insight into how cell migration capacities are affected by various carcinogens. Untreated HBECs showed different migration characteristics across the two methods used to study cell migration. According to results by IncuCyte ZOOM, untreated HBEC-3KT migrated faster than untreated HBEC-2KT and untreated HBEC-12KT, the ladder two showing similar migration. Results from *in vitro* scratch assay indicated that untreated HBEC-2KT migrated faster than both untreated HBEC-3KT and untreated HBEC-12KT. The migration assays with untreated HBECs have only been done once, so this needs to be repeated to be able to draw solid conclusions. The HBECs originate from different donors, thus their gene expression profiles may vary due to different genetic and epigenetic factors. However, all the untreated HBECs show relatively high migration compared with transformed HBEC derived cell lines. This might be due to additives in the media, such as L-glutamine and serum. L-glutamine has been documented to

play an essential role during cell proliferation and enhance the function of immune cells. In addition L-glutamine is important during injury, and creating a wound in the cell monolayer mimics the healing process during for example injury, as the cells migrate to close the wound (Newsholme, 2001). Serum contains TGF-β, which might have a role in cell migration and invasion as changes in the microenvironment upon its activity favour cell migration and capillary formation (Derynck et al., 2001). TGF-β is also known to induce EMT, which again is involved in cell migration (Tang et al., 2011). Untreated HBECs were grown in serum-free media, so TGF-β cannot trigger their migration. However, control cells (DMSO) and transformed cells are grown in media supplemented with serum, which might contribute to their observed migration. Control cells (DMSO) tend to have a more rapid migration than untreated HBECs, which might indicate that TGF-β in serum may be related to the observed increased migration.

Transformed HBEC-2KT derived cell lines closed the wound approximately halfway during the 12-hour observation period, as was observed by both methods. HBEC-2KT control cells (DMSO) showed higher migration than the transformed cells when analysed by IncuCyte ZOOM, which is in contrast to data obtained from *in vitro* scratch assay, where migration by HBEC-2KT control cells (DMSO) apparently was much slower compared to transformed cell lines. However, these migration assays on HBEC-2KT control cells (DMSO) were only carried out once by *in vitro* scratch assay and thus it will be necessary to repeat the experiments on these cells to be able to draw solid conclusions. Also, due to equivocal results from the two migration analysis methods, further studies are needed to explain these results. HBEC-12KT control cells (DMSO) showed a more rapid migration compared to its transformed cell lines. Transformation of HBEC-12KT seemed to decrease the migration to varying degrees, as determined by both methods. Overall, the migration percentages of the HBEC-12KT transformed cells were in the range between 30-60 %. Migration of control cells (DMSO) was in the range between 85-100 %.

EMT is indicated to be a process in the development of cancer cells due to the acquired potential of invasion and metastasis. In a study from 2007, B[*a*]P was shown to induce EMT-related gene expression in A549 cells, which lead to a migratory phenotype (Yoshino et al., 2007). Previous short-time exposure studies indicated that higher concentrations of CSC inhibited wound closure in primary bronchial epithelial cells, whereas exposure to lower concentrations of CSC resulted in a significant increase in wound closure (Luppi et al., 2005).

A recent study indicated that CSC might silence the expression of genes involved in downregulation of EMT, which is characterised by increased cell migration (Veljkovic et al., 2011). It can, however, not be excluded that the observed changes in migration capacity among transformed cell lines in the present study also might be related to the selection process in soft agar. In addition, in our laboratory we have tested five different *in vitro* transformed cell lines (HBEC-2KT-CSC.L-2A, HBEC-2KT-CSC.H-2A, HBEC-12KT-CSC.L-A-2A, HBEC-12KT-CSC.H-2A, HBEC-12KT-B[*a*]P.H-2A) for growth in nude mice by subcutaneous injection (six mice per cell line). The mice have now been observed for five months and there are no signs on formation of tumours. This is in accordance with Damiani et al. (2008), and indicates that additional genetic and epigenetic alterations are required to facilitate tumour formation.

The transcription factors FOXA1 and FOXA2 are considered to be involved in carcinogenesis. Changes in their gene expression were observed with carcinogen-induced transformation. Thus, in previous experiments at STAMI the expression of several genes were observed to be altered upon transformation with B[*a*]P, CSC and MNU. A significant downregulation of *FOXA1*, *FOXA2* and *CDH1* genes was found in transformed cells compared to their control cells (DMSO). Contrary, an upregulation of the *CDH2* gene in transformed cells compared to its control cells (DMSO) was found. Downregulation of the *FOXA1* and *FOXA2* genes might indicate EMT. This includes hallmarks as gain of mesenchymal phenotype and increased migration. In addition, a switch from E-cadherin (*CDH1* gene) to N-cadherin (*CDH2* gene) is characteristic for EMT. The process of EMT is closely related to cancer progression, and has been observed in NSCLC (Byers et al., 2013; Guarino et al., 2007).

A observed change in phenotype from rounded, epithelial form of non-transformed cells to a more elongated shape of transformed cells was observed, consistent with EMT. However, our results did not confirm any increase in migration in the transformed cell lines compared to control cells (DMSO), except for in HBEC-2KT derived cell lines analysed by *in vitro* scratch wound. This suggests that not only EMT contributes to cell migration and also that transformation is not only dependent on EMT. Thus, other genetic and epigenetic changes might have been taking place in the transformed cell lines contributing to their overall diminished migration percentage compared to non-transformed cells. It is, however, clear that cell migration and EMT are not directly linked in this *in vitro* transformation model.

Oversaturation was observed for some cell lines during cell migration assays. This might indicate loss of contact inhibition, which is also observed in various types of cancer cells. Merlin is a protein that couples cell-surface adhesion molecules, as E-cadherin, to transmembrane receptor tyrosine kinases, as epidermal growth factor receptor. Hence, the adhesiveness of cadherin-mediated intercellular attachments is strengthened. In addition, Merlin sequesters growth factor receptors and limits their release of mitogenic signals (Hanahan and Weinberg, 2011). Oversaturation may also indicate that communication capabilities of the cells are lagging behind. Components of gap junctions are shown to induce cell contact growth inhibition via cell communication. Recent studies imply EMT-mediated loss of contact inhibition in hepatocarcinoma cells, indicating that cancer cells have the ability of oversaturation (Ke et al., 2008).

4.2.2 DNA methylation

Epigenetic mechanisms have been shown to be involved in carcinogenesis and DNA methylation analysis was carried out to study if hypermethylation was associated with the observed downregulation of the *FOXA1* and *FOXA2* genes in transformed cell lines. In the FOXA1_pyro1 assay, overall highly methylated DNA (above 70 %) was observed in transformed HBEC-12KT cell lines and their control cells (DMSO). However, DNA from HBEC-2KT derived cell lines showed varying methylation percentages in the CpG sites in this assay. Control cells (DMSO) and HBEC-2KT exposed to high dose CSC showed higher overall methylation than HBEC-2KT transformed by low dose CSC, where there in general was observed approximately 50 % methylation. However, HBEC-12KT-CSC.H showed a drop in DNA methylation in CpG's 8-11.

The CpG's studied in the FOXA1_pyro2 assay showed an overall high degree of methylation, above 70 %, in both transformed cell lines (HBEC-2KT and HBEC-12KT) and their control cells (DMSO). Methylation in both of the *FOXA1* regions studied has been indicated by previous studies in carcinoma cell lines as A549, HeLa-S3 (only in FOXA1_pyro2), HepG2 and MCF-7 (ENCODE). Correspondingly, methylation studies in normal breast and lung cells do not indicate methylation in these CpG sites. This suggests a difference between normal and carcinoma cell lines in the degree of methylation. However, in this study, control cells (DMSO) from both HBEC-2KT and HBEC-12KT derived cell lines showed an overall high

CpG methylation in *FOXA1*. Thus, it is difficult to draw conclusion on whether the measured methylation levels are responsible for the observed downregulation of *FOXA1*. In addition, it cannot be deduced whether DNA methylation is a result of transformation as non-transformed cell lines already had high methylation levels in the studied CpG sites.

An overall low DNA methylation was observed in FOXA2_cpg1 assay for both transformed cell lines (HBEC-2KT and HBEC-12KT) and their control cells (DMSO). According to ENCODE, no methylation data for this region has been reported yet. The CpG sites studied in the FOXA2_TSS assay in DNA from both transformed HBEC-2KT and control cells (DMSO) showed overall methylation levels below 50 %. DNA from transformed HBEC-12KT and their control cells (DMSO) showed overall methylation levels between 20-50 % in the FOXA2_TSS assay. For HBEC-12KT-CSC.L-B, more than 70 % methylation in three of four colonies was observed in CpG 11 of the FOXA2_TSS assay. This might contribute to the observed downregulation of *FOXA2* in the cell line, as this increase in methylation was not observed in the control cells (DMSO). In this region methylation has been observed in MCF-7 cells (ENCODE). However, only minor or no DNA methylation in A549 and HepG2 has been observed. *FOXA2* gene expression was downregulated despite no outstanding differences in DNA methylation between transformed and non-transformed cells. Thus, it might be speculated that DNA methylation in the inspected sites are not involved in gene silencing. In addition, there are many factors contributing to the regulation of gene expression, as transcription factors, miRNA, cell signalling, mRNA splicing and degradation (Chen and Rajewsky, 2007). Several studies indicate that hypermethylation at CpG islands in promoter has important roles in the progression of cancer and it is considered to be a common hallmark of many types of cancer. Methylation at CpG islands may lead to repression of normal functions (Esteller, 2007). It was found that the *FOXA2* gene was methylated in two out of five transformed cell lines (Damiani et al., 2008). A study from 2012 showed that 48 % of the studied NSCLC cell lines had more than 10 % CpG dinucleotide hypermethylation in the FOXA2 promoter, and an inverse correlation between absence of FOXA2 mRNA or FOXA2 protein and degree of hypermethylation was observed (Basseres et al., 2012).

Generally, for the FOXA2_TSS assay there was red colour code for CpG's 13-20 after analyses by the PyroMark Q24 software, and thus, these data points were not considered in the analyses. The instrument does a quality assessment and gives the CpG's a colour code, as explained in section 2.10.6. Red indicates that the data are not approved. When inspecting the

results in the PyroMark Q24 software the red points at CpG's 13-20 was due to signals that did not correlate with the expected references. Also, high sum deviation in the variable position was observed in some CpG sites. This might be related to incorrect incorporation of bases by DNA polymerase, due to the length of this assay (337 bp's). According to the PyroMark PCR Handbook (2009) amplicons for CpG assays should ideally be shorter than 200 bp's. The amplicons for FOXA1_pyro1 and FOXA2_cpg1 were also longer than 200 base pairs (264 and 251 bp's, respectively), but in those cases that did not appear to interfere significantly with the quality of the data. An obvious further improvement would be to design a new sequencing primer situated a couple of CpG sites before CpG 13 in the FOXA2-TSS assay to be able to study DNA methylation levels in the remaining part of the region. This work is ongoing in the lab.

In the present study, the whole procedure of bisulfite treatment of DNA followed by pyrosequencing for quantification of DNA methylation was repeated twice on all samples. Overall, a high degree of consistency between the data from the two independent analyses was observed.

In a parallel master thesis MeDIP was used to assess the degree of methylation in the *FOXA1* and *FOXA2* genes. In general, experiments with MeDIP resulted in overall lower methylation percentages compared with results obtained by pyrosequencing. Theoretically, there can be various reasons for the observed difference between the methods. First, it might be due to failed bisulfite treatment. However, this appears not to be the case in this present study as controls for bisulfite conversion are included and insufficient conversion would have resulted in red colour code. Second, differences could have been due to overtreatment with bisulfite. However, this would have lead to DNA damage and reduced or no PCR products, so this is also not a likely explanation for the differences across the two methods. Last, it might be related to positioning of the primers. Assays for FOXA1_pyro1 and FOXA1_C1 (MeDIP) overlap, so a big difference in methylation percentages would not be expected. However, FOXA1_pyro1 indicated high methylation as observed from pyrosequencing results, and this area also stood out in MeDIP analyses. This might indicate that the CpG's studied in FOXA1_pyro1 has higher methylation than the other CpG's examined.

The FOXA2_cpg1 assay is located close to the FOXA2_C1 assay (MeDIP) and they are placed in the same CpG island. The FOXA2_TSS assay is located in the same CpG island as

the FOXA2_C3 assay (MeDIP). Hence, similar results could have been expected. Results from pyrosequencing showed an overall lower methylation in the CpG sites within *FOXA2* compared with *FOXA1*. Results from MeDIP analyses indicated higher methylation in the FOXA2_C1 assay compared to other CpG regions. In the FOXA2_cpg1 assay analysed by pyrosequencing results indicated less than 10 % DNA methylation in this area, which was lower than other CpG's studied. Only HBEC-2KT-CSC.L-2B showed higher levels of methylation in the FOXA2_C3 assay compared to the other cell lines. Results from pyrosequencing in FOXA2_TSS indicated low DNA methylation for all the studies cell lines. It might be difficult to compare pyrosequencing and MeDIP considering methylation levels, as MeDIP results showed rather low methylation values. It is, along with MeDIP results, difficult to draw any conclusions for alterations in methylation between transformed and non-transformed cell lines. This is rather unexpected especially regarding FOXA2, as Basseres et al. (2012) presented results suggesting that DNA methylation is correlated with downregulation of FOXA2 in lung tumours.

4.2.3 Future work

For future work, it would be interesting to perform gene expression analyses of DNMTs in the HBEC derived cell lines. DNMT1 has shown to be overexpressed in several cancers, including lung. Also, DNMT3a and 3b have shown to be overexpressed in tumours, and cooperates with DNMT1 (Damiani et al., 2008). Furthermore, it would be interesting to investigate whether cell adhesion genes are methylated during carcinogen-induced transformation of HBEC derived cell lines used in this study. Methylation of for example E-cadherin has been observed in bronchial epithelial cells from smokers. Consequently, demethylation strategies might improve primary cancer prevention in smokers (Damiani et al., 2008).

Additionally, it could be relevant to go into more detail about what other factors than DNA methylation that can contribute to alterations in expression of the *FOXA1* and *FOXA2* genes in the HBEC derived cell lines. Subjects of such studies could be transcription factors, cell signalling and microRNAs.

5 Conclusion

The aims of this study were to investigate mechanisms involved in development of lung cancer. The first aim was to investigate how *in vitro* transformation by tobacco smoke carcinogens affected cell migration, and the second aim was to investigate whether DNA methylation could explain the downregulation of the *FOXA1* and *FOXA2* genes in transformed cell lines.

Cell migration was shown to both decrease and increase in transformed cell lines relative to its control cells (DMSO). Two methods were used to study cell migration: the manual *in vitro* scratch assay and a semi-automated technique using IncuCyte ZOOM. However, it is clear that cell migration and EMT are not directly linked in this *in vitro* transformation model even though previous gene expression analyses indicated cadherin switch. Nevertheless, transformation of HBECs with tobacco-related carcinogens was shown to induce changes in cell migration.

It might be speculated that the inspected sites in the *FOXA1* gene not are involved in gene silencing since control cells express the gene despite high levels of methylation. Further, no outstanding alterations in DNA methylation in CpG sites were detected between non-transformed and transformed cell lines. Consequently, it cannot be concluded whether DNA methylation caused the observed downregulation of the *FOXA1* and *FOXA2* genes in this *in vitro* transformation model.

References

Ambros V. (2004) The functions of animal microRNAs. *Nature* 431: 350-355.

Ananthakrishnan R and Ehrlicher A. (2007) The forces behind cell movement. *International journal of biological sciences* 3: 303-317.

Aran D, Toperoff G, Rosenberg M, et al. (2011) Replication timing-related and gene body-specific methylation of active human genes. *Human molecular genetics* 20: 670-680.

Avner P and Heard E. (2001) X-chromosome inactivation: counting, choice and initiation. *Nature Reviews Genetics* 2: 59-67.

Barbas CF, Burton DR, Scott JK, et al. (2007) Quantitation of DNA and RNA. *Cold Spring Harbor Protocols* 2.

Basseres DS, D'Alò F, Yeap BY, et al. (2012) Frequent downregulation of the transcription factor Foxa2 in lung cancer through epigenetic silencing. *Lung cancer* 77: 31-37.

Bertram JS. (2001) The molecular biology of cancer. *Molecular Aspects of Medicine* 21: 167-223.

Brambilla E and Lantuejoul S. (2008) Histopathology of lung tumours. In: Hansen H (ed) *Textbook of Lung Cancer.* Informa Healthcare, 61-74.

Byers LA, Diao L, Wang J, et al. (2013) An Epithelial–Mesenchymal Transition Gene Signature Predicts Resistance to EGFR and PI3K Inhibitors and Identifies Axl as a Therapeutic Target for Overcoming EGFR Inhibitor Resistance. *Clinical Cancer Research* 19: 279-290.

Cantral DE, Sisson JH, Veys T, et al. (1995) Effects of cigarette smoke extract on bovine bronchial epithelial cell attachment and migration. *American Journal of Physiology - Lung Cellular and Molecular Physiology* 268: 723-728.

Carpenter AE, Jones TR, Lamprecht MR, et al. (2006) CellProfiler: image analysis software for identifying and quantifying cell phenotypes. *Genome biology* 7: 1-11.

Chen K and Rajewsky N. (2007) The evolution of gene regulation by transcription factors and microRNAs. *Nature Reviews Genetics* 8: 93-103.

Colella S, Shen L, Baggerly K, et al. (2003) Sensitive and quantitative universal Pyrosequencing™ methylation analysis of CpG sites. *Biotechniques* 35: 146-151.

Croce CM. (2008) Oncogenes and cancer. *New England journal of medicine* 358: 502-511.

Dahl C and Guldberg P. (2003) DNA methylation analysis techniques. *Biogerontology* 4: 233-250.

Damiani LA, Yingling CM, Leng S, et al. (2008) Carcinogen-Induced Gene Promoter Hypermethylation Is Mediated by DNMT1 and Causal for Transformation of Immortalized Bronchial Epithelial Cells. *Cancer research* 68: 9005-9014.

De Craene B and Berx G. (2013) Regulatory networks defining EMT during cancer initiation and progression. *Nature* 13: 97-110.

Debeir O, Adanja I, Kiss R, et al. (2008) Models of cancer cell migration and cellular imaging and analysis. In: Lambrechts A and Ampe C (eds) *The Motile Actin System in Health and Disease.* 123-156.

DeMarini DM. (2004) Genotoxicity of tobacco smoke and tobacco smoke condensate: a review. *Mutation research* 567: 447-474.

Derynck R, Akhurst RJ and Balmain A. (2001) TGF-β signaling in tumor suppression and cancer progression. *Nature genetics* 29: 117-129.

Deutsch L, Wrage M, Koops S, et al. (2012) Opposite roles of FOXA1 and NKX2‐1 in lung cancer progression. *Genes, Chromosomes and Cancer* 51: 618-629.

Dupont J-M, Tost J, Jammes H, et al. (2004) De novo quantitative bisulfite sequencing using the pyrosequencing technology. *Analytical Biochemistry* 333: 119-127.
England R and Pettersson M. (2005) Pyro Q-CpG™: quantitative analysis of methylation in multiple CpG sites by Pyrosequencing®. *Nature Methods* 3: 1-2.
Esteller M. (2007) Cancer epigenomics: DNA methylomes and histone-modification maps. *Nature Reviews Genetics* 8: 286-298.
Faustman-Watts EM and Goodman JI. (1984) DNA-purine methylation in hepatic chromatin following exposure to dimethylnitrosoamine or methylnitrosourea. *Biochemical Pharmacology* 33: 585-590.
Freshney RI. (1987) *Culture of Animal Cells: A Manual of Basic Technique,* Wiley-Liss.
Friedl P and Wolf K. (2003) Tumour-cell invasion and migration: Diversity and escape mechanisms. *Nature* 3: 362-374.
Gazdar AF, Gao B and Minna JD. (2010) Lung cancer cell lines: Useless artifacts or invaluable tools for medical science? *Lung cancer* 68: 309-318.
Glaß M, Möller B, Zirkel A, et al. (2012) Cell migration analysis: Segmenting scratch assay images with level sets and support vector machines. *Pattern Recognition* 45: 3154-3165.
Gravdal K, Halvorsen OJ, Haukaas SA, et al. (2007) A Switch from E-Cadherin to N-Cadherin Expression Indicates Epithelial to Mesenchymal Transition and Is of Strong and Independent Importance for the Progress of Prostate Cancer. *Clinical Cancer Research* 13: 7003-7011.
Guarino M, Rubino B and Ballabio G. (2007) The role of epithelial-mesenchymal transition in cancer pathology. *Pathology* 39: 305-318.
Hanahan D and Weinberg RA. (2000) The Hallmarks of Cancer. *Cell* 100: 57-70.
Hanahan D and Weinberg RA. (2011) Hallmarks of cancer: the next generation. *Cell* 144: 646-674.
Haugen A and Mollerup S. (2008) Etiology of lung cancer. In: Hansen H (ed) *Textbook of Lung Cancer.* Informa Healthcare, 1-9.
Hazan RB, Phillips GR, Qiao RF, et al. (2000) Exogenous Expression of N-Cadherin in Breast Cancer Cells Induces Cell Migration, Invasion and Metastasis. *The Journal of Cell Biology* 148: 779-790.
Hazan RB, Qiao R, Keren R, et al. (2004) Cadherin Switch in Tumor Progression. *Annals of the New York Academy of Sciences* 1014: 155-163.
Hecht SS. (2012a) Lung carcinogenesis by tobacco smoke. *International Journal of Cancer* 131: 2724-2732.
Hecht SS. (2012b) Research Opportunities Related To Establishing Standards for Tobacco Products Under the Family Smoking Prevention and Tobacco Control Act. *Nicotine & Tobacco Research* 14: 18-28.
Hellermann GR, Nagy SB, Kong X, et al. (2002) Mechanism of cigarette smoke condensate-induced acute inflammatory response in human bronchial epithelial cells. *Respiratory research* 3: 22-30.
IARC. (1978) IARC Monographs on the Evaluation of Carcinogenic Risks to Humans - Some N-Nitroso Compounds. *IARC* 17: 227.
Jacinto FV, Ballestar E and Esteller M. (2008) Methyl-DNA immunoprecipitation (MeDIP): Hunting down the DNA methylome. *Biotechniques* 44: 35-43.
Jemal A, Bray F, Center MM, et al. (2011) Global cancer statistics. *CA: a cancer journal for clinicians* 61: 69-90.
Jinn Y, Ichioka M and Marumo F. (1998) Expression of connexin32 and connexin43 gap junction proteins and E-cadherin in human lung cancer. *Cancer letters* 127: 161-169.

Jjingo D, Conley AB, Soojin VY, et al. (2012) On the presence and role of human gene-body DNA methylation. *Oncotarget* 3: 462-474.
Jones PA and Baylin SB. (2002) The fundamental role of epigenetic events in cancer. *Nature Reviews Genetics* 3: 415-428.
Kanwal R and Gupta S. (2010) Epigenetics and cancer. *Journal of Applied Physiology* 109: 598-605.
Katoh M, Igarashi M, Fukuda H, et al. (2013) Cancer genetics and genomics of human *FOX* family genes. *Cancer letters* 328: 198-206.
Ke X-S, Qu Y, Goldfinger N, et al. (2008) Epithelial to mesenchymal transition of a primary prostate cell line with switches of cell adhesion modules but without malignant transformation. *PLoS One* 3: 1-11.
Klaassen CD and Watkins III JB. (2010) *Casarett & Doull's Essentials of Toxicology*: The McGraw-Hill Companies.
Laird PW. (2010) Principles and challenges of genome-wide DNA methylation analysis. *Nature* 11: 191-203.
Langaee T and Ronaghi M. (2005) Genetic variation analyses by Pyrosequencing. *Mutation research* 573: 96-102.
Liang C-C, Park AY and Guan J-L. (2007) *In vitro* scrach assay: a convenient and inexpensive method for analysis of cell migration *in vitro*. *Nature Protocols* 2: 329-333.
Lin L, Miller CT, Contreras JI, et al. (2002) The hepatocyte nuclear factor 3 α gene, HNF3α (FOXA1), on chromosome band 14q13 is amplified and overexpressed in esophageal and lung adenocarcinomas. *Cancer research* 62: 5273-5279.
Lin RK, Hsu HS, Chang JW, et al. (2007) Alteration of DNA methyltransferases contributes to 5′ CpG methylation and poor prognosis in lung cancer. *Lung cancer* 55: 205-213.
Lunt SY and Heiden MGV. (2011) Aerobic Glycolysis: Meeting the Metabolic Requirements of Cell Proliferation. *Annual Review of Cell and Developmental Biology* 27: 441-464.
Luppi F, Aarbiou J, van Wetering S, et al. (2005) Effects of cigarette smoke condensate on proliferation and wound closure of bronchial epithelial cells *in vitro*: role of glutathione. *Respiratory research* 6: 140-152.
Nagathihalli NS, Massion PP, Gonzalez AL, et al. (2012) Smoking Induces Epithelial-to-Mesenchymal Transition in Non-Small Cell Lung Cancer through HDAC-Mediated Downregulation of E-cadherin. *Molecular Cancer Therapeutics* 11: 2362-2372.
Nelson T, Riggs AJ, Endsley E, et al. (s.a.) Essen BioScience Cell Player™ Cell Migration 96-Well Assay. Essen BioScience.
Newsholme P. (2001) Why is L-glutamine metabolism important to cells of the immune system in health, postinjury, surgery or infection? *The Journal of nutrition* 131: 2515-2522.
Oakeley EJ. (1999) DNA methylation analysis: a review of current methodologies. *Pharmacology and Therapeutics* 84: 389-400.
Okano M, Bell DW, Haber DA, et al. (1999) DNA methyltransferases Dnmt3a and Dnmt3b are essential for de novo methylation and mammalian development. *Cell* 99: 247-257.
Parkin DM, Bray F, Ferlay J, et al. (2005) Global cancer statistics, 2002. *A Cancer Journal for Clinicians* 55: 74-108.
Pleasance ED, Stephens PJ and O'Meara S. (2009) A small-cell lung cancer genome with complex signatures of tobacco exposure. *Nature* 463: 184-190.
Ponder BAJ. (2001) Cancer genetics. *Nature* 411: 336-341.
Ramirez RD, Sheridan S, Girard L, et al. (2004) Immortalization of human bronchial epithelial cells in the absence of viral oncoproteins. *Cancer research* 64: 9027-9034.
Reece RJ. (2004) *Analysis of Genes and Genomes*: John Wiley & Sons Ltd.

Ridley AJ, Schwartz MA, Burridge K, et al. (2003) Cell migration: integrating signals from front to back. *Science* 302: 1704-1709.
Roddy M, Nelson T, Appledorn DM, et al. (s.a.) CellPlayer™ 96-Well Kinetic Cell Migration and Invasion Assays. Essen BioScience.
Rodriguez LG, Wu X and Guan JL. (2005) Wound-healing assay. *Methods Mol Biol* 294: 23-29.
Sérandour AA, Avner S, Percevault F, et al. (2011) Epigenetic switch involved in activation of pioneer factor FOXA1-dependent enhancers. *Genome research* 21: 555-565.
Shapiro GI. (2006) Cyclin-Dependent Kinase Pathways As Targets for Cancer Treatment. *Journal of Clinical Oncology* 24: 1770-1783.
Sharma S, Kelly TK and Jones PA. (2010) Epigenetics in cancer. *Carcinogenesis* 31: 27-36.
Shen L, Guo Y, Chen X, et al. (2007) Optimizing annealing temperature overcomes bias in bisulfite PCR methylation analysis. *Biotechniques* 42: 48-58.
Sjøberg M. (2012) Lung Carcinogenesis. Department of Biology, University of Oslo, 99.
Song Y, Washington MK and Crawford HC. (2010) Loss of FOXA1/2 Is Essential for the Epithelial-to-Mesenchymal Transition in Pancreatic Cancer. *Cancer research* 70: 2115-2125.
Tang Y, Shu G, Yuan X, et al. (2011) FOXA2 functions as a suppressor of tumor metastasis by inhibition of epithelial-to-mesenchymal transition in human lung cancers. *Cell research* 21: 316-326.
Tekpli X, Zienolddiny S, Skaug V, et al. (2012) DNA methylation of the CYP1A1 enhancer is associated with smoking‐induced genetic alterations in human lung. *International Journal of Cancer* 131: 1509-1516.
Tost J and Gut IG. (2007) Analysis of Gene-Specific DNA Methylation Patterns by Pyrosequencing® Technology. *Methods in Molecular Biology: Pyrosequencing® Protocols.* Humana Press, 89-102.
van Eijk KR, de Jong S, Boks MP, et al. (2012) Genetic analysis of DNA methylation and gene expression levels in whole blood of healthy human subjects. *BMC genomics* 13: 636-648.
Veljkovic E, Jiricny J, Menigatti M, et al. (2011) Chronic exposure to cigarette smoke condensate *in vitro* induces epithelial to mesenchymal transition-like changes in human bronchial epithelial cells, BEAS-2B. *Toxicology in Vitro* 25: 446-453.
Wan H, Dingle S, Xu Y, et al. (2005) Compensatory roles of Foxa1 and Foxa2 during lung morphogenesis. *Journal of Biological Chemistry* 280: 13809-13816.
Wang W, Goswami S, Sahai E, et al. (2005) Tumor cells caught in the act of invading: their strategy for enhanced cell motility. *Trends in cell biology* 15: 138-145.
Weinberg RA. (2007) *The biology of cancer*: Garland Science.
Word B, Lyn-Cook LE, Mwamba B, et al. (2013) Cigarette Smoke Condensate Induces Differential Expression and Promoter Methylation Profiles of Critical Genes Involved in Lung Cancer in NL-20 Lung Cells In Vitro Short-Term and Chronic Exposure. *International journal of toxicology* 32: 23-31.
Xu H, Ferro TJ and Chu S. (2007) Cigarette smoke condensate inhibits ENaC alpha-subunit expression in lung epithelial cells. *European Respiratory Journal* 30: 633-642.
Xu H, Zheng L, Dai H, et al. (2011) Chemical-induced cancer incidence and underlying mechanisms in *Fen1* mutant mice. *Oncogene* 30: 1072-1081.
Yamaguchi H, Wyckoff J and Condeelis J. (2005) Cell Migration in Tumors. *Current Opinion in Cell Biology* 17: 559-564.
Yang AS, Estécio MRH, Doshi K, et al. (2004) A simple method for estimating global DNA methylation using bisulfite PCR of repetitive DNA elements. *Nucleic acids research* 32: 38-43.

Yoshino I, Kometani T, Shoji F, et al. (2007) Induction of epithelial‐mesenchymal transition‐related genes by benzo [a] pyrene in lung cancer cells. *Cancer* 110: 369-374.
Youlden DR, Cramb SM and Baade PD. (2008) The international epidemiology of lung cancer: geographical distribution and secular trends. *Journal of Thoracic Oncology* 3: 819-831.

Appendix

Content

A. Materials

In the following tables is information regarding instruments (A.1), materials (A.2), cell culture media (A.3), chemicals (A.4), solutions (A.5), kits (A.6) and computer software (A.7) used during the work with this thesis.

Instruments

Table A.1: Instruments and their labels that were used in this thesis.

Instrument	Name/label
Agitator	Thermolyne Speci-Mix, Sybron, Thermolyne
Autoclave	Systec DX-90
Cell Counter	Countess Automated Cell Counter, Invitrogen
Centrifuges	Eppendorf Centrifuge 5702 Sigma 2-6E Thermo Scientific MicroCL21 VWR Galaxy Mini
Centrifuges (Cooler)	Eppendorf Centrifuge 5417R Sigma 4K15
Heating Blocks	Grand Instruments QBT2 Eppendorf Thermomixer Comfort
Imaging System	Bio-Doc® 220 Imaging System, Benchtop UV Transilluminator, UVP
Incubator	Thermo Forma Binder
IncuCyte ZOOM	Essen BioScience
Microscope	Nikon Diaphoto light microscope
PyroMark Q24	Qiagen
PyroMark Q24 Vacuum Station	Qiagen
Spectrophotometer	Eppendorf Biophotometer NanoDrop 8000 Spectrophotometer
Thermal Cyclers (cDNA and PCR)	Perkin Elmer Cetus DNA Cycler 480 Techne TC-3000X

	MJ Research, PTC-200, Peltier Thermal Cycler MJ Research, DNA Engine Dyad, Peltier Thermal Cycler
Vacuum Pump	2511 Dry Vacuum Pump/Compressor, Welch
Vacuum Station (Bisulfite procedure)	Promega
Vortex	Heidolphreax 2000 Whirlmixer Fision
Water bath	GFL (Gesellschaft für Labortechnik m.b.H)

Materials

Table A.2: Materials that were used in this thesis.

Materials	Manufacturer
100 mm dishes	NUNC, Nunclon surface sterile
96- and 6-well plates	NUNC, Nunclon surface sterile
96-Well ImageLock Plates	Essen BioScience
96-Well WoundMaker	Essen BioScience
12 ml, 50 ml Falcontubes	Falcon
Cell Counter chamber slides	Invitrogen
Container for electrophoresis	2012 Maxiphor, Electrophoresis Unit, LKB Bromma
DNA LoBind tubes (2 ml)	Eppendorf Tubes
Electronic Pipettes	Pipetboy, Integra Biosciences Pipetus®-akku, Hirschmann Laborgerate Gilson
Flat 8 Cap Strips	Thermo Scientific
Gel electrophoresis chambers	BioRad
Lid with wires (electrophoresis)	BioRad
Microsentrifuge tubes (0.5, 1.5 ml)	Trefflab
Multichannel Pipette	Micronic Systems
PCR plates	Thermo Scientific
Plastic film for 96-well plate	MicroAmp, Applied Biosystems

Plastic Pipettes	VWR
PyroMark Q24 Plate	Qiagen
PyroMark Q24 Cartridge	Qiagen
Quarts kuvettes	QS-Hellma
Sterile filter	Pall Corporation, Acrodisc Syringe filters
Twist top vials, with cap	Sorensen Bioscience Inc.
Volt Source	Gene Power Supply GPS 200/400, Pharmacia

Cell Culture Media

Table A.3: Cell culture media that were used in the thesis, including additives, manufacturer and catalogue number.

Medium	Additives	Manufacturer	Catalogue no.
GIBCO® LHC-9 Serum-free medium	L-glutamine, serum-free, phenol red	Invitrogen	12680-013
GIBCO® DMEM/F-12	15 mM HEPES buffer, L-glutamine	Invitrogen	11039-021

Chemicals

Table A.4: Chemicals used in this thesis, their manufacturer and catalogue number.

Chemical	Manufacturer	Catalogue no.
100 bp DNA ladder	New England Biolabs	3231S
Acrylamide	Bio-Rad	161-0146
Ammonium acetate	BDH	100124T
Benzo(*a*)pyrene (B[*a*]P)	Sigma Aldrich	B-1760-1G
Buffer EB (elution buffer)	Qiagen	19086
Chloroform	Sigma Aldrich	C2432
Cigarette smoke condensate (CSC)	Murty Pharmaceuticals	
Collagen (PureCol)	Advanced BioMatrix	5005B

Crystal Violet	Sigma Aldrich	C3886
Difco Agar Noble	BD	214220
Dimethylsulfoxide (DMSO)	Koch Licht	2228-00
EDTA	Fluka Biochemika	03690
Ethanol (rectified, absolute)	Kemethyl	600051
Fetal Bovine Serum (FBS)	Gibco	10099-141
GelRed	Biotium Inc.	41003
HEPES	Sigma Aldrich	H9136
Hydroquinone	Sigma Aldrich	H9003
Loading buffer	Sigma Aldrich	G2526
Sodium hydroxide (NaOH)	Sigma Aldrich	S8045
NuSieve® 3:1 Agarose	Lonza	50090
Phenol red	Sigma Aldrich	P3532
PhiX174 RF DNA	Promega	5018402
Propan-2-ol (isopropanol)	Merck	2006617
PyroMark Annealing Buffer	Qiagen	979009
PyroMark Binding Buffer	Qiagen	979006
PyroMark Denaturation Solution	Qiagen	979007
PyroMark Gold Q24 Reagents	Qiagen	970802
PyroMark Wash Buffer, 10x	Qiagen	979008
SeaKem® GTG® Agarose	Lonza	50070
Sodium Bisulfite, A. C. S reagent	Sigma Aldrich	2439739
Streptavidin Sepharose High Performance	GE Healthcare	17-5113-01
Penicillin Streptomycin	Gibco	15 140-114
Isol-RNA lysis reagent	5’ prime	2302700
Trizma hydrochloride solution	Sigma Aldrich	T3038
Trypan Blue Stain	Invitrogen	T10282
Trypsin	Sigma Aldrich	T1147

Solutions

All solutions were made with dH_2O and solutions for cell culturing were sterile filtered before use.

Table A.5: Solutions.

Solution	Content
Ammonium acetate (10M)	77 g ammonium acetate, 100 ml dH_2O, pH adjusted to 7.03, sterile filtered
Antibiotic freezing (AF) media	76 % L-15 medium, 2 % 1M HEPES, 2 % PS, 20 % FBS
Collagen	1 % collagen solution (3.13 mg/ml), 99 % PBS
DMSO for cell culture storage	50 % L-15 medium, 2 % 1M HEPES, 8 % DMSO, 40 % FBS
Ethylenediaminetetraacetic acid (EDTA)	9.3 ml EDTA, 50 ml dH_2O, pH adjusted to 8
FBS	Heat inactivated (56 ℃ for 45 minutes)
HEPES	238.3 g HEPES, 1 ml 0.12 % phenol red in 1 L dH_2O, pH 7.3
Phenol red	125 g phenol red. 360 μl 1M NaOH, 100 ml dH_2O
Phosphate Buffered Saline (PBS)	7.07 g NaCl, 0.20 g KCl, 1.94 g $NaHPO_4*H_2O$, dH_2O to 1 L
TAE buffer (50X)	242 g Tris base, 57.2 ml acetic acid, 100 ml EDTA (0.5 M, pH 8.0), dH_2O to 1000 ml
Tris-EDTA (TE) buffer	500 μl 1M Tris pH 8, 10 μl 0.5 M EDTA, dH_2O to 50 ml
Trypsin (1 %)	50 ml trypsin, 50 ml PBS

Kits

Table A.6: Kits, their manufacturer and catalogue number.

Process	Kit Name	Manufacturer (catalogue no.)
cDNA synthesis	qScript^{TM} cDNA Synthesis Kit	Quanta (95047-500)

Genomic DNA isolation	Wizard ® Genomic DNA Purification Kit	Promega (A1125)
DNA purification during bisulfite treatment	Wizard® DNA Clean-Up System	Promega (A7280)
Pyro-PCR	PyroMark PCR Kit	Qiagen (978703)

Computer Software

Table A.7: Computer software used during this thesis, including their function and manufacturer.

Function	Software	Manufacturer	Location
Assay design for RT-qPCR	SDS Software 2.4	Applied Biosystems	Carlsbad, California, USA
Data analysis	SigmaPlot 12.3	Systat Software Inc.	San Jose, California, USA
IncuCyte ZOOM assay design and data analysis	IncuCyte ZOOM 2012A	Essen BioScience	Ann Arbor, Michigan, USA
Manual analysis of cell migration	Cell Profiler 2.0	Broad Institute	Massachusetts, USA
Pyrosequencing assay design and data analysis	PyroMark Q24 2.0.6.20	Qiagen	Hilden, Germany
Pyrosequencing primer design	PyroMark Assay Design 2.0	Qiagen	Hilden, Germany
Writing and data analysis	Microsoft Office 2007/2011 Excel and Word	Microsoft Corporation	Redmond, Washington, USA

B. General cell culture work

Thawing of cells

1. Cells were taken from a nitrogen tank at STAMI, and the ampoule was thawed in a water bath (37 °C).
2. The cells were transferred to a centrifuge tube and LHC-9 medium (5 ml) was added
3. The vial was centrifuged (1000 rpm, 4 minutes).
4. The supernatant was discarded and the pellet was re-suspended in medium (3 ml).
5. Cell suspension was transferred to a petri dish (100 mm), with added medium (5 ml) to make a total of 8 ml.
6. The cells were incubated at 37 °C.

Passaging cells

1. The media over the cells was removed.
2. Washed twice with PBS (10 ml).
3. Trypsin (1 ml) was added to the plates.
4. The cells were incubated (37 °C) until detachment from the petri dish, this was monitored in a light microscope.
5. Medium was added (5 ml) and the cells were washed up and down for separation of cells and washing of petri dish.
6. The cell suspension was transferred to a centrifuge tube and centrifuged (1000 rpm, 4 minutes).
7. The supernatant was discarded.
8. The pellet was re-suspended in medium (volume depended on dilution) and transferred to a 100 mm petri dish, with added medium to make a total volume of 8 ml.
9. The cells were incubated at 37 °C.

Freezing of cells

Followed passaging cells to point 7.

1. Cells were re-suspended in AF media (500 µl) and transferred to a twist top vial.
2. DMSO freezing medium (500 µl) was added and the solution was mixed.

3. The ampoule was placed in an isolated box at -80 °C for 4-6 hours or overnight.
4. The ampoule was further placed in a nitrogen tank for long-term storage.

Collagen coating of petri dished

1. PureCol was diluted in PBS to a total concentration of 0.03 mg/ml.
2. Collagen was added to 100 mm petri dishes (3 ml), to each well in 6-well plates (1 ml) and 96-well plates (100 µl) to completely cover the dishes/wells.
3. Incubated in the LAF-bench (room temperature) for minimum 2 hours.
4. The collagen solution was removed and washed twice with PBS.

Placed the dishes in the freezer (-80 °C).

C. CellProfiler pipeline

A pipeline was developed in CellProfiler to analyse the migration data acquired from the manual *in vitro* scratch assay. Tested different combinations of algorithms to obtain the best-suited pipeline for these particular experiments.

First, the images were made into a grey scale; this was necessary for a later identification of objects. Edges and certain image features were enhanced to improve subsequent identification of the objects, speckles were chosen as the features to enhance. Speckles are an area of increased intensity in relation to its immediate neighbourhood and was considered to be best suited for this analysis due to increased intensity of cells. Subsequently, the image was smoothened to remove artefacts of a particular size. Primary objects could now be identified based on the image processing done. In the end, the total image area occupied by objects could be measured. This algorithm reports the sum of the areas of the objects defined by the identification algorithm. The data was exported to a spreadsheet and further processed for presentation of results.

Below is an overview of the pipeline.

- Load images
- ColorToGray
- SaveImages
- EnhanceOrSuppressFeatures
- SaveImages
- EnhanceEdges
- SaveImages
- Smooth
- SaveImages
- IdentifyPrimaryObjects
- SaveImages
- MeasureImageAreaOccupied
- ExportToSpreadsheet

D. Cell images from IncuCyte ZOOM

Cells were placed in the instrument IncuCyte ZOOM and it was programmed to take images on an hourly basis for 24 hours. Images of HBEC derived cell lines 0, 12 and 24 hours after wounding are presented below (figure D.1-D.13).

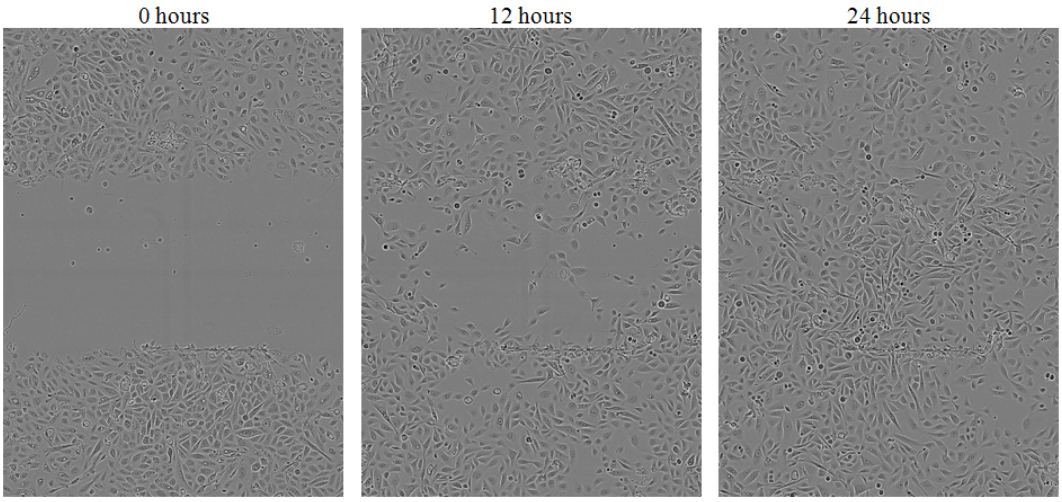

Figure D.1: Migration of untreated HBEC-2KT 0, 12 and 24 hours after wounding.

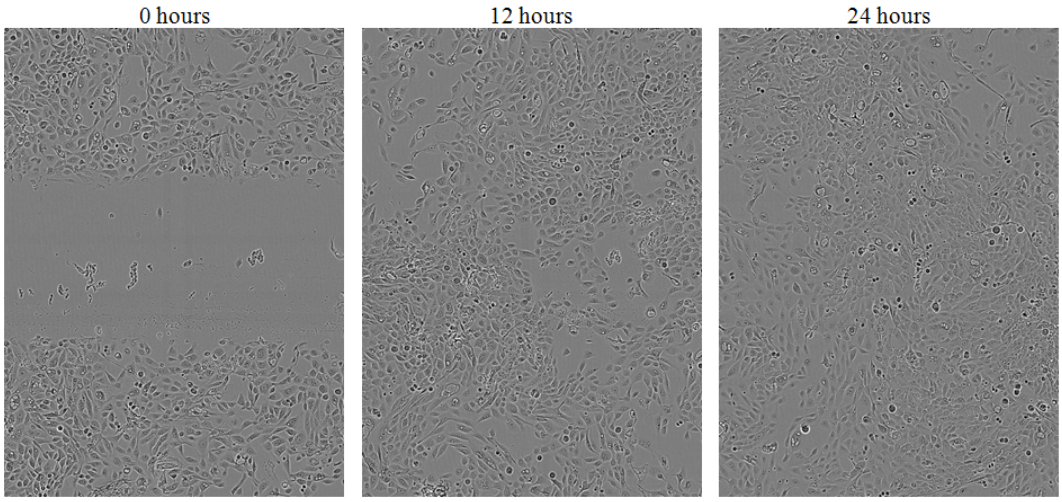

Figure D.2: Migration of HBEC-2KT control cells (DMSO) 0, 12 and 24 hours after wounding.

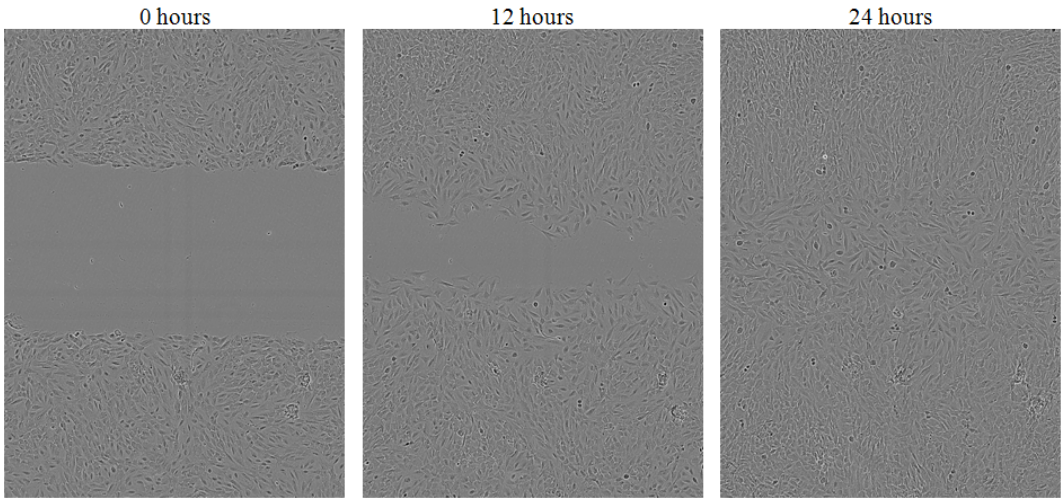

Figure D.3: Migration of HBEC-2KT-CSC.L 0, 12 and 24 hours after wounding.

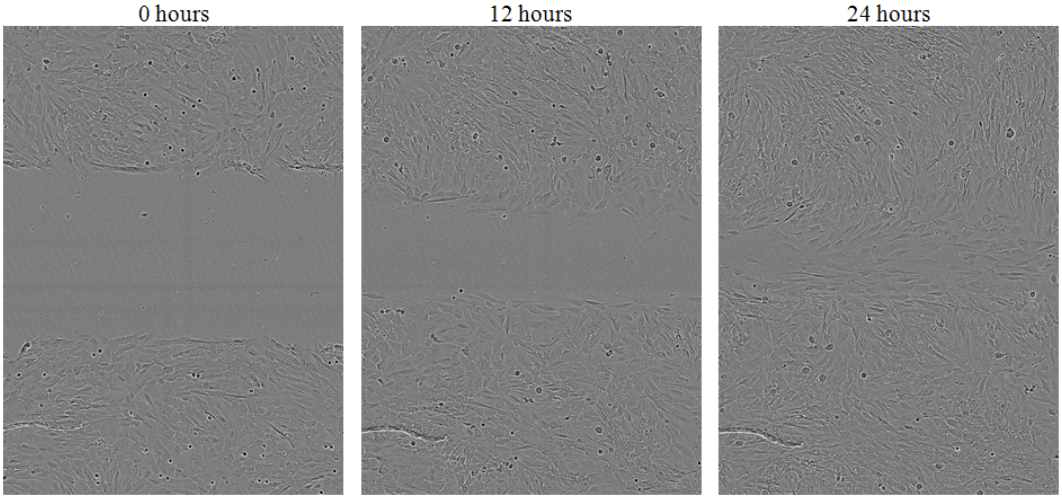

Figure D.4: Migration of HBEC-2KT-CSC.H 0, 12 and 24 hours after wounding.

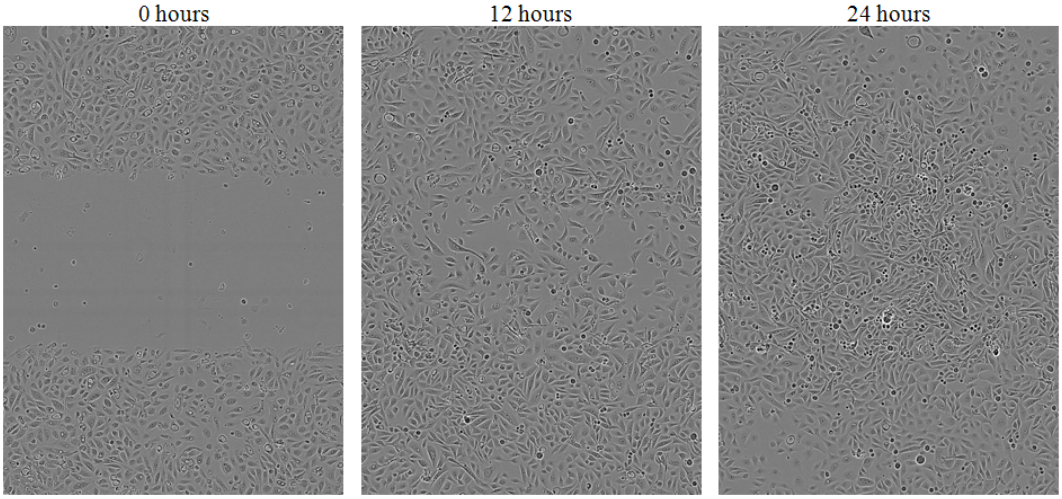

Figure D.5: Migration of untreated HBEC-3KT 0, 12 and 24 hours after wounding.

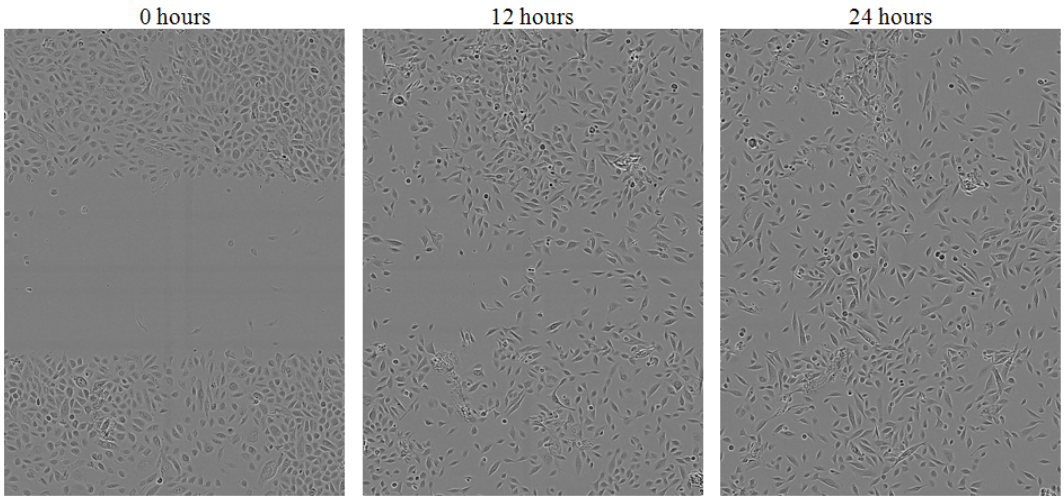

Figure D.6: Migration of untreated HBEC-12KT 0, 12 and 24 hours after wounding.

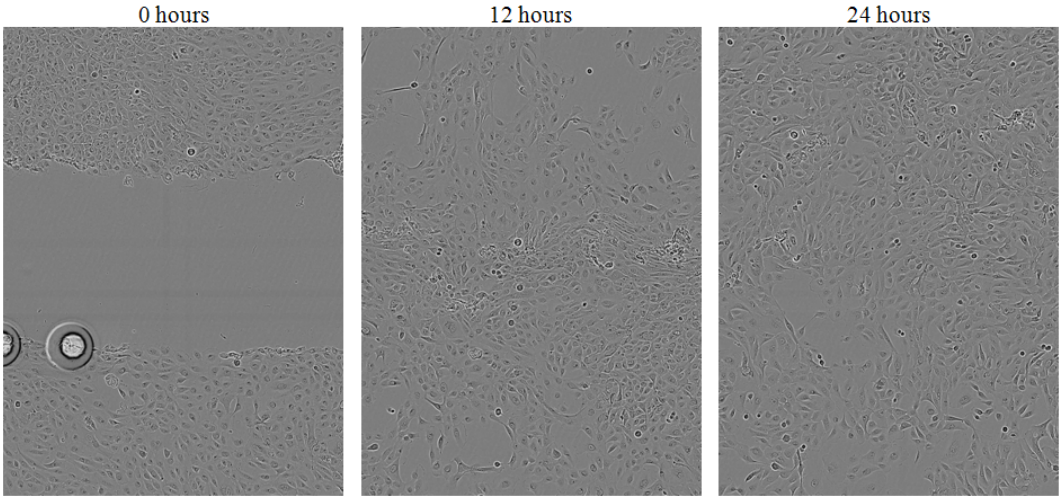

Figure D.7: Migration of HBEC-12KT control cells (DMSO) 0, 12 and 24 hours after wounding.

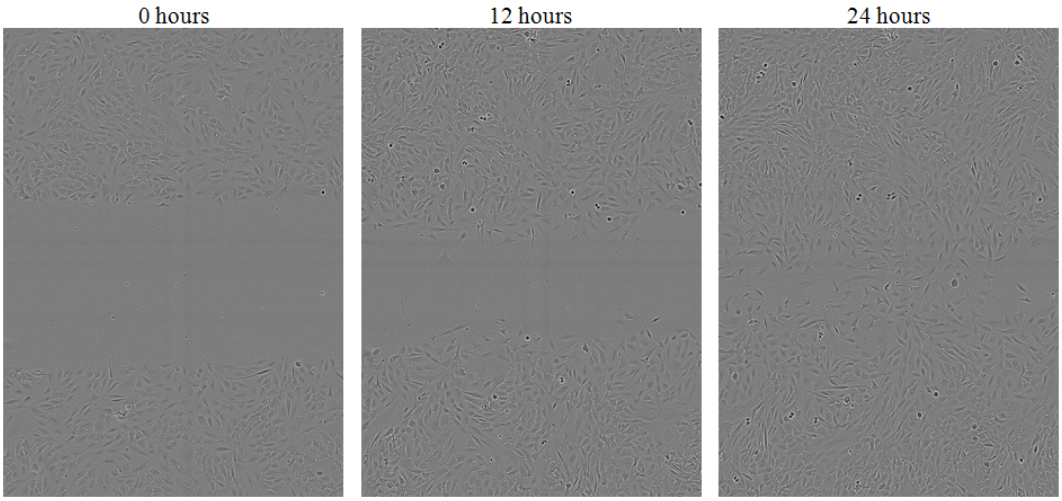

Figure D.8: Migration of HBEC-12KT-CSC.L-A 0, 12 and 24 hours after wounding.

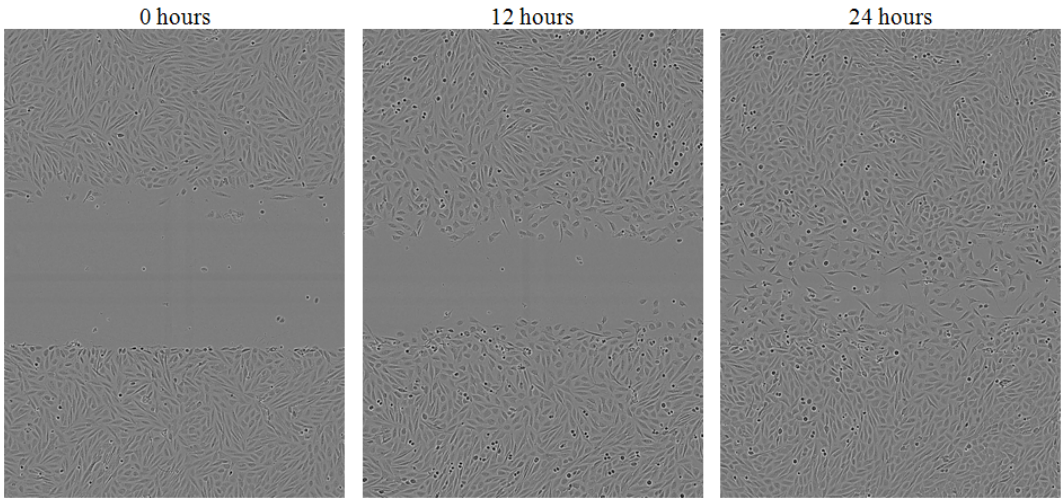

Figure D.9: Migration of HBEC-12KT-CSC.L –B 0 hours, 12 hours and 24 hours after wounding.

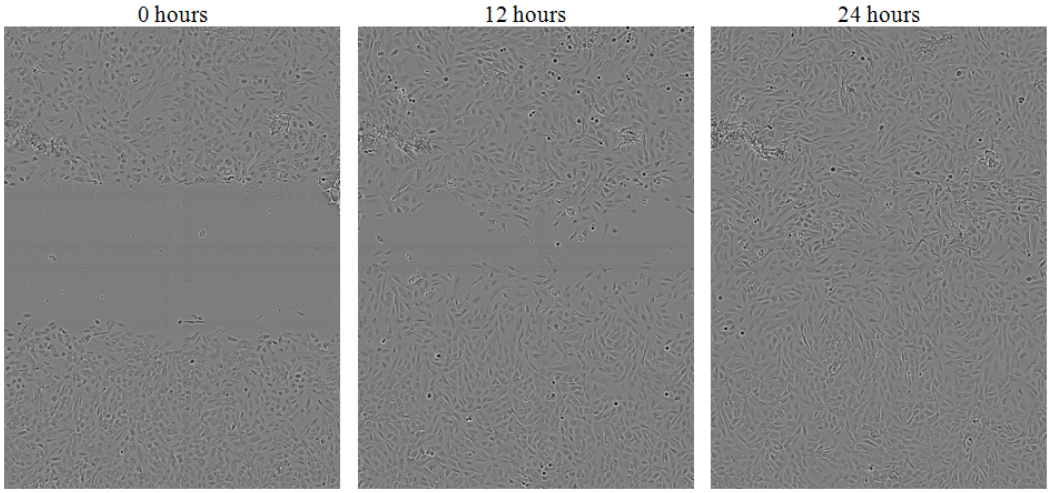

Figure D.10: Migration of HBEC-12KT-CSC.H 0 hours, 12 hours and 24 hours after wounding.

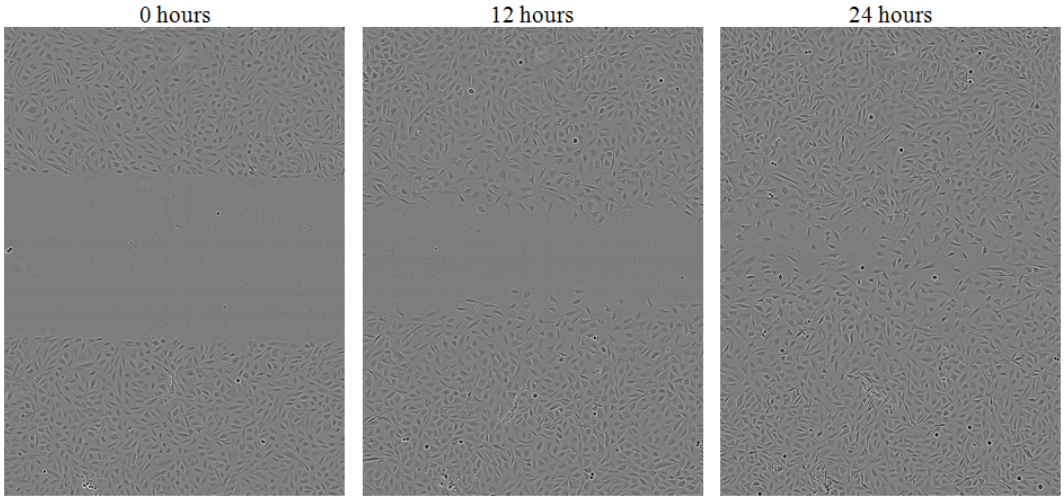

Figure D.11: Migration of HBEC-12KT-B[*a*]P.L 0 hours, 12 hours and 24 hours after wounding.

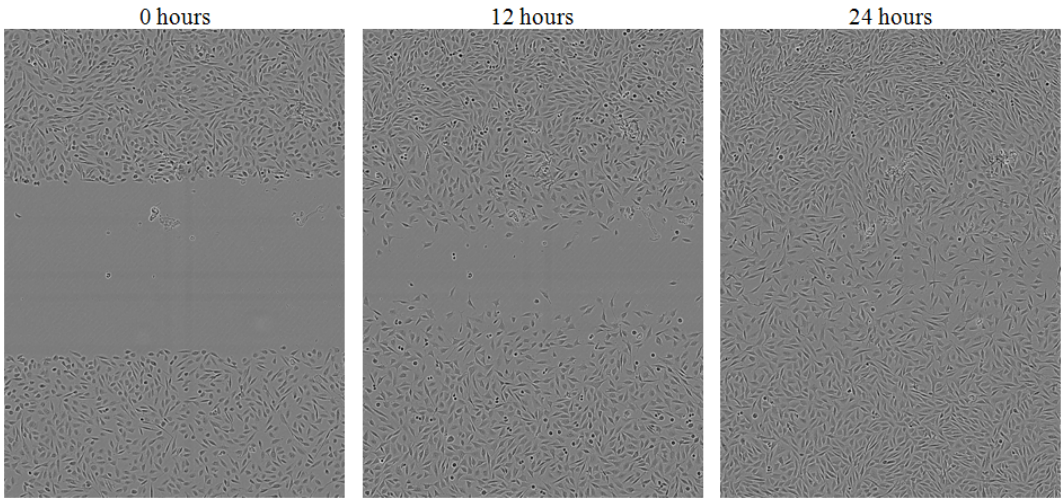

Figure D.12: Migration of HBEC-12KT-B[*a*]P.H 0 hours, 12 hours and 24 hours after wounding.

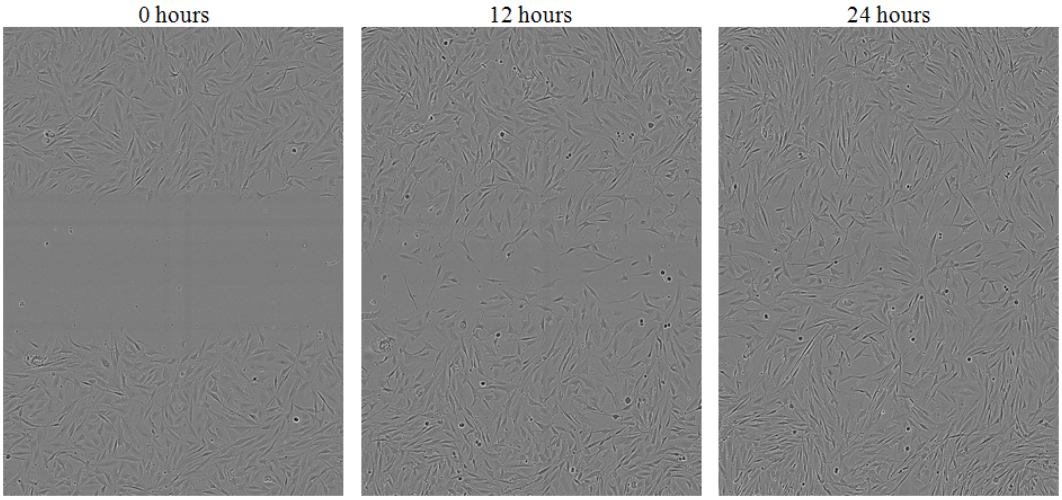

Figure D.13: Migration of HBEC-12KT-MNU 0 hours, 12 hours and 24 hours after wounding.

E. Migration analysis of HBEC derived cell lines using IncuCyte ZOOM

Migration assay using IncuCyte ZOOM was repeated several times. In the figures E.1-E.10 below the consistency between the independent experiments of each cell line is noticeable. The chosen parallel is marked with a red circle. The parallel chosen is the one that best represents the independent migration assays for each cell line. Untreated HBECs (HBEC-2KT, HBEC-3KT and HBEC-12KT) were only examined once and are not represented here. This is due to time pressure and experimental errors.

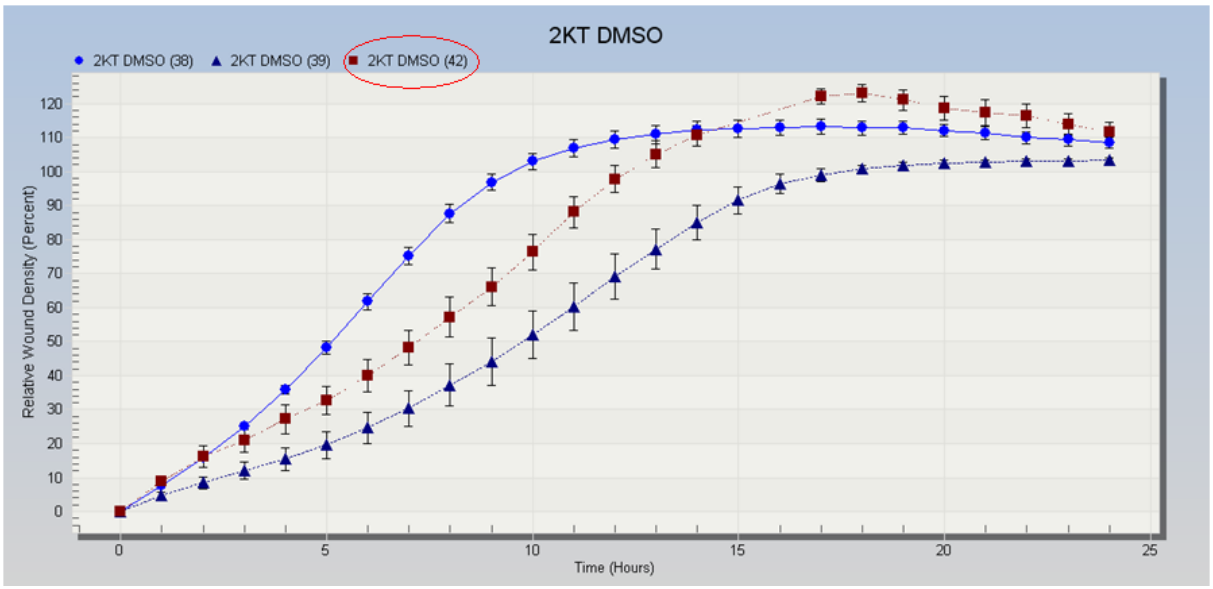

Figure E.1: Three independent migration experiments with HBEC-2KT control cells (DMSO) over a time course of 24 hours. Migration is represented as relative wound density (%). The red ring denotes the parallel chosen as a representative for the three experiments.

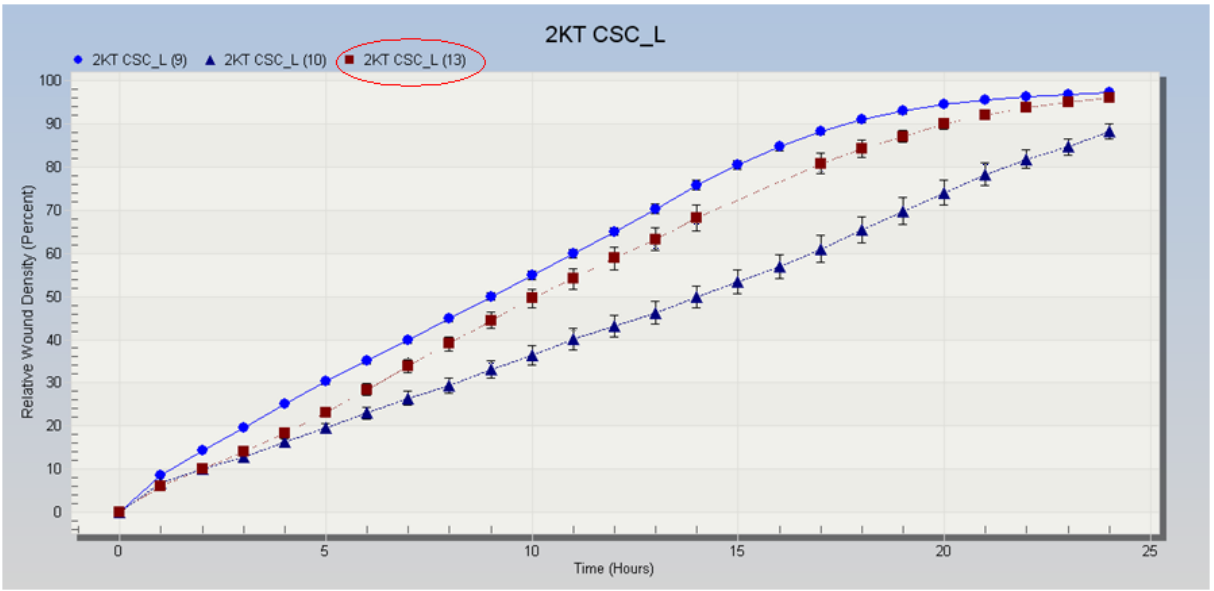

Figure E.2: Three independent migration experiments with HBEC-2KT-CSC.L over a time course of 24 hours. Migration is represented as relative wound density (%). The red ring denotes the parallel chosen as a representative for the three experiments.

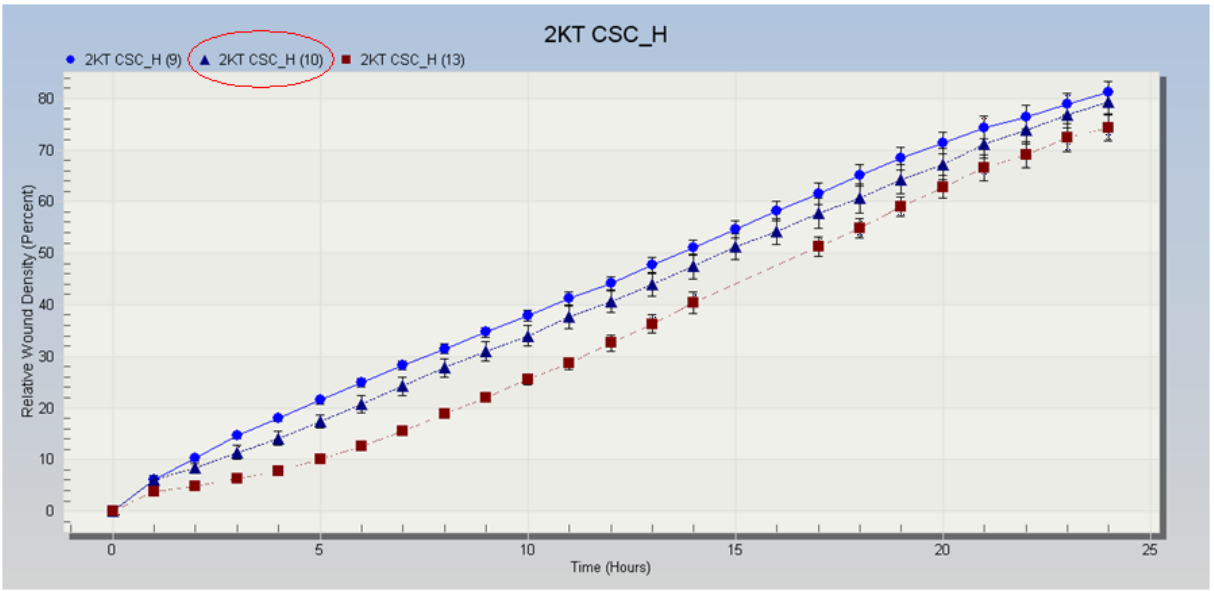

Figure E.3: Three independent migration experiments with HBEC-2KT-CSC.H over a time course of 24 hours. Migration is represented as relative wound density (%). The red ring denotes the parallel chosen as a representative for the three experiments.

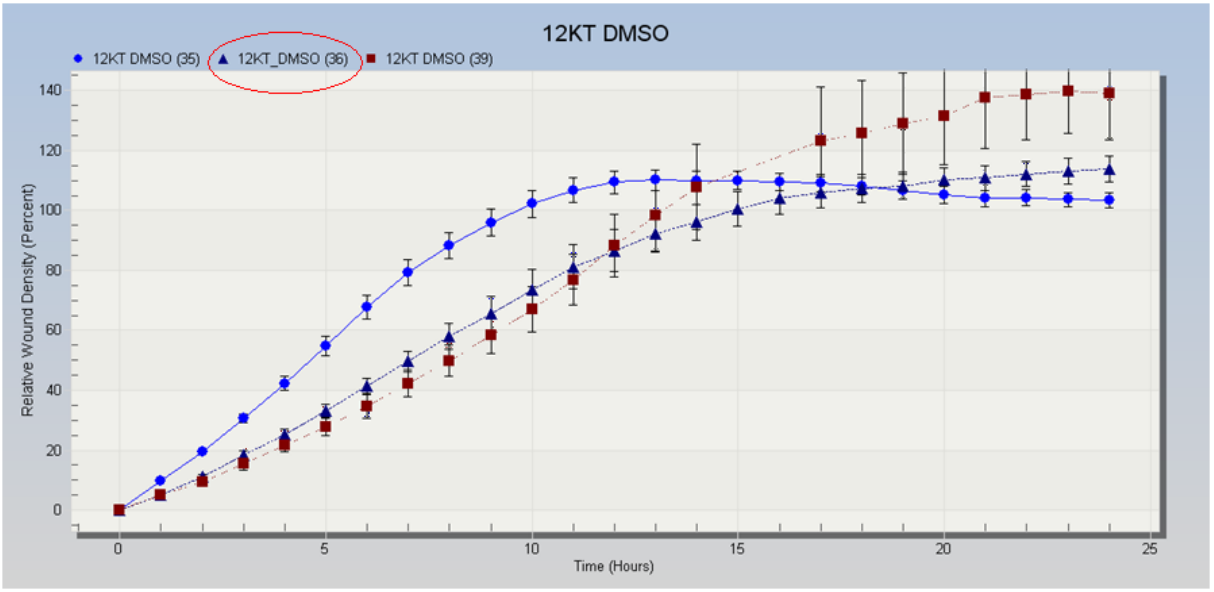

Figure E.4: Three independent migration experiments with HBEC-12KT control cells (DMSO) over a time course of 24 hours. Migration is represented as relative wound density (%). The red ring denotes the parallel chosen as a representative for the three experiments.

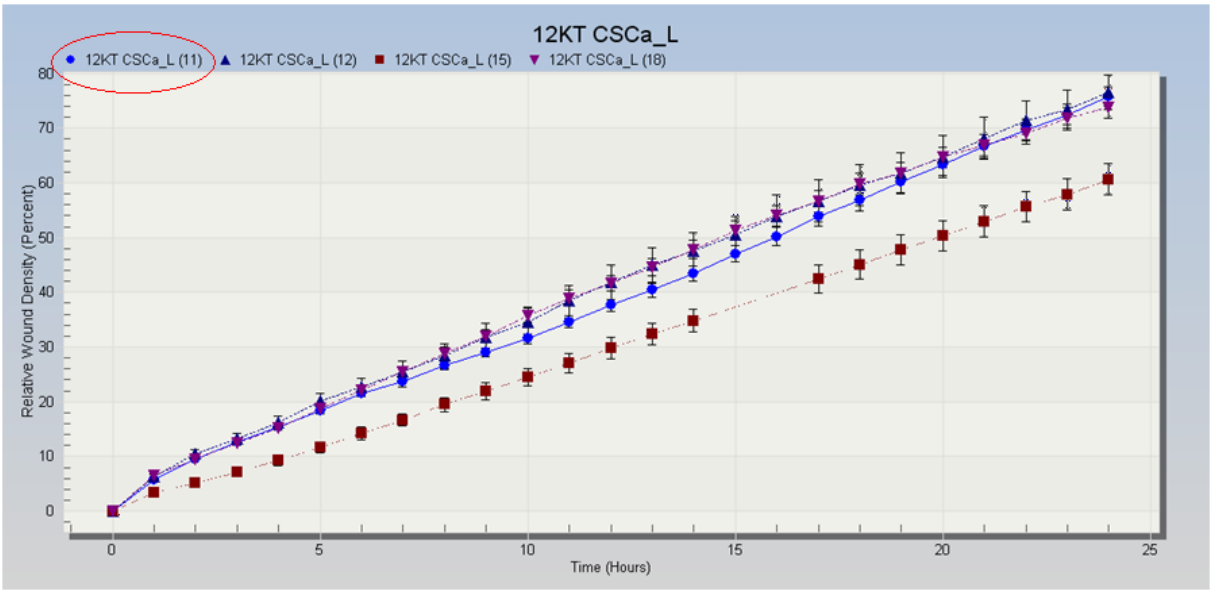

Figure E.5: Four independent migration experiments with HBEC-12KT-CSC.L-A over a time course of 24 hours. Migration is represented as relative wound density (%). The red ring denotes the parallel chosen as a representative for the four experiments.

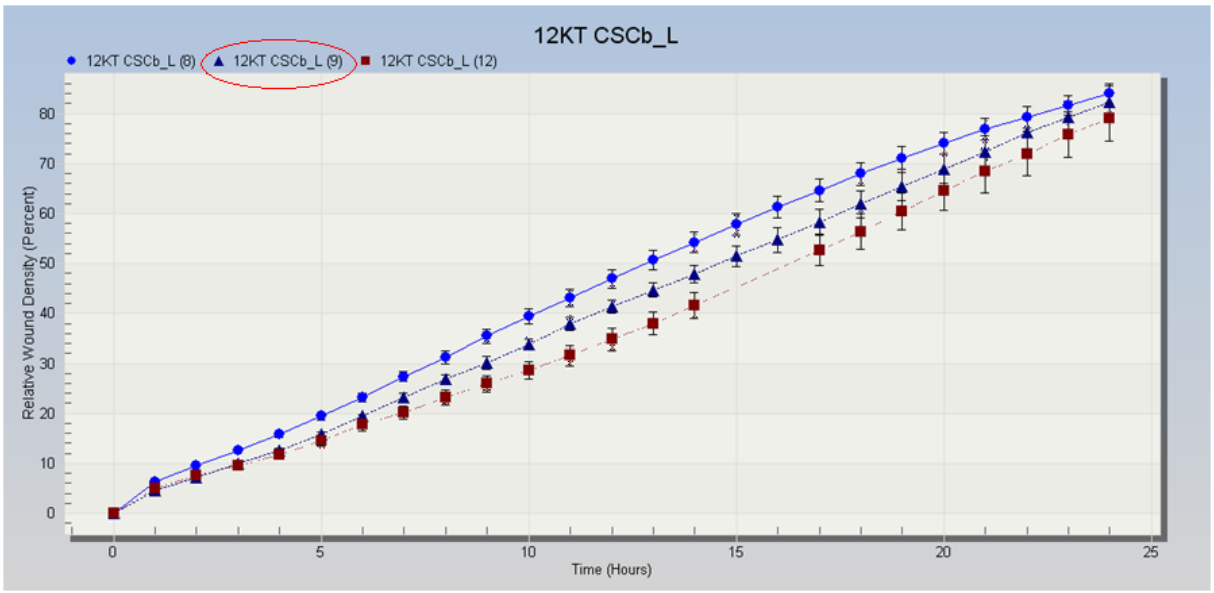

Figure E.6: Three independent migration experiments with HBEC-12KT-CSC.L-B over a time course of 24 hours. Migration is represented as relative wound density (%). The red ring denotes the parallel chosen as a representative for the three experiments.

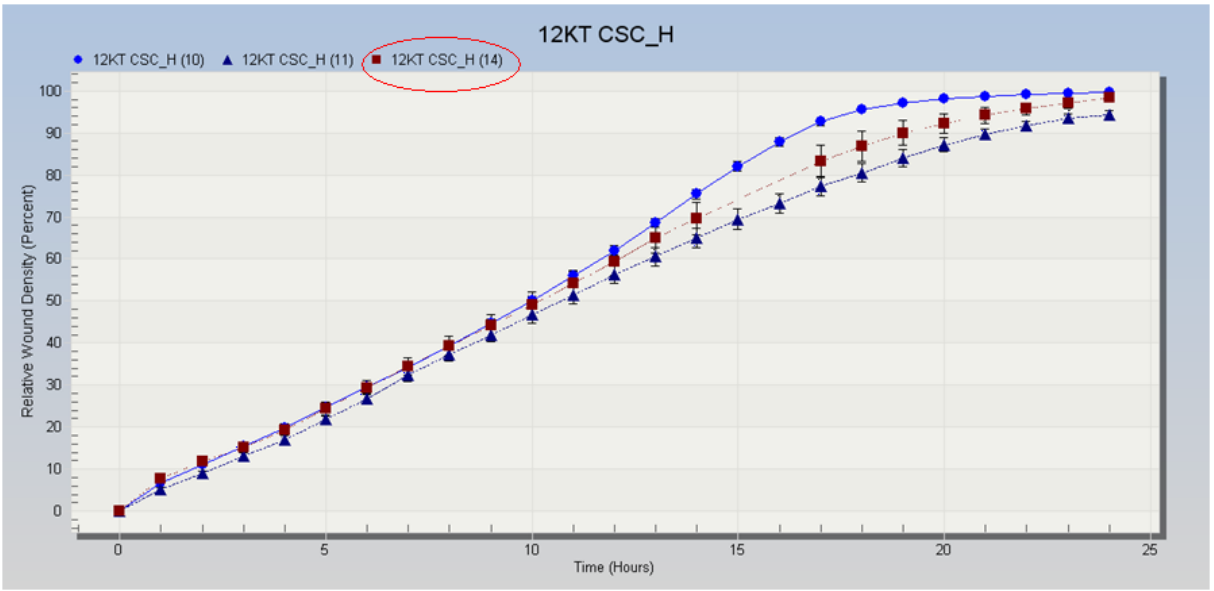

Figure E.7: Three independent migration experiments with HBEC-12KT-CSC.H over a time course of 24 hours. Migration is represented as relative wound density (%). The red ring denotes the parallel chosen as a representative for the three experiments.

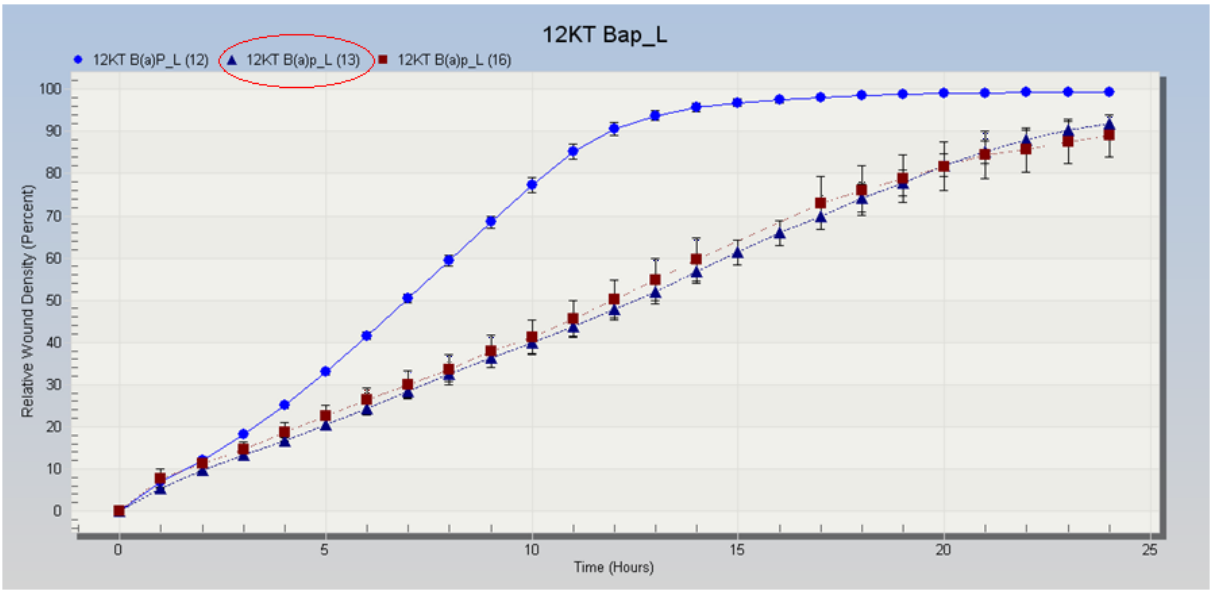

Figure E.8: Three independent migration experiments with HBEC-12KT-B[*a*]P.L over a time course of 24 hours. Migration is represented as relative wound density (%). The red ring denotes the parallel chosen as a representative for the three experiments.

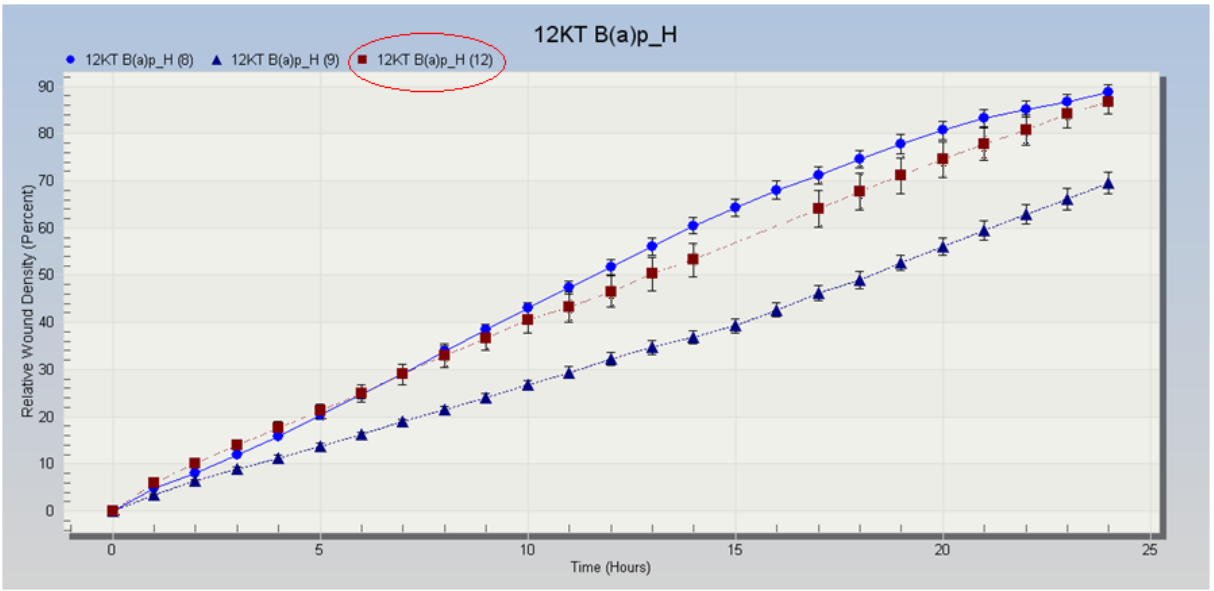

Figure E.9: Three independent migration experiments with HBEC-12KT-B[*a*]P.H over a time course of 24 hours. Migration is represented as relative wound density (%). The red ring denotes the parallel chosen as a representative for the three experiments.

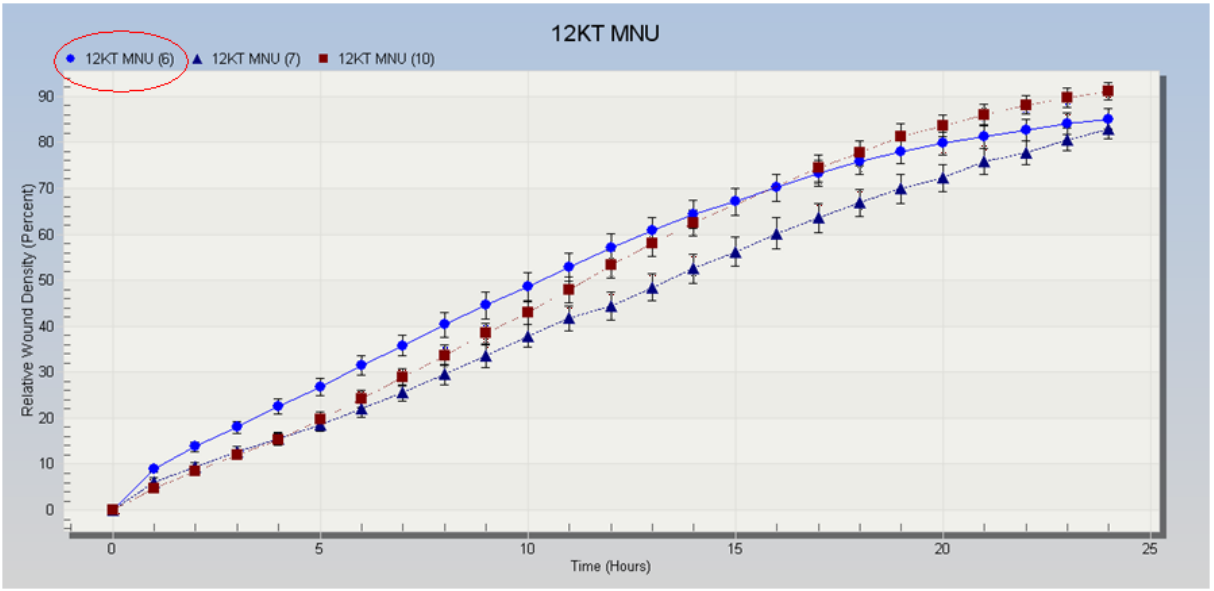

Figure E.10: Three independent migration experiments with HBEC-12KT-MNU over a time course of 24 hours. Migration is represented as relative wound density (%). The red ring denotes the parallel chosen as a representative for the three experiments.

F. Parallels to include in migration analysis by IncuCyte ZOOM

For various reasons some parallels were left out when analysing data acquired from IncuCyte ZOOM. An example can be seen in figure F.1 below, all parallels of HBEC-12KT-CSC.L-B and HBEC-2KT-CSC.L show the same overall trend on their graphs. Whereas for HBEC-12KT, parallels with a red cross clearly deviate from the overall trend, hence they are left out. One parallel of HBEC-2KT-CSC.H is missing some data points for some reason. This is an instrumental error and the parallel is left out of the calculations.

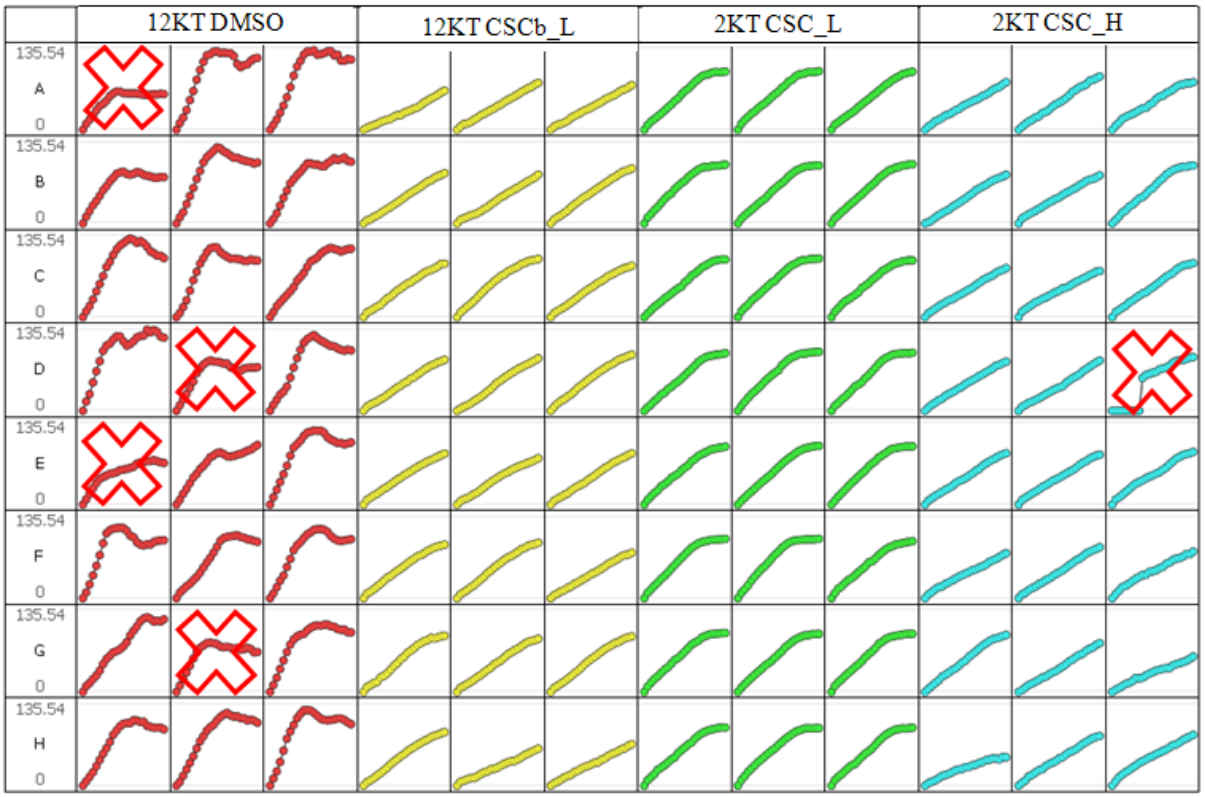

Figure F.1: Microplate graph from IncuCyte ZOOM. HBEC-12KT control cells (DMSO) is represented in red, HBEC-12KT-CSC.L-B in yellow, HBEC-2KT-CSC.L in green and HBEC-2KT-CSC.H in blue. The red crosses denote the parallels not taken into account, for various reasons, during analyses.